Aras Mirfendreski

Powertrain Development with Artificial Intelligence

History, Work Processes, Concepts, Methods and Application Examples

Springer

Powertrain Development with Artificial Intelligence

Aras Mirfendreski

Powertrain Development with Artificial Intelligence

History, Work Processes, Concepts, Methods and Application Examples

Springer

Aras Mirfendreski
Köln, Germany

ISBN 978-3-662-63862-0 ISBN 978-3-662-63863-7 (eBook)
https://doi.org/10.1007/978-3-662-63863-7

Responsible Editor: Markus Braun
This Springer imprint is published by the registered company Springer-Verlag GmbH, DE
part of Springer Nature.
The registered company address is: Heidelberger Platz 3, 14197 Berlin, Germany

Contents

List of Figures

List of Tables

Introduction

1

When did we actually start to subject everything around us and not least ourselves to continuous optimization? The idea behind optimization has been around for as long as human existence. To reduce physical labor, to increase the speed of an action in order to shorten its duration or to increase yield and thus the efficiency of an action is a sign of intelligence that is deeply anchored in our thought processes. In the eighteenth century, the agricultural revolution arose out of a necessity to feed the growing population of Western Europe. As a result, innovative processes had to be developed to increase the fertility of the soil and increase the yield of harvest. Evolutionary breeding behaviors helped to raise more powerful farm animals to support agriculture or to breed animals with a higher meat content for consumption. This era went hand in hand with the industrial revolution of the nineteenth and twentieth centuries. The development of power machines and drives changed the attitude toward physical labor. New working communities, as created by industries, as well as new and closer societies emerged, which promoted social networking. This led to the rise of the proletariat for the first time, which in a broader sense was also motivated by the optimization of social structures.

Our natural drive for development has taken us to a highly efficient and highly technological level in which we live today. Once a system has reached higher orders of optimization, it is inevitable to switch to alternative systems in order to conquer new business areas and reposition in the highly dynamic and competitive market. Does this perhaps explain why the combustion engine is experiencing a renaissance?

Drive concepts of the future will have to meet the granular demands of society as well as the strict requirements of politics. Based on demanding expectations, the entire automotive industry is collectively preparing to set the right course at an early stage for a visionary future landscape. Recent publications show that by 2040, a variety of hybrid variants, with a share of $53\% - 65\%$, should cover the new registration market. The concepts can primarily be divided into mild 48V hybrids with different powertrain variants ($P_0 - P_4$ topology), conventional serial or parallel hybrids and plug-in hybrids up to range extenders, where the

A. Mirfendreski, *Powertrain Development with Artificial Intelligence*,
https://doi.org/10.1007/978-3-662-63863-7_1

engine takes over a passive role of the drive. The range $11\% - 15\%$ of the market share is to be covered by pure electric vehicles, and the remaining $22\% - 29\%$ will be split between pure internal combustion engines, which will be powered to a higher degree by synthetic fuels (e-fuels) and bio-fuels, as well as gas and hydrogen-powered vehicles.

As a result of the targeted and versatile drive variants, the development costs of automobile manufacturers will increase dramatically in the coming years. Combustion engines have already reached an almost maximum potential regarding their efficiency and thus a minimum of CO_2 emissions. Further optimization attempts are now only bringing marginal improvements at the same or even higher investment volume. This, however, does not mean that it can be replaced so easily. Yet, one thing is certain: investment trends for the development of internal combustion engines will no longer be sustained in this form, as they have been in recent decades. An investment basis resulting from more versatile drive concepts will only be profitable in the future if significant leaner development processes and more efficient methods replace the current ones.

For this purpose, the right tools are available at the right time: Artificial intelligence (AI). AI is the science of intelligent agents combined with the power of neural networks that primarily computer scientists have dealt with over the past decades. Their versatile fields of application have settled in the world of IT and have significantly advanced the digitization process since the 1970 s. In the meantime, the concepts of AI have become versatile, reliable and highly efficient. How can the topics of a digital IT sector be transferred to industrial fields?

The term artificial intelligence is used in an inflationary way in the vernacular and meanwhile rather conveys an image or a feeling that a certain process can be carried out cleverly, mechanically and by self-learning. This book is intended as a concept book and serves to consolidate the possible uses of AI for industrial applications. It aims to present AI topics in all its complexity and to provide conceptual and creative ideas on how it can be used in powertrain development. Engineers with a focus on drive development who want to get to know more about the possibilities and levels of AI should benefit from this. This book is also aimed at AI users and IT experts who do not have a classical engineering background and would like to gain a clear impression of how their techniques can be applied to specific powertrain development topics.

Aras Mirfendreski

2 The Combustion Engine at the Turn of Industrialization

2.1 The Prehistory

Industrialization changed the world. It began in the late eighteenth century and brought about a revolutionary change through technology. The abrupt change challenged centuries-old structures at various levels that were unprepared. It seemed to possess extraordinary power and revolutionized agriculture, trade, transport, textile production, housing, politics, cultures and last but not least the entire society.

The need for industrialization was first determined by the agricultural revolution. This took place between 1760 and 1815 and enabled farmers to achieve significant growth in food production through the modernization of technologies in agriculture and animal husbandry. Western Europe and especially Great Britain were traditional trading regions at that time. The combination of ever-increasing population density and poor arable land forced farmers and peasants to become more efficient and to develop new methods to increase their productivity. In arable farming, grazing livestock was used as a fertilizer supplier for pasture land, which increased the fertility of cereal fields. Great successes in the efficient management of fields were achieved by growing new crops that simultaneously served the food cycle between humans and livestock, and by cultivating new and more robust grass varieties that not only grew faster but also extracted fewer nutrients from the soil.

In the field of **agricultural technologies**, the seed drill was invented at the beginning of the eighteenth century, replacing the plowing and sowing by human labor. This machine not only saved a considerable amount of time when sowing fields but also made it easier to harvest with the precision of evenly spaced seeds and hence increased efficiency. Other technical innovations included a horse-drawn hoe, introduced by Jethro Tull around 1708, which was used for weeding, and a lathe by Andrew Meikle around 1760, which separated the grain from its husk.

In the **livestock** sector, Robert Bakewell introduced groundbreaking innovations. For grassland management, he worked close to the river, diverting waterways and canals to

A. Mirfendreski, *Powertrain Development with Artificial Intelligence*,
https://doi.org/10.1007/978-3-662-63863-7_2

irrigate the land. This enabled him to ensure that crops did not fail even in dry periods and to eliminate the dependence on rain. He experimented with different animal fertilizers on trial fields and promoted the fertility of the soil. And in the field of animal breeding, he moved away from uncontrolled breeding of cattle on free pasture. He deliberately brought together healthy and strong sheep, cattle and cows, and, through evolutionary breeding behavior, from generation to generation, was able to raise more breed animals with a higher portion of meat.

The agricultural revolution of the seventeenth century and the subsequent industrial revolution in the late eighteenth and nineteenth centuries were pioneered by Britain, which served as a model for Western Europe, the United States and, in the late nineteenth century, Japan. Britain's rapidly growing population, high supply of labor, involvement in world trade and availability of raw materials were important prerequisites—all of which arrived at the same time, making technological change both necessary and possible.

The driving raw material of industrialization was coal, not only because it has an energy density up to four times higher than wood, but also because it burns much more slowly and thus releases its energy more moderately. Great Britain had large coal deposits. Unlike in many other countries, its coal was not deep, so it was accessible without the need for technologies for deep mining. This and the lack of alternatives to coal, as the country had only a small amount of forested land to supply wood for industries with high energy needs, catapulted Britain forward and gave it a great developmental advantage over other countries.

Toward the end of the eighteenth century, Scottish engineer James Watt developed an efficient version of the steam engine. In the subsequent decades, it found its way into mining, metal and textile industries as a reliable machine. This technology enabled mechanized mining of coal lay in deeper layers of the earth such as coal fields found in the northern France Walloon region, the German Ruhr and Saar areas, as well as Silesia and Ukraine. The industrial revolution followed in its wake.

The favorable position of Great Britain and its lead in both agriculture and industry enabled the country to develop national and international trade quickly. As a result, a large fortune in the form of capital was built up, and new business areas were created through lucrative investments. The concept of monetizability through capital investments was understood early on. Investments resulted in the financing of industrial enterprises, which led to the development of a well-functioning banking system. In the late eighteenth century, banks were founded, and increasingly loans, bills of exchange and bonds developed into a new field of business for traders. Central European countries did not follow to establish joint-stock banks until half a century later. From the past, it is clear that England still plays a dominant role in the financial and banking sectors.

The technological advantages afforded by coal-fired railroad and industrialization consolidated Great Britain's lead on world trade. The aforementioned technological limitations in mining and thus in steel production for rail transport delayed the industrial development of the United States of America and German Reich by 30–40 years. In the meantime, England had become the undisputed center of the world in international capital transfer.

Until that time, Great Britain had not been exposed to any competition, and determined the market price solely through imports of raw materials and exports of products. It was only with the competitiveness of other countries, which had caught up with the market over the following decades, that price regulation through supply and demand began.

The leading sectors in German industrial development were coal mining, iron production and mechanical engineering. The dominant demand and thus the breakthrough of the industrial structures enabled the railroad and the expansion of the railroad network. Around 1840, the length of the railways in the later German Empire was less than 500 km. Ten years later, it was 6000 km and, at the foundation of the Empire in 1871, 19000 km.

The United States, but especially the Northern States, benefited enormously on their first steps toward industrialization through their common history and language and the predominant origin of many immigrants and settlers from Great Britain. Various technologies were also brought and transmitted to the states by British settlers during the industrialization process. Due to the large area of land, it was recognized early on that an expansion of the railroad network would be of crucial importance in order to rapidly advance industrialization. Around 1840, the expansion of the network began drastically in the Northern States and was pushed forward at the same time as Germany.

The southern states, on the other hand, hardly took part in industrialization until 1880. Many regions here had concentrated on the agricultural cultivation of cotton. The sale of raw products played the main role in trade, so that for a long time industrial machines were not necessary. Slavery offered large landowners the opportunity to run their fields at a low cost. The need for efficiency and cost optimization through mechanization was no longer necessary.

Industrialization brought a fundamental change and a reversal of social orders. On the one hand, it brought far-reaching opportunities and a financially rapid rise of the middle class; on the other hand, it brought a loss of position and significance for the nobles and elites due to the changes in modern economic practices. From a political point of view in particular, companies became more prominent and exerted an increasingly strong influence. Improved transportation facilities allowed the population to leave their habitats and settle in urban agglomerations in the industrialized regions. When the population density in industrialized regions increased, this often resulted in desolate working and living conditions. On the other hand, the living conditions such as nutrition, health care and education improved considerably. In its many forms, industrialization was a creeping and peaceful process that gradually changed the world [1].

2.2 The Technological Revolution

For more than two centuries, mankind has benefited from machines. It has helped to multiply the yield of the soil and to transport people over the barriers of space and time. It is not only a mechanical substitute for the human hand, but through the speed of its work, it changed

the nature of its products and the lifestyle of generations. Although machines had existed for centuries, the engine provided mechanical power for the first time. Power derived from wind and water was bound to place and opportunity. This problem was overcome by the engine. When James Watt developed the steam engine in 1769, he opened up an inexhaustible source of energy for mankind and thereby triggered the industrial revolution. The lordship over power was once preserved for the most powerful of this world. Horses, slaves, servants and warriors—for thousands of years, influence was driven by animal and human labor [1, 2].

The eighteenth century was initially reserved for the development of the steam engine and not the internal combustion engine. Its rapid development is not a coincidence. Steam can be generated in a heated boiler, and it is then continuously available as long as water is in the boiler. In contrast, fuel, at that time in the form of powder, had to be put back into the cylinder of the engine after each working cycle. The pressures were higher, the control more difficult. This explains why the steam engine was brought to life earlier.

The awareness of having a mechanical force available at all times gradually changed the population's attitude to physical labor. If a process required the performance of heavy physical work, from then on it was an obvious thought to find ways to replace its load with power machines. In addition to agricultural and other activities, as well as textile production, trade and transport, new and industrial professions for the production of machines and other technological products were developed. The production of machines was not the work of a single person. Large enterprises and working communities as well as new forms of life emerged in the industrial boom. It was during this period that the idea of socially linked living and working emerged.

The door to early mobility was opened by the steam locomotive, the beginnings of which were in the1820 s. It was the first means of transport available for everyone that revolutionized the perception of space and time. The history of the American Civil War shows that four decades after the invention of the steam locomotive, railroad played a decisive role in both political and strategic change. The industrial, social and political revolutions since the second half of the eighteenth century were closely related both intellectually and materially.

In the middle of the nineteenth century, the Belgian inventor Etienne Lenoir undertook the development of the two-stroke gas engine. In 1862, the principle was improved by Nicolaus August Otto through the four-stroke process which was named after him. By this time, these new forms of propulsion were large and heavy and were mainly suitable as power engines for industrial purposes. In the middle of 1869, the construction of a factory was started. In Cologne, where the world's first engine factory was built, the center of the large company still stands today. At that time, there were only 40 workers who produced 87 engines under Otto's management in 1869. With the development of the combustion engine, power was available anywhere. It was brought into the hands of the proletariat, and with the revolution of power their rise gradually began [3].

The locomotive only marked the beginning of a new era of mobility. It could not, in the long run, satisfy people's aspiration for freedom as it was tied to rails, stations and railroad networks. In 1878, Amédée Bollée reconsidered the technology of steam power in terms of

individual forms of transport and adopted it in the serial production of steam-powered cars. The first models were created by integrating the drives into already existing carriages. The main advantages were that the steam cycle was a closed process and water was available to everyone at all times. Coal and firewood were also cheap fuels that were used to heat the water in the steam boiler. However, the concept also had a major disadvantage: preheating the water until it had reached its operating temperature, which could take up to half an hour before the journey began.

After the steam engine, the electric motor was the second type of mechanical drive that was used as a standard for vehicles. The Flocken electric car, which was developed and presented by Andreas Flocken in Coburg in 1888, was considered the first four-wheeled electric vehicle. The limited range and the long time it took to recharge the battery posed major challenges for this type of drive back then.

At the same time, the first pioneers were working on combustion engines as alternative drive concepts. In 1886, Carl Friedrich Benz applied for a patent for his motor vehicle in Mannheim. In 1889, he presented his Motor Car Number 3 to a broad public at the World Exhibition in Paris. This marked the birth of the internal combustion engine as a standard drive concept, and from then on it took its course. At the same time, Gottlieb Daimler and Wilhelm Maybach presented their version of the first four-wheeled automobile in Stuttgart in 1886. The Daimler-Maybach engine of 1885 was small and light and used a carburetor with fuel injection.

Two decades after the development and series production of the driving concepts—steam, electricity and combustion—it was unclear which of these three would prevail on the market. All of them brought their individual advantages and disadvantages. In 1900, about 4200 cars were built in the USA. Of these, 1600 were steam-powered, 1572 were electrically powered and 1028 had a combustion engine or other drive concept. Only a handful of about 200 manufacturers who had a more or less mature concept to offer survived until 1920. The development of the starter for an internal combustion engine in 1909 was groundbreaking and simplified the cumbersome starting of the engine by means of a hand crank. The higher efficiency and improved driving range, cheap price of oil and the gradual establishment of a network of filling stations were all factors that spoke in favor of the internal combustion engine and gave reason to believe that it would win the race over its competitors [2].

Revolution through Simulation for the Development of Powertrains

3

The computer-aided use of simulation tools for the development of powertrains has become more and more established over the last decades and is indispensable today. For this purpose, simulations are divided into the areas of flow dynamics (3D-CFD), concept simulation (1D/0D), elastohydrodynamics (EHD), kinematics, structure dynamics and reliability (finite element method (FEM) and multi-body simulation (MBS)) and acoustics. Different simulation products are provided for different development phases of powertrains. These mesh with each other throughout the entire development process chain with a strong interaction accordingly. Beginning with the concept phase up to the application of electronic control units, software products contribute their individual strengths and hence allow to benefit from a technologically efficient and targeted application.

Figure 3.1 gives a general overview as to which simulation products are used in the respective phases of powertrain development. In today's modern development units of car manufacturers, development processes are all model-based and in a strong interaction with each other, which makes the use of the complete chain inevitable. The following chapters aim to elaborate the theoretical foundations of the simulation levels and to introduce the fundamental physics behind them.

3.1 Flow Calculation

3D-, 1D- and 0D-CFD tools are generally used to predict the flow path of fluids and to conclude on thermal and thermodynamic behaviors. The selection of a suitable method is made according to the required level of detail. A higher level of detail is always accompanied by a higher computational effort.

The time required for 3D-CFD applications is so high that they are not suitable for overall process calculations. Instead, they are used for the calculation of individual components.

A. Mirfendreski, *Powertrain Development with Artificial Intelligence*,
https://doi.org/10.1007/978-3-662-63863-7_3

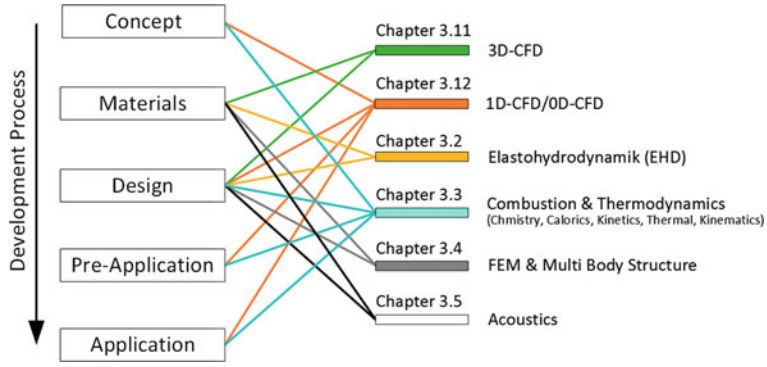

Fig. 3.1 Application areas of simulation for powertrain development

For 1D calculations, the time factor is playing an increasingly important role today. The combination of the increasing performance of computational processors and more efficient algorithms of computational solvers are leading to a new age which allows a complete engine run to be solved within real time. This results in the possibility of coupling simulation tools with real components from the field of electronics. Especially for engine control units, completely new application possibilities open up, which bring significant advantages for the development chain.

A 0D application does not resolve for the location of dependent effects. It predicts identical thermodynamic states for mass, pressure and temperature independent of the spatial coordinate. This level is especially useful if complex overall systems have to be calculated in a short time (vehicle + drive + electronics) or if the effects of a higher resolution are not desired.

3.1.1 3D-CFD

3D-CFD allows gaining differentiated insights into complex flow phenomena. Through its application, fluid-flowing components can be optimized with regard to their design. The following list enumerates some common powertrain areas that are calculated using 3D-CFD:

- Fuel cells: Flow, heat transfer, electrochemical reactions, transport of species in PEM fuel cells,[1] etc.
- Electric drives: thermal management of the electric motor, battery cooling, electrochemical modeling of the battery, aerodynamics, etc.
- Components for the cooling circuit: oil and water circuit (pump, inflow, thermostat, etc.).

[1] PEM: Proton Exchange Membrane.

- Internal combustion engine cylinder intake: airflow, compressor, intercooler (IC), manifold system, port design, valve design (charge movement for tumble and swirl generation), etc.
- Internal combustion engine cylinder: injector position, injection jet (nozzle holes, injection angle, etc.), piston geometry (compression ratio, bowl, cooling channels, etc.).
- Combustion engine cylinder outlet: port design, valve design (charge movement), manifold, EGR path, EGR cooler, turbine inlet and internal flow, VTG, wastegate, aftertreatment, muffler, etc.

The conservation laws for mass, momentum and energy, which are collectively known as the Navier-Stokes equations are the underlying equations forming the basis of numerical fluid mechanics. A flow field is completely characterized by its velocity vector and the state variables pressure, density and temperature as a function of coordinate and time. The **conservation law of mass** is described as follows [4]:

$$\frac{dm}{dt} = 0 \tag{3.1}$$

The equation expresses that the temporal change of mass within a fixed control volume corresponds to the masses added or removed over the boundaries of the volume element. The absolute mass can only increase or decrease if the density of the fluid changes. For incompressible fluids, the conservation equation for the mass in integral form is expressed as follows:

$$\text{Integral}: \frac{\partial}{\partial t}\int_V \rho \mathrm{d}V + \int_S \rho u \cdot n \mathrm{d}S = 0 \tag{3.2}$$

V denotes the control volume, S its surface, n the unit vector perpendicular to S (directed outwards), u the fluid velocity and ρ its density. A corresponding coordinate-free differential form of the continuity equation can be derived by applying the Gauss theorem [4].

$$\text{Vector}: \frac{\partial \rho}{\partial t} + \nabla \cdot \rho u = 0 \tag{3.3}$$

Another, often used representation notation is the Cartesian tensor:

$$\text{Cartesian}: \frac{\partial \rho}{\partial t} + \frac{\partial \rho u_x}{\partial x} + \frac{\partial \rho u_y}{\partial y} + \frac{\partial \rho u_z}{\partial z} = 0 \tag{3.4}$$

Here, (u_x, u_y, u_z) describe the Cartesian components of the velocity vector u. Newton's second equation of motion describes the **conservation of momentum**. It expresses that the momentum of a control volume can be influenced by external forces f [4].

$$\frac{m \cdot u}{\partial t} = \sum f \tag{3.5}$$

The momentum conservation in integral form is described as follows:

$$\text{Integral}: \frac{\partial}{\partial t}\int_V \rho u \mathrm{d}V + \frac{\partial}{\partial t}\int_S \rho u u \cdot n \mathrm{d}S = \int_S T \cdot n \mathrm{d}S + \int_V \rho b \mathrm{d}V \tag{3.6}$$

The left side of the equation describes the momentum of a fluid within a control volume. Its change over time corresponds to the sum of acting surface forces (shear and normal forces) and external forces. These may consist of gravitational, centrifugal, Coriolis or electromagnetic forces. These are summarized in the variable b [4].

The stress tensor T for a Newtonian fluid describes the molecular transport rate of a momentum and can be represented in the Cartesian coordinate system as follows [4]:

$$T_{ij} = -\left(p + \frac{2}{3}\mu\frac{\partial u_j}{\partial x_i}\right)\delta_{ij} + 2\mu D_{ij} \tag{3.7}$$

D represents the tensor of the deformation rate, δ_{ij} the Kronecker symbol ($\delta_{ij} = 1$ for $i = j$, $\delta_{ij} = 0$ for $i \neq j$), and p and μ represent the pressure and the dynamic viscosity of the fluid, respectively [4].

For the description of the viscous part of the stress tensor, the following notation is also used in the literature:

$$\tau_{ij} = 2\mu D_{ij} - \frac{2}{3}\mu\delta_{ij}\nabla u \tag{3.8}$$

with

$$D_{ij} = \frac{1}{2}\left(\frac{\partial u_i}{\partial x_j} + \frac{\partial u_j}{\partial x_i}\right) \tag{3.9}$$

The coordinate-free vector representation of the conservation of momentum is

$$\text{Vector}: \nabla u_i \rho u = u_i \nabla \cdot (\rho u) + \rho u \cdot \nabla u_i \tag{3.10}$$

If the viscous part of the stress tensor τ_{ij} is used in Eq. 3.6 and gravity is considered the only external force, the shape is obtained in Cartesian tensor notation:

$$\text{Cartesian}: \frac{\partial \rho u_i}{\partial t} + \frac{\partial \rho u_j u_i}{\partial x_j} + \frac{\partial \tau_{ij}}{\partial x_j} - \frac{\partial p}{\partial x_i} + \rho g_i = 0 \tag{3.11}$$

The **energy conservation equation** can be represented in different forms, depending on which physical quantity is considered as variable (temperature, internal energy, thermal enthalpy, total enthalpy, etc.). A common representation for a flow can be described using the enthalpy h and the thermal conductivity k [4]:

$$\text{Integral}: \frac{\partial}{\partial t}\int\limits_V \rho h \mathrm{d}V + \int\limits_S \rho h u \cdot n \mathrm{d}S = \int\limits_S k \nabla T \cdot n \mathrm{d}S + \int\limits_V (u \cdot \nabla p + S' \cdot \nabla u)\mathrm{d}V + \frac{\partial}{\partial t}\int\limits_V p \mathrm{d}V \tag{3.12}$$

S' corresponds to the viscous part of the stress tensor. For the coordinate-free vector representation of the conservation of energy theorem, the following results:

$$\text{Vector}: \frac{\partial(\rho\phi)}{\partial t} + \nabla \cdot (\rho\phi u) = \nabla \cdot (\Gamma \nabla \rho) + q_\phi \tag{3.13}$$

For the conservation of a scalar, ϕ represents the amount of the scalar per unit mass, e.g. the specific enthalpy or the internal energy. The differential form of the generic conservation equation in Cartesian coordinates and tensor notation is

$$\text{Cartesian}: \frac{\partial(\rho\phi)}{\partial t} + \frac{\partial(\rho u_i \phi)}{\partial x_j} = \frac{\partial}{\partial x_j}\left(\Gamma \frac{\partial \phi}{x_j}\right) + q_\phi \tag{3.14}$$

The variable Γ here describes the diffusion coefficient for the quantity ϕ, and q_ϕ designates sources and sinks of ϕ, which are supplied or discharged to the control system. By the conservation laws for mass, momentum and energy, a system is completely described together with the thermal equation state for ideal gases and the relations between the specific gas constant R, the isentropic exponent κ and the specific heat capacities c_p as well as c_v [5]:

$$p \cdot v = m \cdot R \cdot T, \kappa = \frac{c_p}{c_v}, R = c_p - c_v \tag{3.15}$$

All in all, a system of equations consisting of nonlinear, partial differential equations (PDE) results. For a 3D-CFD calculation process, these are iteratively calculated at each point of the discretized structure (mesh) at each individual time step.

3.1.2 1D-CFD

If a complete engine process including an existing air path system is the objective of investigation, a 1D approach is a good choice. In a 1D simulation, the fluid flow is considered exclusively along the main flow direction, which results in a moderate computational effort in relation to the 3D-CFD. In addition to the calculation of an air path, 1D flow models using the example of an engine are suitable for the calculation of charge exchange, exhaust gas turbocharger design, geometry optimization, and the design and dimensioning of cooling and oil circuits.

1D models are also based on the conservation equations of mass, momentum and energy. As a result of the reduced dimensions, a 1D flow calculation can be expressed in a much simpler way compared to 3D-CFD. The following basic equations are presented in [5].

With regard to **mass conservation**, the following simplification is made for the 1D, starting from the 3D, view, by omitting the local coordinate resolution in y- and z-directions:

$$\frac{\partial}{\partial t} + \frac{\partial m_x}{\partial x} + \cancelto{0}{\frac{\partial m_y}{\partial y}} + \cancelto{0}{\frac{\partial m_z}{\partial z}} = 0 \tag{3.16}$$

$$\rightarrow \frac{\partial}{\partial t} + \frac{\partial m_x}{\partial x} = 0 \tag{3.17}$$

By applying the continuity equation, the mass can be replaced. This results in the vectorial notation:

$$\frac{\partial}{\partial t} + \frac{\partial m_x}{\partial x} = \frac{\partial}{\partial t} + \frac{\partial (\rho_x u_x A_x)}{\partial x} \tag{3.18}$$

A_x corresponds to the flow area of a pipe transverse to the flow direction. Due to the 1D approach, the x-component of the flow velocity corresponds to the entire flow vector $u_x = u$. Hence, the conservation of mass for 1D leads to

$$\frac{\partial \rho}{\partial t} + \rho \frac{\partial u}{\partial x} + u \frac{\partial \rho}{\partial x} + \frac{\rho u}{A} \frac{\partial A}{\partial x} = 0 \tag{3.19}$$

For the **conservation of momentum**, the reduction of the single terms below can be performed based on the 3D view. The surface forces and the external forces are combined and represented by a friction coefficient f_R:

$$\frac{\partial \rho u_i}{\partial t} + \frac{\partial \rho u_j u_i}{\partial x_j} + \frac{\partial \tau_{ij}}{\partial x_j} - \frac{\partial p}{\partial x_i} + \rho g_i = 0 \tag{3.20}$$

$$\rightarrow \frac{\partial \rho u}{\partial t} + u \frac{\partial u}{\partial x} + \frac{\partial p}{\partial x} + f_R = 0 \tag{3.21}$$

If one follows the same scheme and tries to get from the 3D view of **energy conservation** to the 1D one, Eq. 3.22 can take different forms depending on which scalar is chosen. By inserting the equations for continuity from Eq. 3.17 and the conservation of momentum from Eq. 3.21, the energy equation can be represented in a generic form as a function of the total pressure differential, see Eq. 3.23, [5, 6]:

$$\frac{\partial (\rho \phi)}{\partial t} + \frac{\partial (\rho u_i \phi)}{\partial x_j} = \frac{\partial}{\partial x_j} \left(\Gamma \frac{\partial \phi}{x_j} \right) + q_\phi \tag{3.22}$$

$$\rightarrow \frac{\partial p}{\partial t} + u \frac{\partial p}{\partial x} + (q_\phi + u \cdot f_R)\rho = 0 \tag{3.23}$$

3.1.3 0D-CFD

A much simpler description of an air path is based on zero-dimensional (0D) models. By decoupling a system from its path and time, the flow process is detached from a path and can be represented solely by a time dependency. In a considered subsystem, the thermodynamic state is spatially constant at any discrete time.

Even in a 1D flow modeling, parts of the air path in the form of air volumes can be considered dimensionless. In this case, the reflection is calculated with a characteristic and representative length of a volume. Additionally, other subsystems of the engine as well as the combustion chamber, exhaust turbocharger, etc. are modeled on the basis of a 0D approach.

Filling and emptying models

The filling and emptying method is a concept commonly used in practice for calculating fluid-flow pipe systems. Here, pipelines of the air path system are combined to spherical containers with corresponding volumes, which is why this type of model is also called "container model". These are separated from each other by means of orifices or valves with fixed or variable cross-sections. Changes of state within a container are calculated considering transient filling and emptying processes. A positive volume flow between adjacent containers is generated by filling the front container and emptying the rear one.

A crucial assumption is that pressure and temperature within the containers are balanced without delay. For each discrete calculation step, a complete mixing of the tank contents takes place. The flow thus moves through the air path system at an infinitely high speed of sound.

For a calculation of transient processes, it is assumed that the flow can be treated stationary for small time intervals, which leads to deviations in the result. Gas dynamic flow effects cannot be reproduced with an R&D method, since the latter is not suitable for the investigation of concepts such as resonance charging at the cylinder inlet and shock charging at the exhaust turbocharger [5].

A system is described by the average values of pressure, temperature, mass, internal energy and the heat flow across the system boundaries.

For the calculation of container models, the conservation laws for mass and energy are calculated, the consideration of the conservation of momentum is omitted due to the absence of a local resolution. Thus, the system is greatly simplified compared to a 1D approach. The **conservation of mass** leads to the following differential form from a simplified 3D consideration:

$$\frac{\partial \rho}{\partial t} + \frac{\partial \rho u_x}{\partial x}^{0} + \frac{\partial \rho u_y}{\partial y}^{0} + \frac{\partial \rho u_z}{\partial z}^{0} = 0 \tag{3.24}$$

$$\rightarrow \frac{\partial \rho}{\partial t} = 0 \tag{3.25}$$

From this, a temporally solvable representation can be derived:

$$\frac{\mathrm{d}}{\mathrm{d}t}m(t) = \dot{m}_{\mathrm{in}}(t) - \dot{m}_{\mathrm{out}}(t) = 0 \tag{3.26}$$

The **conservation law for energy**, based on the 3D view, can be reduced accordingly to the following form:

$$\frac{\partial(\rho\phi)}{\partial t} + \cancelto{0}{\frac{\partial(\rho u_j \phi)}{\partial x_j}} = \cancelto{0}{\frac{\partial}{\partial x_j}\left(\Gamma\frac{\partial\phi}{x_j}\right)} + q_\phi \tag{3.27}$$

$$\rightarrow \frac{\partial\rho\phi}{\partial t} = q_\phi \tag{3.28}$$

If, for example, for the scalar ϕ the internal energy of a system is considered, the temporal change takes the following form:

$$\frac{\mathrm{d}U}{\mathrm{d}t} = \frac{\mathrm{d}Q_{\mathrm{W}}}{\mathrm{d}t} + \frac{\mathrm{d}H_{\mathrm{zu}}}{\mathrm{d}t} - \frac{\mathrm{d}H_{\mathrm{ab}}}{\mathrm{d}t} \tag{3.29}$$

Using the thermal equation of state for ideal gases, the internal energy can also be expressed as a function of pressure, temperature and the isentropic exponent κ:

$$\frac{\partial U}{\partial t} = \frac{\partial}{\partial t}\cdot\frac{p\cdot V}{\kappa-1} = \frac{1}{\kappa-1}\cdot\frac{\partial p}{\partial t}\cdot V + \frac{1}{\kappa-1}\cdot p\cdot\frac{\partial V}{\partial t} \tag{3.30}$$

Together with the caloric correlations

$$U = m\cdot c_v\cdot T,\ H = m\cdot c_p\cdot T \tag{3.31}$$

and Eqs. 3.29 and 3.31 while disregarding the heat flows over the walls result in the following derivations for p and T:

$$\frac{\mathrm{d}T}{\mathrm{d}t} = \frac{T\cdot R}{c_v\cdot p\cdot V}\left[\left(\dot{H}_{\mathrm{zu}}(t) - \dot{H}_{\mathrm{ab}}(t)\right)\left(1-\frac{c_v}{c_p}\right)\right] \tag{3.32}$$

$$\frac{\mathrm{d}p}{\mathrm{d}t} = \frac{\kappa\cdot R}{V\cdot c_p}\left[\dot{H}_{\mathrm{zu}}(t) - \dot{H}_{\mathrm{ab}}(t)\right] \tag{3.33}$$

To determine the mass flow over the throttling points (see Fig. 3.2), a flow equation according to *de Saint-Venant* is used for stationary, adiabatic flows. A detailed derivation can be read in [5]:

$$\dot{m} = \alpha_K\cdot A_{\mathrm{zu}}\cdot\sqrt{p_0\cdot\rho_0}\cdot\psi,\ \psi = \sqrt{\frac{2\kappa}{\kappa-1}\left(\left(\frac{p_1}{p_2}\right)^{\frac{2}{\kappa}} - \left(\frac{p_1}{p_2}\right)^{\frac{\kappa+1}{\kappa}}\right)} \tag{3.34}$$

Here, A_{in} is the geometric cross-section, p_0 and ρ_0 the pressure and density in the tank in front of the orifice, α_{K} the flow coefficient and p_1 the pressure in the cross-section. The term ψ is also called outflow function.

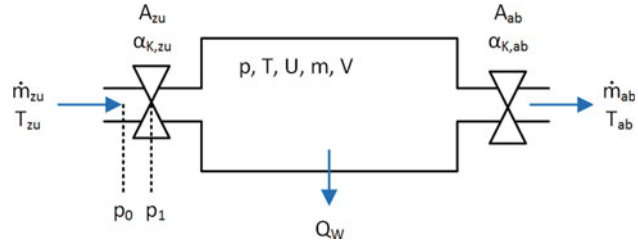

Fig. 3.2 State variables, fluid and energy flow of a container model

By means of the flow coefficients, real effects on the flow through a valve, such as constriction, are taken into account, whereby the actual flow cross-section is smaller than the geometric one. This coefficient describes the ratio of the actual mass flow to the theoretically possible mass flow.

The maximum of the outflow function results from an extreme value determination. At the point $\psi_{\max}$, the critical pressure ratio $\left(\frac{p_1}{p_0}\right)_{\text{krit}}$ is just reached, as the following equation results:

$$\frac{\partial \psi}{\partial \left(\frac{p_1}{p_0}\right)} = 0, \left(\frac{p_1}{p_0}\right)_{\text{krit}} = \left(\frac{2}{\kappa + 1}\right)^{\frac{\kappa}{\kappa - 1}} \tag{3.35}$$

As can be seen in Fig. 3.3, the value of the function increases up to the critical pressure ratio. At this point, the speed of sound and thus the maximum possible mass flow is reached in the narrowest cross-section. To the left, the mass flow can be increased by increasing p_0 or decreasing p_1 [5, 7].

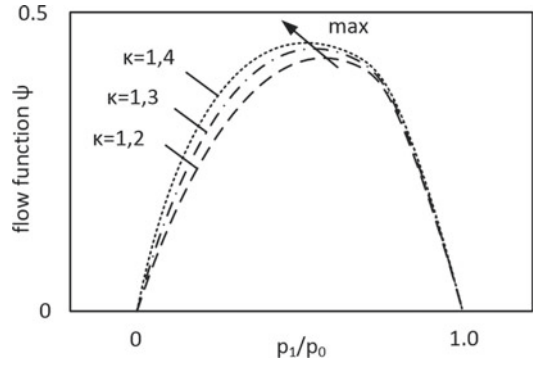

Fig. 3.3 Flow function as a function of isentropic exponent and pressure ratio [5]

Mean value models

A mean value model (MVM) is a subordinate and compressed form of the filling and emptying models. The difference lies in the fact that, in contrast to a conventional engine process calculation, the working process is not crank angle-resolved but considered averaged over a cycle.

Such models are used when a crank angle-resolved view of the engine can be dispensed with, or when even shorter computing times are required in contrast to the filling and emptying method. This can be the case, for example, for fast parameter studies, integration of the engine model into a complete vehicle environment (longitudinal dynamics) or for the coupling of electronic control units, where real-time capability is mandatory.

3.2 Elastohydrodynamics (EHD) and Tribology

Tribology deals with the science of interactions of surfaces in relative motion, which includes the principles of friction, lubrication and wear. Its application is interdisciplinary and is based on physics, chemistry, materials science and engineering (Fig. 3.4).

One of the most important applications of tribology in the field of engineering can be found in the design and layout of bearings. In sliding roller contacts, such as rolling bearings, gears and cam followers, the treads are elastically deformed due to high contact pressures. For plastics such as seals, deformation can even occur at low pressure. This results in a much larger surface area for carrying the load force than would be the case without deformation. During operation, material stresses can hence be kept within specified limits despite high forces [8].

Lubrication under consideration of deformations has been increasingly understood in the last decades as a describable phenomenon and transferred into mathematical models. This has led to the development of simulation tools that help to carry out sensitivity studies, influence processes, understand effects more precisely and ultimately transfer studied knowledge to implement it into the design.

Elastohydrodynamic lubrication is generally referred to when the elastic deformation of two contact bodies is equal to or approximately greater than the thickness of the lubricant film. If the deformation is negligible, on the other hand, the lubrication is referred to as purely hydrodynamic. If the contact bodies are stiff, as is the case with metals, this is referred to as hard EHD lubrication. Soft EHD lubrication, on the other hand, occurs when one or both contact bodies have a low modulus of elasticity. In the case of endurance runs, it is a matter of stationary EHD lubrication. If, on the other hand, a time-discrete behavior is of interest, such as during a warm-up or dynamic load on contact bodies, this is referred to as transiently loaded EHD lubrication.

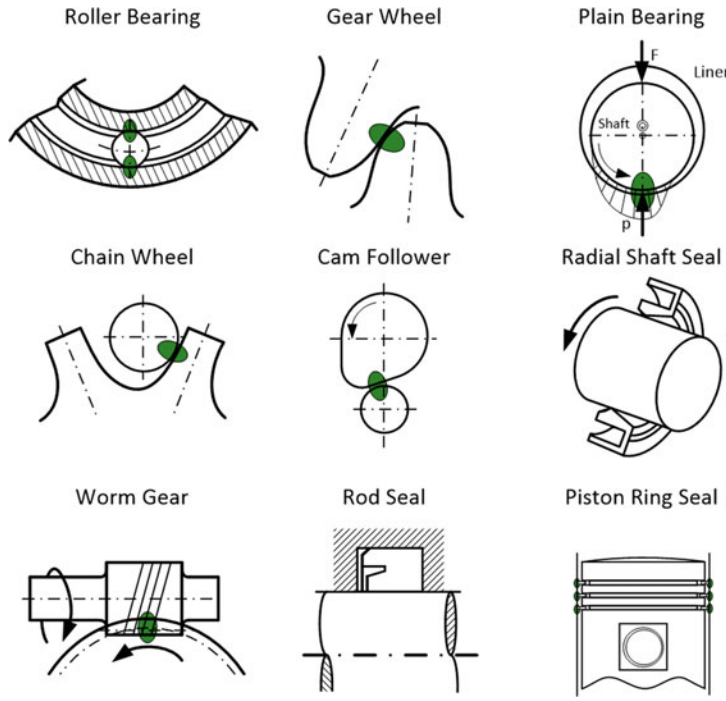

Fig. 3.4 Examples of EHD-lubricated contacts [8]

In general, a contact between any two bodies locally forms an elliptical pressure surface. In one extreme case, the load state can reach a circular contact, i.e. a point contact, or approximately a bath-shaped contact or line contact in the other extreme case. In a line contact, the bodies are in a plane deformation state.

To describe a tribological system, it is necessary to know important parameters such as lubricant film thickness and pressure, load capacity, friction and material stresses. Problems of the EHD can generally be divided into stationary hard EHD, stationary soft EHD, thermal EHD and transient EHD.

The course of the friction force as a function of the friction velocity in the case of hydrodynamic friction is typically described by the so-called Stribeck curve (see Fig. 3.5). This curve gives insight into the effect of the lubricant film thickness on the friction coefficient as a function of oil viscosity, relative speed of the material pairings and the normal force.

If there is no relative movement between two pairs of materials, this is called dry friction. If a force greater than the static friction force is applied, a relative movement is initiated. In the first phase, the lubricant separates the material pairings from each other only at the molecular level—this phase is called boundary lubrication.

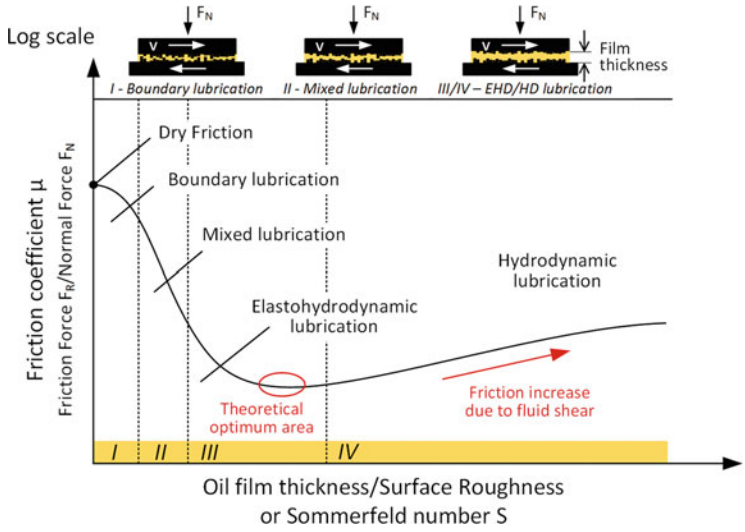

Fig. 3.5 Stribeck curve: Effect of the lubricant film on the friction coefficient of two materials [9]

If a thin lubricating film forms between the bodies so that they are only separated by slight material roughness, the bodies can slide off on the lubricant—this phase is known as mixed lubrication.

When mixed friction is overcome, the material pairs are completely separated by the lubricating film in the next phase. This phase, which is called liquid friction, can be divided into an elastohydrodynamic and a hydrodynamic phase, where material wear is lowest. As more and more layers of the lubricant slide on top of each other with increasing relative speed, the frictional force increases again in the hydrodynamic phase. In general, it is desirable to achieve a coefficient of friction in the range of the minimum for any design of material pairings and oil [8].

In its simplest form, the entire problem of elastic hydrodynamic lubrication (EHL) is described by five equations as follows.

1. The Reynolds equation describes the flow of a Newtonian fluid in a narrow gap.

It was derived from the Navier-Stokes equation to express the character of a slow and viscous flow. Inertial forces as well as external forces versus viscous forces are neglected for simplification. A second simplification is done based on the geometrical conditions of a narrow gap: The dimensions in z-direction are much smaller than in x- and y-directions, see Fig. 3.6. Applying the condition of slip resistance along the wall, the velocity profile is

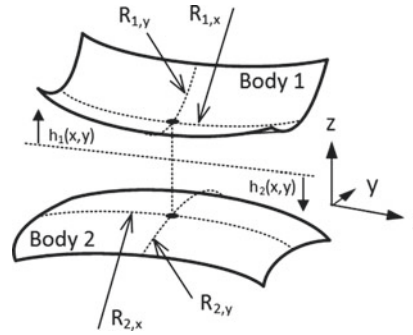

Fig. 3.6 Coordinate system in the contact point of two bodies

obtained as a function of the z-coordinate. The continuity of the mass flow in a narrow gap, extending from one surface to the other, results as follows:

$$\frac{\partial}{\partial x}\left(\frac{\rho h^3}{12\eta}\frac{\partial p}{\partial x}\right)\frac{\partial}{\partial y}\left(\frac{\rho h^3}{12\eta}\frac{\partial p}{\partial y}\right) - \frac{\partial\left(u_m \rho h\right)}{\partial x} - \frac{\partial(\rho h)}{\partial t} = 0 \tag{3.36}$$

In the case of a line contact, the contact dimensions in the y-direction are very large compared to those in the x-direction, so that the following simplified equation applies:

$$\frac{\partial}{\partial x}\left(\frac{\rho h^3}{12\eta}\frac{\partial p}{\partial x}\right) - u_m \frac{\partial h}{\partial x} = 0 \tag{3.37}$$

Here p is the pressure, h the film thickness, u_m the average surface speed, η the viscosity and ρ the density of the oil.

2. The elastic deformation equation describes the influence on the deformation of the oil gap.

To approximate the elastic deformations of real bodies, two assumptions are made: The deformation is linearly elastic and the two contact bodies have uniform and isotropic properties. The contact dimensions a are small compared to the dimensions of the body ($a << R_x$), so that the additional assumption of an approximation of the bodies by two semi-infinite half-spaces can be made.

Both hypotheses are generally valid and the obtained approximate values agree very well with experimental results. Thereby, the elastic deformation $h(x, y)$ according the pressure distribution $p(x, y)$ can be approximated by

$$h(x, y) = h_0 + \frac{x^2}{2R_x} + \frac{y^2}{2R_y} + \frac{2}{\pi E'}\iint_{-\infty}^{\infty} \frac{p(x', y')\mathrm{d}x'\mathrm{d}y'}{\sqrt{(x - x')^2 + (y - y')^2}} \tag{3.38}$$

For a line contact with a large contact length in the y-direction compared to that one in the x-direction, the equation can be simplified to

$$h(x) = h_0 + \frac{x^2}{2R_x} + \frac{2}{\pi E'} \iint_{-\infty}^{\infty} p(x') \ln \left(\frac{x - x'}{x_0} \right)^2 \mathrm{d}x' \tag{3.39}$$

3. The viscosity-pressure relationship describes viscosity as a function of pressure. The simplest form is known under the exponential approach of Barus:

$$\eta(p) = \eta_0 \cdot e^{(\alpha \cdot p)} \tag{3.40}$$

Here, η_0 is referred to as the atmospheric viscosity and α as the pressure viscosity coefficient.

4. The density-pressure relationship expresses the density as a function of pressure according to the approach of Dowson and Higginson:

$$\rho(p) = \rho_0 \frac{5.9 \cdot 10^8 + 1.34p}{5.9 \cdot 10^8 + p} \tag{3.41}$$

5. The principle of interaction means that the integral of the pressure distribution from the Reynolds equations must balance the externally applied load w in order to establish a balance of forces. For the 2D problem, this condition is

$$w = \iint_{-\infty}^{\infty} p(x', y') \, \mathrm{d}x' \mathrm{d}y' \tag{3.42}$$

w stands for the applied load in the 2D case. For the one-dimensional load case (line contact), the applied load is

$$w = \iint_{-\infty}^{\infty} p(x') \, \mathrm{d}x' \tag{3.43}$$

For both the 1D and the 2D problem, the local equations for describing pressure and film thickness distributions $p(x, y)$ and $h(x, y)$ are supplemented by the global Eqs. 3.42 and 3.43, so that the film thickness h_0 can be determined using the Eqs. 3.38 and 3.39 [10].

3.3 Combustion Chamber (Combustion and Thermodynamics)

The Science of Combustion is a discipline that deals with the physical and chemical processes of combustion and the different characteristics of flames. Its complexity results from the contact and interaction of many other fields of physics. Examples mentioned are fluid dynamics, thermodynamics, calorics, reaction kinetics, mechanics and more. If the aim is to simulate combustion, a chain of consecutive calculations and thus boundary conditions must be well predicted in order to make further reliable calculations.

Figure 3.7 illustrated the chamber of a cylinder. It is geometrically limited by the cylinder walls to the sides, the piston to the bottom and the valves (cylinder head) to the top. The complexity of the combustion process from the viewpoint of multiple physical and chemical processes all taking place in the cylinder gets very clear from this picture.

According to the law of conservation of mass, the change of mass in a control volume is always constant, which corresponds to the sum of all mass flows entering and leaving the volume:

$$dm = dm_{in} - dm_{out} + dm_{Fuel} - dm_{Blowby} \tag{3.44}$$

In their entirety, all the processes mentioned generate incoming and outgoing energy flows that can be summarized in an overall energy balance according to the first law of thermodynamics. Putting them into equilibrium results in the following differential function over time:

$$dU = dH + dQ_B - dQ_W - dW \tag{3.45}$$

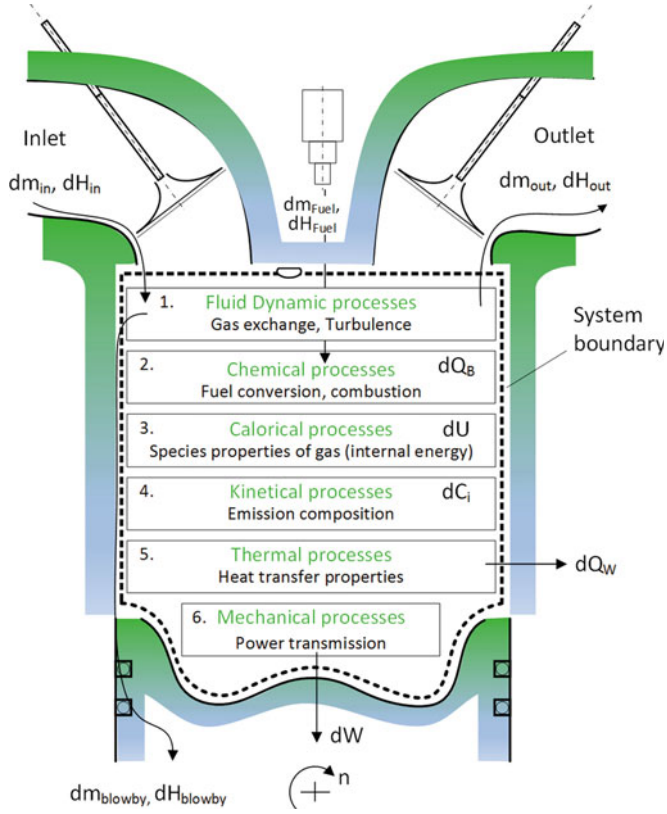

Fig. 3.7 Physical/chemical process sequences in a cylinder

U stands for the internal energy within the system boundaries, H for the supplied and removed enthalpy flows, Q_B for the released combustion energy, Q_W for the heat losses and W for the mechanical power output. If the enthalpy flow in the system boundary "combustion chamber" shown in the figure are resolved, the following results are obtained:

$$dU = dH_{in} - dH_{out} - dH_{blowby} + dH_{Fuel} + dQ_B - dQ_W - dW \tag{3.46}$$

For the temporal change of the internal energy during a working cycle, usually the differential from U is solved according to the crank angle, which results in the following term:

$$\frac{dU}{d\varphi} = h_{in}\frac{dm_{in}}{d\varphi} - h_{out}\frac{m_{out}}{d\varphi} - h_{out}\frac{dm_{Blowby}}{d\varphi} + h_{Fuel}\frac{dm_{Fuel}}{d\varphi} + \frac{dQ_{Fuel}}{d\varphi} - \frac{dQ_W}{d\varphi} - \frac{dW}{d\varphi} \tag{3.47}$$

In the following sections, all six physical processes are discussed in sequence according to Fig. 3.7 and their theoretical foundations are presented.

1. Fluid dynamics (dH): During the charge exchange, the calculation basis of fluid dynamics is used to determine the mass flow of fresh air (in case of direct injection) or fuel-air mixture (in the case of mixture intake) into the cylinder. In addition to the pressure gradient between the inlet channel and the cylinder chamber, it is crucial that the pulsations of the inlet pressure are composed in such a way that there is a pressure peak during the opening phase of the inlet valve, thus promoting better filling. The basics of fluid dynamics for this were presented in Chap. 3.1. A change of enthalpy dH that is fed to or discharged from a system is basically obtained from the specific heat capacity c_p, the mass m and the temperature difference $dT = (T_{out} - T_{in})$ [5].

$$dH = c_p \cdot m \cdot dT \tag{3.48}$$

2. Chemical processes (dQ_B): The introduction of a fuel into the combustion chamber and the conversion of its bound chemical energy into heat follows in this process step. The ignition of the fuel-air mixture can be effected externally by a spark plug (petrol engine) or self-ignition (diesel engine) or by one of many alternative combustion processes such as compressed auto ignition (CAI) or homogeneous charge compressed ignition (HCCI).

The burning speed and thus the time needed to convert the chemical energy of the fuel are very decisive. Typically, one tries to make it as quick as possible, since the highest thermodynamic efficiency can be achieved with an early center of combustion ($\sim 6° - 8°$ crank angle). To achieve this, a high level of turbulence is required by the end of the gas exchange phase.

Engine power, efficiency and emissions are controlled by the combustion of the fuel-air mixture. In order to understand the engine operation in its entirety, many individual building blocks are required for relevant combustion phenomena. The phenomena differ for the main engine type spark ignition and diesel. In gasoline engines, the fuel is either mixed with air

in the engine intake system or injected directly into the cylinder. After compression of the fuel-air mixture, an electrical discharge of the spark plug triggers the combustion process. The ignition spark develops into a flame which spreads into the cylinder space until it reaches the walls of the combustion chamber on the sides or the piston downwards and extinguishes. An undesirable phenomenon that occurs is the spontaneous or uncontrolled self-ignition of a significant portion of the fuel-air mass before it is ignited by the flame. The explosive phenomenon is the cause of engine knocking, which can lead to engine damage due to the high pressures generated.

In diesel engines, the fuel is injected into the cylinder at high pressure and high temperature. The self-ignition of parts of the developing mixture of already injected and vaporized fuel with the hot air initiates the combustion process. Unlike the gasoline engine, this process is turbulent. The composition of the fuel-air mixture therefore plays a decisive role in diesel combustion.

The composition of fuel and air is called stoichiometry and describes the reactants of a combustible mixture and the composition of the products. Since the relationships depend on the conservation of the mass of each chemical element of the reactants, the relative compositions of the fuel and the fuel/air ratio are used as the basis for calculation. If sufficient oxygen is available, a hydrocarbon fuel can completely oxidize. The carbon in the fuel is then converted into carbon dioxide CO and the hydrogen H_2 into water H_2O [5].

For a fuel with the composition $C_xH_yS_qO_z$, the following reaction takes place in the case of complete conversion:

$$C_xH_yS_qO_z + \left(x + \frac{1}{4}y + q - \frac{1}{2}z\right) \cdot O_2 = xCO_2 + \frac{y}{2} \cdot H_2O + qSO_2 \tag{3.49}$$

with the stoichiometric coefficients and the mass fractions of the elements carbon c, hydrogen h, sulfur s and oxygen o contained in the fuel:

$$x = \frac{M_B}{M_C}c,\ y = \frac{M_B}{M_H}h,\ q = \frac{M_B}{M_S}s,\ z = \frac{M_B}{M_O}o \tag{3.50}$$

The stoichiometric air requirement leads to

$$L_{st} = \frac{1}{x_{O_{2,L}}} \cdot \frac{m_{O_{2,st}}}{m_B} = \frac{1}{x_{O_{2,L}}} \left(\frac{M_{O_2}}{M_C} \cdot \frac{1}{4}\frac{M_{O_2}}{M_H} \cdot h + \frac{M_{O_2}}{M_S} \cdot s - o\right) \tag{3.51}$$

$$= \frac{1}{0.232} \cdot (2.664 \cdot c + 7.937 \cdot h + 0.998 \cdot s - o)$$

For an engine combustion, the ratio of actual air mass m_L is related to the stoichiometric air mass $m_{L,st}$ and expressed the air ratio λ:

$$\lambda = \frac{m_L}{m_{L,st}} = \frac{m_L}{m_B} \cdot L_{st} \tag{3.52}$$

The mixing heating value H_G of air and fuel is composed of the fuel mass m_B. In case of external mixture formation (naturally aspirated engine), the lower fuel heating value H_u and the mixture volume V_G are applied in the following equation:

$$H_G = \frac{m_B \cdot H_u}{V_G} = \frac{\rho_G \cdot H_u}{\lambda \cdot L_{st} + 1} \tag{3.53}$$

For engines with internal mixture formation (diesel engines, DI gasoline engines), the fuel mass and the lower heating value are related to the air volume V_L:

$$H_G = \frac{m_B \cdot H_u}{V_L} = \frac{\rho_L H_u}{\lambda L_{st}} \tag{3.54}$$

3. Caloric processes (dU): After the flow-relevant processes of the gas exchange and the chemical processes of the fuel have been discussed, the next sequence according to Fig. 3.7 is followed by the determination of the caloric content. This deals with the material properties of the working gas and is ultimately used to determine the internal energy U within the system boundaries of the combustion chamber and to calculate the term dU from the energy balance according to Eq. 3.45 [5].

A possible approach to the calculation of the internal energy U lies in the description of the individual components of a gas mixture and can be described as

$$dU = \sum_i m_i du_i = \sum_i m_i d(h_i - RT_i) \tag{3.55}$$

The best known approaches to describing the specific internal energy of flue gas, i.e. the combustion products, were developed by Justi in 1938 and Zach-arias in 1968 [11, 12]. Neglecting dissociation effects, i.e. backward reactions of already formed species, and the pressure dependence of reactions, Justi presented a polynomial approach, which represents the specific internal energy as a function of temperature and air ratio. Zacharias' approach made it possible to determine the flue gas more precisely by breaking it down into its components, an approach that could only be overcome with the use of the first mainframe computers.

The internal energy of each gas component can be calculated separately, since its standard enthalpies of formation, reaction enthalpies and the respective molar heat are given in tables as in NIST JANAF [13]. By knowing the respective proportions of these individual components, the total internal energy of a gas can be calculated.

Typical gases emitted by an internal combustion engine such as oxygen, nitrogen, fuel vapor, carbon dioxide and water vapor may be considered ideal, described by the following equation:

$$pV = mRT = n\tilde{R}T \tag{3.56}$$

where p is pressure, V volume, m gas mass, $\tilde{R}$ universal gas constant, T temperature and n molar mass.

Considering the cylinder charge, an ideal gas, the specific heat capacity, and enthalpy and entropy for any reaction can be determined according to the following formulas:

$$\frac{\tilde{c}}{\tilde{R}} = a_1 + a_2 T + a_3 T^2 + a_4 T^3 + a_5 T^4 \tag{3.57}$$

$$\frac{\tilde{h}}{\tilde{R}T} = a_1 + \frac{a_2}{2} T + \frac{a_3}{3} T^2 + \frac{a_4}{4} T^3 + \frac{a_5}{6} T^4 + \frac{a_6}{T} \tag{3.58}$$

$$\frac{\tilde{s}}{\tilde{R}} = a_1 \cdot lnT + a_2 T + \frac{a_3}{2} T^2 + \frac{a_4}{3} T^3 + \frac{a_5}{4} T^4 + a_7 \tag{3.59}$$

4. Kinetic processes (dC_i): Kinetics is a subarea of physical chemistry and deals with the time sequence of chemical reactions or physical-chemical processes. It can generally be divided into the subareas of micro- and macrokinetics. While microkinetics is mainly concerned with the time sequence of chemical reactions and their mathematical description, macrokinetics takes global influences of thermodynamics as well as heat and mass transport processes (diffusion) into account.

In the application for the internal combustion engine and the area of simulation, reaction kinetics is particularly relevant, since it ensures the calculation basis for many fundamental processes. These include influences of different fuel types on the chemical processes in the combustion chamber (including combustion speed and knock resistance), the generation of raw emissions and catalytic processes of exhaust gas aftertreatment [5].

Reaction speed

A chemical reaction with the educts A and B, which form the products C and D, is described according to the following formalism:

$$\alpha \mathrm{A} + \beta \mathrm{B} + \gamma \mathrm{C} \underset{k_{1,r}}{\overset{k_{1,v}}{\rightleftharpoons}} \delta \mathrm{D} + \varepsilon \mathrm{D} \tag{3.60}$$

α, β, γ, δ and ε represent the stoichiometric coefficients of the reaction, and k_f and k_r describe the reaction rate of the forward and backward reactions, respectively. The temporal change of a species concentration (taking component A as an example) can be determined for the given chemical reaction equation with the following empirical approach:

$$\frac{dC_A}{dt} = \alpha \left(k_f [\mathrm{A}]^{\alpha} \cdot [\mathrm{B}]^{\beta} \cdot [\mathrm{C}]^{\gamma} - k_r [\mathrm{D}]^{\delta} \cdot [\mathrm{E}]^{\varepsilon} \right) \tag{3.61}$$

The reaction rate k_f and k_r are experimentally determined quantities, which are summarized in extensive tables for all chemical reactions. The measurements originate from experiments in shock wave reactors or similar. Since they are also strongly temperature-dependent, they are corrected using an Arrhenius approach:

$$k = A \cdot T^b \cdot e^{-\frac{E_A}{R \cdot T}} \tag{3.62}$$

In particular, the speed of the reaction depends on the activation energy E_A, which must be applied to initiate the reaction, and the absolute temperature T. For very high temperatures, the term converges against the pre-exponential factor AT^b. In this case, the velocity is described by the shock kinetics of the molecules. The constant A, the temperature coefficient b and the activation energy E_A can also be taken from tables.

Reaction equilibrium

At the molecular level, a chemical reaction always takes place in two directions. From the difference between the forward and backward reactions, it is possible to draw conclusions about the direction of the reaction. The chemical equilibrium is therefore only a special case in which the forward and backward reactions take place at the same speed, so that macroscopically no visible conversion of substances occurs. On the molecular level, however, reactions continue to take place. Although the macroscopic reaction rate always aims at the chemical equilibrium, equilibrium analysis does not provide information about the time required to reach this state. Information on this is provided by the reaction kinetics.

If one takes into account that in the special case of a chemical equilibrium the reaction proceeds equally fast in both directions, the conversion rate of the concentrations of the individual species becomes zero. Eq. 3.61 results in

$$0 = \alpha \left(k_f \cdot [\mathrm{A}]^\alpha \cdot [\mathrm{B}]^\beta \cdot [\mathrm{C}]^\gamma - k_r \cdot [\mathrm{D}]^\delta \cdot [\mathrm{E}]^\varepsilon \right) \tag{3.63}$$

When transforming the equation as the ratio between forward and backward speed,

$$\rightarrow \frac{k_f}{k_r} = \frac{[\mathrm{D}]^\delta \cdot [\mathrm{E}]^\delta}{[\mathrm{A}]^\alpha \cdot [\mathrm{B}]^\beta \cdot [\mathrm{C}]^\gamma} = K_c \tag{3.64}$$

K_c is a function of the molar concentration of all involved species and is called equilibrium constant.

In order to get an idea of the equilibrium composition of a combustion, an example of octane with the chemical formula C_8H_{18} is given next. According to Burcat, the equilibrium composition of the combustion products and their dependence on the air ratio λ, the temperature and the process pressure is shown (Fig. 3.8).

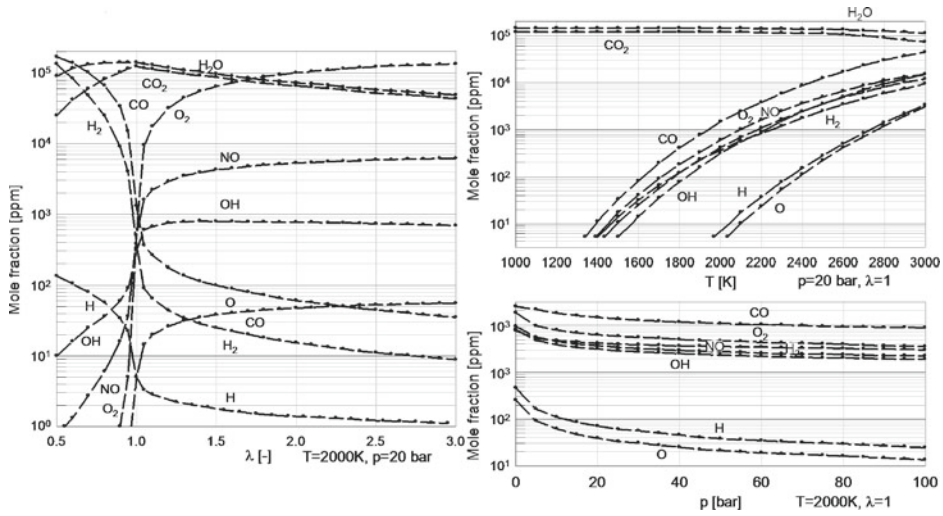

Fig. 3.8 Exhaust gas equilibrium composition for C_8H_{18} fuel according to Burcat. Representation of the dependencies of air/fuel ratio, temperature and pressure

Reaction order

Looking at the reaction equation from 3.65–3.67, this literally means that on the reactant side a number α of A particles collide with β numbers of particles B and γ number of particles C to form D and E on the product side. The probability that the three particles A, B and C collide at the same time and with sufficiently high kinetic energy is very low. It is more likely that two particles first collide, forming an intermediate product and then, if necessary, forming further intermediates to finally form the products D and E. If the overall reaction is broken down into individual steps, their elementary reactions result as follows:

$$\alpha\mathrm{A} + \beta\mathrm{B} \rightarrow \mathrm{A}_\alpha\mathrm{B}_\beta \tag{3.65}$$

$$\mathrm{A}_\alpha\mathrm{B}_\beta + \gamma\mathrm{C} \rightarrow \mathrm{D} \tag{3.66}$$

$$\mathrm{A}_\alpha\mathrm{B}_\beta + \mathrm{D} \rightarrow \mathrm{E} \tag{3.67}$$

Experimentally, it can be determined how the reaction rates of the elementary reactions depend on the respective concentrations of the components A, B, C and D. The dependence of the reaction rate on the exponent, with which the concentration of a certain reactant enters into the law of rates, is called reaction order of the respective reactant. The overall order of a reaction is the sum of the reaction orders of all reactants involved in it. The reaction rate of the individual elementary reactions are multiplied together to give the rate of the total reaction.

Partial balance

In a complex reaction system, it can happen that a large number of reactions take place simultaneously, only some of which proceed so quickly that one can speak of a partial equilibrium of this particular species. The reaction as a whole does not necessarily have to be in chemical equilibrium.

In 1946, Y.B. Zeldovich presented the elementary reaction of nitrogen oxide production for the first time. These describe the formation of thermal nitrogen oxide (NO), which in combustion engines accounts for the largest proportion of all total nitrogen oxides ($\sim$ 90–95% of all NO_x).

$$N_2 + \dot{O} \underset{k_{1,r}}{\overset{k_{1,v}}{\rightleftharpoons}} NO + \dot{N} \tag{3.68}$$

$$\dot{N} + O_2 \underset{k_{2,r}}{\overset{k_{2,v}}{\rightleftharpoons}} NO + \dot{O} \tag{3.69}$$

$$\dot{N} + OH \underset{k_{3,r}}{\overset{k_{3,v}}{\rightleftharpoons}} NO + \dot{H} \tag{3.70}$$

Using a gasoline engine combustion process at stoichiometric condition ($\lambda = 1$), the species concentrations over time are examplarily shown below. After the ignition timing and the corresponding increase of the process temperature $T > 2500\,\mathrm{K}$, the reactions get activated. The graph shows that the components O and OH are intermediate products that are formed for a short time and then suddenly decomposed again. The partial equilibrium can be represented to determine the species concentration: $dC_O/dt = 0$, $dC_{OH}/dt = 0$ (Fig. 3.9).

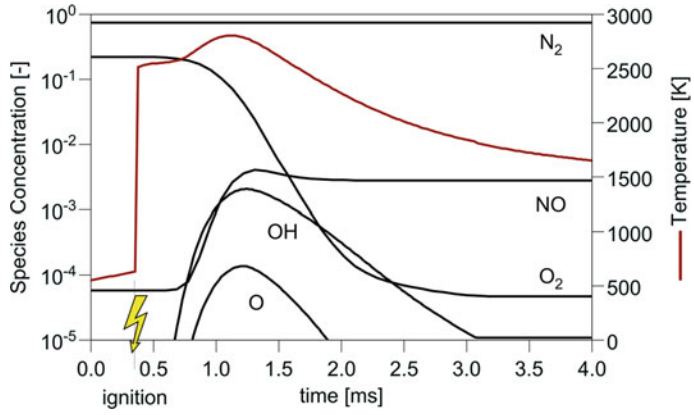

Fig. 3.9 Partial equilibrium using the example of the extended Zeldovich mechanism (nitrogen oxide formation) for the components O and OH

5. Thermodynamics dQ_W: The description of the heat transfer in the cylinder is subject to complex interrelationships. Due to the relatively large proportion and losses that occur on the thermal processes, it is of constant interest to reproduce them with high accuracy on the basis of models in order to identify potential for improvement. The additional difficulty in modeling the thermal process is that a number of consecutive processes as for the charge exchange (fluid dynamic processes), combustion process (chemical processes), internal energy (caloric processes) and kinematics, each introduces an individual error which adds up to an exponential error (looking back to Fig. 3.7). Finally, the summed error has a decisive influence on the calculation of the thermal behavior, so that an accurate prediction becomes a great challenge.

In principle, the heat transfer through the walls Q_w is composed of a convective component Q_e and a radiation component Q_ε:

$$dQ_w = dQ_e + dQ_\varepsilon \tag{3.71}$$

Usually, the radiation part is added to the convective part and is found in the heat transfer coefficient α. The combustion chamber is usually divided at least into three different areas: 1. piston, 2. liner and 3. cylinder head. To achieve a higher quality of resolution, theoretically more sections up to infinitesimal elements can be selected. The valves are usually added to the cylinder head. The description of the heat flow through the cylinder walls follows Newton's equation using the heat transfer coefficient α_i, the transfer area A_i and the temperature difference between the cylinder wall T_w and the gas T_{gas}:

$$dQ_w = \sum_i \alpha_i A_i \left(T_{w,i} - T_{gas,i}\right) \tag{3.72}$$

The determination of a suitable heat transfer coefficient presupposes that the gas temperature in the combustion chamber as well as the wall temperatures are very well represented. For 3D-CFD simulations, it is usual to determine temperature distributions of the burned and unburned gas to different cells i ($T_{gas,i}$) over the entire combustion chamber. In 1D, however, the combustion is determined quasi-dimensionally, so that the mean gas temperature is calculated from the local averaging of the gas temperature in the combustion chamber and the index i is omitted (T_{gas}) [5].

For this purpose, usually semi-physical approaches are used, which provide a fast prediction and, at the same time, take into account a sufficiently high degree of boundary conditions. In the literature, there is a large number of presented approaches for the calculation of the heat transfer through the walls [14–17].

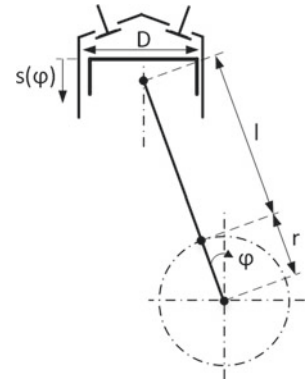

Fig. 3.10 Geometry of the crank mechanism

6. Kinematic processes dW: The mechanism of an engine converts the oscillating motion of the pistons into a rotating motion of the crankshaft (Fig. 3.10). The work dW converted at the piston can be determined through the cylinder pressure and the volume change [5]:

$$dW = -pdV \tag{3.73}$$

Resolving for the crank angle, the work can be derived from the following term. This requires additional inputs as the angular frequency ω, the cylinder bore diameter D and the piston stroke s:

$$\frac{dW}{d\varphi} = -p\omega\frac{dV}{d\varphi} = -p\omega D^2\frac{\pi}{4}\frac{ds}{d\varphi} \tag{3.74}$$

The piston stroke is directly related to the crank angle. The term $\frac{ds}{d\varphi}$ can be calculated as a function of the crank radius r and the conrod ratio $\lambda_s = \frac{r}{l}$:

$$s(\varphi) = r \cdot [[1 - cos\varphi] + \frac{1}{\lambda} \cdot [1 - \sqrt{1 - \lambda_s \cdot sin^2(\varphi)}]] \tag{3.75}$$

$$\frac{ds}{d\varphi} = r\omega \cdot [sin\varphi + \frac{\lambda_s}{2}sin(2\varphi)] \tag{3.76}$$

3.4 Material Strength and Structure

Multi-body simulation

Multi-body simulation (MBS) is a method of numerical simulation, in which simple as well as complex multi-body systems are considered, which are composed of individual components. The composition is realized by simple, rigid or elastic bodies, which are connected by joints, springs, dampers or other contact connections. The MBS is a very useful tool for motion analysis with special focus on the interactions between single components. This enables the

determination of loads that result as a consequence of superimposed loads and mass inertia of a system. These loads are used for the early detection of deformations and stresses. New and fast designs of modified kinematics finally help to find optimized solutions. Frequently, MBS tools are used during product development to evaluate the characteristics of safety, comfort, durability and performance.

Basically, the MBS is divided into kinematic and dynamic calculations. In a kinematic view, the systems have no dynamic degrees of freedom. Since the change over time is insignificant here, stationary observations are sufficient to evaluate these. For more complex problems, on the other hand, it is often not sufficient to regard bodies as rigid in order to meet higher accuracy requirements. In this respect, the structural elasticity of the components is included, so that additional, deformation-induced stresses are taken into account. A more detailed representation of a rigid MBS can be realized by integrating additional simulation methods such as the finite element method (FEM), flow simulation (CFD) and thermodynamics. Along with minor additional modeling effort and corresponding higher computational effort, the predictions are much more accurate over deformations, dynamics and stresses of components.

Finite Elemente

Finite Element Analysis (FEM) is a numerical calculation method for the investigation of the strength and deformation of bodies with static and dynamic load conditions. FEM has become widely accepted in the development of mechanical components for industrial applications over the last decades and is indispensable today. In the application of Finite Element Analysis (FEA) software, CAD-manufactured components are imported and divided into a multitude of small finite units (mesh). If the investigation of a load on critical zones of a body is of high interest, these selected areas are resolved higher than others, so that detailed results can be obtained. Depending on the choice of the resolution (shape function) of the smallest volume elements (tetrahedron, hexahedron, octahedron, etc.), deeper insights into the structural behavior can be obtained at the expense of more computational time.

The application possibilities of FEM have expanded massively, especially in the last few years, thanks to the availability of high-performance computers. This allows to increasingly investigate coupled problems, such as the combination with multi-body systems and the interaction between structures and fluids from (CFD), acoustics, thermomechanics, thermochemistry, ferroelectrics, electromagnetics and other relevant areas. FEM applications are basically divided into static, dynamic and modal problems. With the help of static analyses, linear static and nonlinear quasi-static structures can be analyzed. With a dynamic analysis, however, oscillating or unsteady loads of components can be analyzed with respect to their structure. Modal analysis is used when the focus is on determining the eigenfrequencies of a structure through vibration excitation and the prevention of undesired interference.

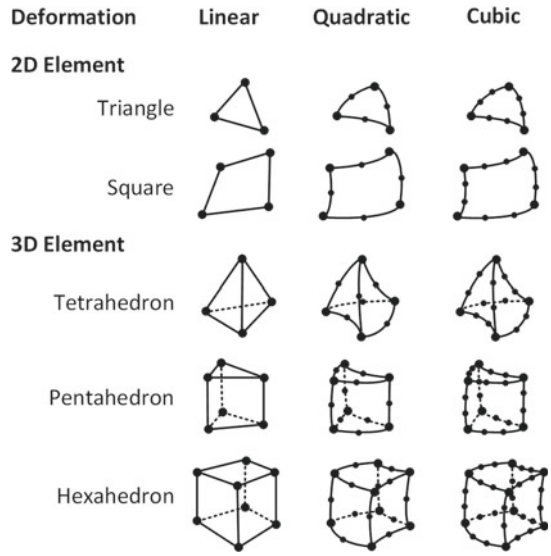

Fig. 3.11 2D and 3D finite elements with linear, quadratic and cubic deformation

In order to examine bodies of any kind with corresponding materials and arbitrary fields of application for load, deformation and durability, they are divided into finite elements for an FEM investigation. This results in a so-called "mesh" of the body. The finer the mesh is divided into finite (finitely small) elements, the higher the resolution of the results, which is directly related to a higher calculation effort. Due to their effectiveness, triangular and quadrangular elements have become widespread for conventional software for 2D surfaces. For 3D bodies, on the other hand, tetrahedral, pentahedral and hexahedral elements as shown in Fig. 3.11 are used. If the deformation of bodies is to be calculated in addition to the load, quadratic or cubic volumes can be selected.

Figure 3.12 shows on a 2D connection beam what a possible transformation of a body into finite elements can look like. The element is fixed to the left and the bottom side. A meshing is exemplarily done with triangular elements (quadratic) with a coarse mesh (center) and a finer mesh (right).

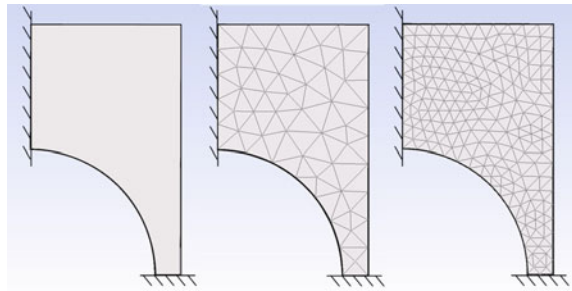

Fig. 3.12 Finite element for a 2D surface with a large and a small mesh size

FEM mainly deals with the solution of boundary value problems. Boundary value problems are problems for which solutions are sought for a given differential equation so that certain conditions arise at the boundaries of the corresponding defined range. Basically, two different methods can be chosen, the application of a force balance or the that of an energy balance. In conventional FEM simulation tools, both methods are provided. Hence, the plausibility of the boundary conditions of an approach selected at the beginning can be checked afterwards by means of an energy balance approach.

In principle, FEM methods can be used to analyze mechanical stress, thermal stress or examine electrical and magnetic flux over solids. The process of an FEM analysis always follows one scheme:

- Definition of a boundary value problem (2D, 3D boundary conditions);
- Creating a model (importing a CAD file);
- Definition of all loads (static or dynamic load);
- Meshing of the model (resolution of the cells, linear, quadratic or cubic deformation);
- Definition of the analysis method (force balance, energy balance).

After a component has been divided into small finite elements, the balances of forces are established at each element and the equations of elasticity theory are applied.

3.4.1 Theory of Elasticity

Using a section of a cubic volume, which in its deformed state corresponds to a hexahedron, all relevant forces and stresses are shown. The normal stresses, which are perpendicular to the squared surfaces, are called $\sigma_x, \sigma_y, \sigma_z$. The shear stresses pointing in the surface direction are called $\tau_{xy}, \tau_{yz}, \tau_{xz}$. Together with the acting forces f_x, f_y, f_z on the volume, the system can be defined and set up as a boundary value problem.

As a result of the elasticity of a body, the forces acting on a volume element lead to deformation and thus to a displacement of the geometry. The determination of the displacement of the individual volumes and hence of the sum of all volume elements forming a body is the actual focus of each FEA calculation. Four steps of the theory of elasticity can be summarized to determine deformations:

1. The force and momentum balance;
2. The strain-displacement relation $\varepsilon - u$ and the material constancy;
3. The stress-strain relation $\sigma - \varepsilon$;
4. Boundary value problem and displacement function u(x);
5. Determining the stiffness matrix [k] and displacement vector {d}.

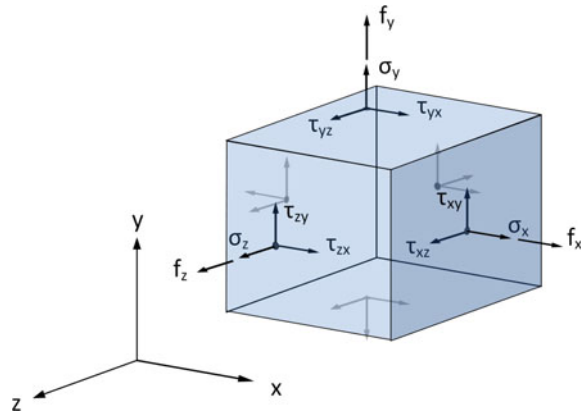

Fig. 3.13 Force balance on a body

1. Force and momentum balance

If one sets up the equations for the equilibrium of forces and moments according to Fig. 3.13, a total of 6 differential equations and 9 unknown quantities (τ_{xy}, $\tau_{yz}\tau_{xz}$, $\tau_{zx}\tau_{yx}$, τ_{zy}, σ_x, σ_y, σ_z) are obtained. The boundary value problem assumes that the forces f_x, f_y, f_z acting on the volume are known. Balance of power:

$$0 = f_x + \frac{\partial \sigma_x}{\partial x} + \frac{\partial \tau_{yx}}{\partial y} + \frac{\partial \tau_{zx}}{\partial z} \quad (1)$$

$$0 = f_y + \frac{\partial \sigma_y}{\partial y} + \frac{\partial \tau_{xy}}{\partial x} + \frac{\partial \tau_{zy}}{\partial z} \quad (2)$$

$$0 = f_z + \frac{\partial \sigma_z}{\partial z} + \frac{\partial \tau_{xz}}{\partial x} + \frac{\partial \tau_{yz}}{\partial y} \quad (3)$$

Equilibrium of moments:

$$\tau_{xy} = \tau_{yx} \quad (4)$$

$$\tau_{yz} = \tau_{zy} \quad (5)$$

$$\tau_{xz} = \tau_{zx} \quad (6)$$

Equations (4), (5) and (6) ensure that 3 of the stress variables are eliminated, leaving 3 differential equations (1), (2), (3) and the 6 unknown variables (τ_{xy}, τ_{yz}, τ_{xz}, σ_x, σ_y, σ_z).

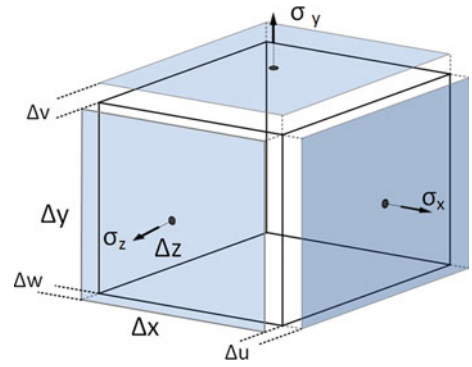

Fig. 3.14 Deformation of a body

2. The strain-displacement relation $\varepsilon - u$ and material constancy

If forces act on a body, a deformation occurs in the direction of the applied force. The deformation is approximately defined as the ratio between the deformation length δu and the total length δx, as shown in Fig. 3.14. Looking at an infinitesimal volume element, the strain can be represented as a partial derivative. This results in 3 new differential equations with 6 unknown quantities, namely the 3 strain quantities (ε_x, ε_y, ε_z) and the 3 deformation variables (u, v, w).

$$\varepsilon_x = \frac{\partial u}{\partial x} \quad (7)$$

$$\varepsilon_y = \frac{\partial v}{\partial y} \quad (8)$$

$$\varepsilon_z = \frac{\partial w}{\partial z} \quad (9)$$

In addition to the deformation, there is also an angular deformation of the volume element as a result of the acting forces, if the volume is not fixed at the edges. In Fig. 3.15, a volume element is fixed at the lower left edge (A-B). If the normal stress σ_x, σ_y, σ_z act on the body, the body deforms with the angle φ_1 due to σ_y, with φ_2 due to σ_x and φ_3 due to σ_z. From this, 3 differential equations for the shear deformations γ_{xy}, γ_{yz}, γ_{xz} can be set up, which result from the forces in the plane.

$$\gamma_{xy} = \varphi_1 + \varphi_2 + \frac{\partial v}{\partial x} + \frac{\partial u}{\partial y} \quad (10)$$

$$\gamma_{yz} = \varphi_2 + \varphi_3 + \frac{\partial u}{\partial y} + \frac{\partial w}{\partial y} \quad (11)$$

$$\gamma_{xz} = \varphi_1 + \varphi_3 + \frac{\partial v}{\partial x} + \frac{\partial w}{\partial y} \quad (12)$$

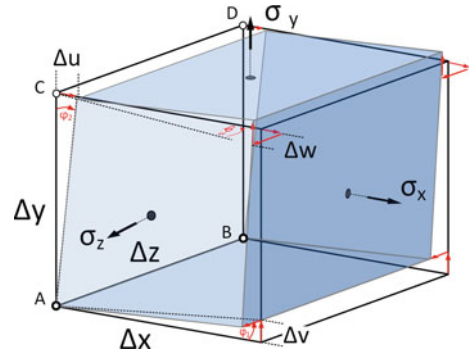

Fig. 3.15 Shear deformation of a body

For practical reasons, the strain variables and shear stresses are combined in a strain vector as shown in Eq. 3.77. The partial derivatives of the deformations are separated from each other on the right side of the equation and divided into a partial derivative operator matrix and deformation vector.

$$\underbrace{\begin{pmatrix} \varepsilon_x \\ \varepsilon_y \\ \varepsilon_z \\ \gamma_{xy} \\ \gamma_{yz} \\ \gamma_{xz} \end{pmatrix}}_{strain\ vector} = \underbrace{\begin{pmatrix} \frac{\partial}{\partial x} & 0 & 0 \\ 0 & \frac{\partial}{\partial y} & 0 \\ 0 & 0 & \frac{\partial}{\partial z} \\ \frac{\partial}{\partial y} & \frac{\partial}{\partial x} & 0 \\ 0 & \frac{\partial}{\partial z} & \frac{\partial}{\partial y} \\ \frac{\partial}{\partial z} & 0 & \frac{\partial}{\partial x} \end{pmatrix}}_{operator\ matrix} \cdot \underbrace{\begin{pmatrix} u \\ v \\ w \end{pmatrix}}_{deformation\ vektor} \tag{3.77}$$

The relationship between strain and displacement can be summarized in the vectorial notation $\varepsilon = [\partial] \cdot u$. In total, this relationship results in 9 unknown quantities ($\varepsilon_x, \varepsilon_y, \varepsilon_z, \gamma_{xy}, \gamma_{yz}, \gamma_{xz}, u, v, w$) and 6 differential equations.

3. The stress-strain relation $\sigma - \varepsilon$

The stress-strain behavior is represented by Hooke's law, which describes a linear relationship between the stress σ and the strain ε by the modulus of elasticity E. By definition, the law applies to materials only in the linear elastic range. As soon as plastic deformation occurs, the physical phenomena behind this follow much more complex laws:

$$\sigma = E \cdot \varepsilon \tag{3.78}$$

Another important material constant comes into play through the Poisson number ν, which is a measure of lateral contraction. The Poisson effect follows the law of material continuity, as it describes the tendency of a material to expand perpendicular to the compression direction. On the other hand, when a material is stretched, it tends to contract transversely to the stretched direction.

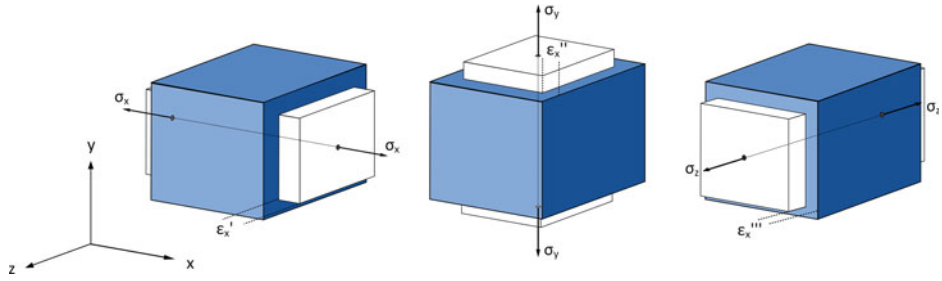

Fig. 3.16 Transversal contraction of a body

Figure 3.79 shows how a body expands in the linear-elastic range under consideration of the transverse contractions when it is exposed to a normal stress. When force is applied in the x-direction, the body expands by the strain ratio $\varepsilon'_x = \frac{\sigma_x}{E}$, when force is applied in the y-direction, it contracts by $\varepsilon''_x = -\nu\frac{\sigma_y}{E}$ and when force is applied in the z-direction, it contracts by $\varepsilon'''_x = -\nu\frac{\sigma_z}{E}$. The total contraction of a body in the x-direction is composed of the individual strains (Fig. 3.16):

$$\varepsilon_x = \varepsilon'_x + \varepsilon''_x + \varepsilon'''_x \tag{3.79}$$

If one proceeds equally for the coordinates y and z, the transverse contraction can be described as follows:

$$\varepsilon_x = \frac{1}{E}\left[\sigma_x - \nu\left[\sigma_y + \sigma_z\right]\right] \quad (13)$$

$$\varepsilon_y = \frac{1}{E}\left[\sigma_y - \nu\left[\sigma_x + \sigma_z\right]\right] \quad (14)$$

$$\varepsilon_z = \frac{1}{E}\left[\sigma_z - \nu\left[\sigma_x + \sigma_y\right]\right] \quad (15)$$

Similarly, the shear deformations γ can be related to the shear stresses τ, which results in 3 further equations:

$$\gamma_{xy} = \frac{\tau_{xy} \cdot 2\,(1+\nu)}{E} \quad (16)$$

$$\gamma_{yz} = \frac{\tau_{yz} \cdot 2\,(1+\nu)}{E} \quad (17)$$

$$\gamma_{xz} = \frac{\tau_{xz} \cdot 2\,(1+\nu)}{E} \quad (18)$$

For practical reasons, the vectorial notation is often used here as well:

$$\begin{pmatrix} \sigma_x \\ \sigma_y \\ \sigma_z \\ \tau_{xy} \\ \tau_{yz} \\ \tau_{xz} \end{pmatrix} = \begin{pmatrix} \frac{1-\nu}{1-2\nu} & \frac{\nu}{1-2\nu} & \frac{\nu}{1-2\nu} & 0 & 0 & 0 \\ 0 & \frac{1-\nu}{1-2\nu} & 0 & 0 & 0 & 0 \\ 0 & 0 & \frac{1-\nu}{1-2\nu} & 0 & 0 & 0 \\ 0 & 0 & 0 & \frac{1}{2} & 0 & 0 \\ 0 & 0 & 0 & 0 & \frac{1}{2} & 0 \\ 0 & 0 & 0 & 0 & 0 & \frac{1}{2} \end{pmatrix} \cdot \begin{pmatrix} \varepsilon_x \\ \varepsilon_y \\ \varepsilon_z \\ \gamma_{xy} \\ \gamma_{yz} \\ \gamma_{xz} \end{pmatrix} \tag{3.80}$$

The stress-strain ratio can be represented in the vectorial notation: $\{\sigma\} = [D]\{\varepsilon\}$. The matrix $[D]$ is a characteristical material matrix or also called the elasticity matrix.

By the laws of stress-strain relations, 6 further equations without additional unknowns are created. Together with the equilibrium of forces and momentums from (1.) and the ratio between strain and deformation from (2.), a total of 18 equations with 18 unknown variables are combined, so that a solvable system of equations results and finally the displacement vector $\{d\}$ can be solved.

4. Boundary value problem and displacement function *u(x)*

To solve the differential equation, an assumption about the displacement field has to be made. Typically, linear displacement fields are assumed for beam elements with a function $u(x) = a_0 + a_1 \cdot x$, see Fig. 3.17. In a mesh, common FEA software offer several possibilities for selection. Using a hexahedron as an example, it is shown that a linear approach, a quadratic, a cubic or a function of a higher order is possible in principle. However, when the order increases, the operations and thus the calculation time increase exponentially as a resulting effect.

5. Determination of the stiffness matrix [*k*] and displacement vector {*d*}

After having defined boundary values for the deformation of all cells in (4.), the last step is to determine the displacement of the nodes for a finite element and, in summary, the displacement of all nodes of an overall system consisting of many finite elements.

If we consider a 2D finite element with a rectangular profile and a linear displacement function (see Fig. 3.17), which is loaded with the forces F_x and F_y, all nodes are shifted by the displacement vector $\{d_i\}$.

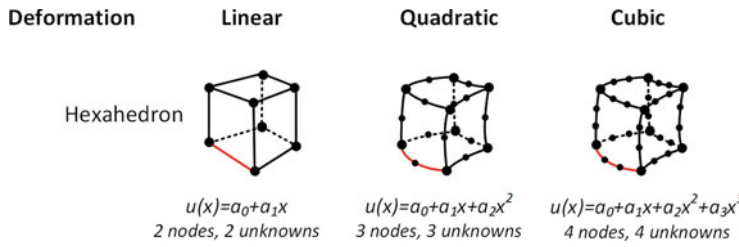

Fig. 3.17 Number of nodes per body edge by a displacement function

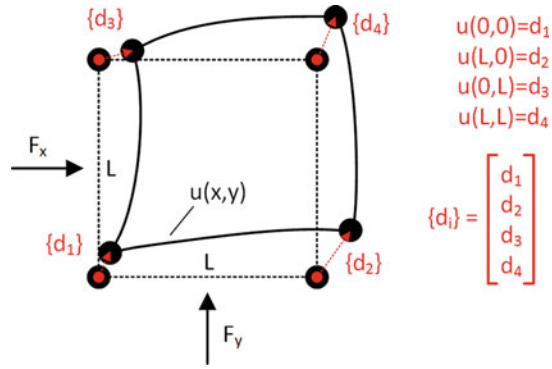

Fig. 3.18 Displacement of all nodes of a body represented by the displacement vector $\{d_i\}$

Together with the stiffness matrix $[k]$, the system of linear equations represents a simplified relationship between loads and displacements in each element for a node i, which must be solved to obtain an approximate solution of the differential equations (1)–(18):

$$\{f\}_i = [k]_i \cdot \{d\}_i \tag{3.81}$$

Finally, the law of continuity is applied to the entire system. This ensures that loads and displacements are connected between all elements and that there is no material gap or overlap within a system:

$$\{F\} = [K] \cdot \{D\} \tag{3.82}$$

The solution of the nodal displacement is found by inverting the matrix solving the equation for $\{D\}$:

$$\{D\} = [K]^{-1} \cdot \{F\} \tag{3.83}$$

Once the displacement vector $\{D\}$ has been determined, all stresses (normal stresses and shear stresses) as well as strains and shear deformations can be determined in each element node by means of the equations presented above [18].

3.4.2 Alternative Methods

In addition to the presented method of solving a boundary value problem by means of the balance of forces, alternative possibilities are also available. The most popular ones are the energy method (Minimal Potential Theory), the principle of virtual work or the Rayleigh-Ritz approximation. In the following, the example of the minimal potential theory is used to show how an identical problem can be solved by applying an energy balance [19].

Minimal Potential Theory

If a body is applied with one or more loads, internal tensions arise in the body. In its entirety, the potential energy π_p of the body can be described as the sum of the internal energy U and the potential of internal and external forces Ω:

$$\pi_p = U + \Omega \tag{3.84}$$

The deformation of a body corresponds to the internal energy and, according to the law of conservation of energy, this must be in balance with the external energy. In this respect, the system of equations can be solved by an extreme value problem.

Of all possible deformations of a body, the equilibrium deformation has the lowest total potential energy, or in other words: The total potential energy of a system is stationary when the system is in equilibrium and the change in potential energy becomes minimal ($\delta\pi_p = 0$). Since the total potential energy depends on the individual deformations of the body, i.e. on the deformations of all nodes, it can be described as a function of the degrees of freedom (node displacements):

$$\pi_p = \{d_1, d_2 \ldots d_n\} \tag{3.85}$$

Using the chain rule for the derivation of nested functions, the derivation of π_p results in

$$\delta\pi_p = \frac{\partial\pi_p}{\partial d_1}\delta d_1 + \frac{\partial\pi_p}{\partial d_2}\delta d_2 + \ldots + \frac{\partial\pi_p}{\partial d_n}\delta d_n \tag{3.86}$$

This means that for the condition delta $\delta\pi_p = 0$, all individual partial derivations must be zero:

$$\frac{\partial\pi_p}{\partial d_1} = 0, \frac{\partial\pi_p}{\partial d_2} = 0, \ldots, \frac{\partial\pi_p}{\partial d_n} = 0 \tag{3.87}$$

The following presentation summarizes the conditions:

$$\frac{\partial\pi_p}{\partial\{d\}} = 0 \tag{3.88}$$

This forms a system of n equations, with which the displacement of the nodes must be determined. The internal energy U of a stressed body is calculated from the integral of the internal stress and the strain of the volume:

$$U = \frac{1}{2}\int_V \{\sigma\}^T\{\varepsilon\}dV \tag{3.89}$$

Compared to Eq. 3.78, an energetic consideration of the stress σ requires an additional stress σ_0, which describes the energetic condition at time 0.

$$\{\sigma\} = \{\sigma_0\} + [D]\left(\{\varepsilon\} - \{\varepsilon_0\}\right) \tag{3.90}$$

According to the product rule for matrices, the transposed equation is obtained after dissolving the bracket:

$$\{\sigma\}^T = \underbrace{\{\sigma_0\}^T}_{\text{initial stresses}} + \underbrace{\{\varepsilon^T\}[D]^T}_{\text{strains from loads}} - \underbrace{\{\varepsilon_0\}^T[D]^T}_{\text{thermal strains}} \tag{3.91}$$

Using Eq. 3.89, the inner energy U results in

$$U = \underbrace{\frac{1}{2}\int_V \{\sigma_0\}^T\{\varepsilon\}dV}_{\text{initial stresses}} + \underbrace{\frac{1}{2}\int_V \{\varepsilon\}^T[D]^T\{\varepsilon\}dV}_{\text{strains from loads}} - \underbrace{\frac{1}{2}\int_V \{\varepsilon_0\}^T[D]^T\{\varepsilon\}dV}_{\text{thermal strains}} \tag{3.92}$$

If we draw up the energy balance for the potential of the forces Ω, which is applied on the system from outside, 3 terms have to be considered—1. forces acting on the body, 2. surface tractions and 3. loads acting on the nodes:

$$\Omega = \underbrace{-\int_V \{u\}^T\{f_B\}dV}_{bodyforce} - \underbrace{\int_S \{u_S\}^T\{f_S\}dS}_{\text{surface tractions}} - \underbrace{\{d\}^T\{f_p\}}_{\text{nodal point loads}} \tag{3.93}$$

In summary, the total potential energy is obtained by inserting the terms U and Ω in Eq. 3.84:

$$\pi_p = \underbrace{\frac{1}{2}\int_V \{\sigma_0\}^T\{\varepsilon\}dV}_{\text{initial stresses}} + \underbrace{\frac{1}{2}\int_V \{\varepsilon\}^T[D]\{\varepsilon\}dV}_{\text{strains from loads}} - \underbrace{\frac{1}{2}\int_V \{\varepsilon_0\}^T[D]\{\varepsilon\}dV}_{\text{thermal strains}} - \underbrace{\int_V \{u\}^T\{f_B\}dV}_{\text{body force}} - \underbrace{\int_S \{u_S\}^T\{f_S\}dS}_{\text{surface tractions}} - \underbrace{\{d\}^T\{f_p\}}_{\text{nodal point loads}} \tag{3.94}$$

According to Fig. 3.18, the deformation $\{u\}$ can be projected by the node matrix $[N]$ onto the displacement vector $\{d\}$ of the nodes by the equation $\{u\} = [N]\{d\}$.

$$\{\varepsilon\} = [\partial]\{u\} = [\partial][N]\{d\} = [B]\{d\} \tag{3.95}$$

By introducing the partial derivative of the nodal matrix $[\partial][N] = [B]$, the following simplified notation for the potential energy results:

$$\pi_p = \frac{1}{2}\int_V \{\sigma_0\}^T[B]\{d\}dV + \frac{1}{2}\int_V \{d\}^T[B]^T[D][B]\{d\}dV - \frac{1}{2}\int_V \{\varepsilon_0\}^T[D][B]\{d\}dV - \int_V \{d\}^T[N]^T\{f_B\}dV - \int_S \{d\}^T[N_S]^T\{f_S\}dS - \{d\}^T\{f_p\} \tag{3.96}$$

If one excludes the vector $\{d\}$ from the integral and applies the equation $\frac{\partial \pi_p}{\partial \{d\}} = \{0\}$ from 3.88 to determine the extremum problem, the result is

$$\{0\} = \left(\frac{1}{2}\int_V \{\sigma_0\}^T\,[B]dV\right)\{d\} + \frac{1}{2}\{d\}^T\left(\int_V [B]^T[D][B]dV\right)\{d\} - \left(\frac{1}{2}\int_V \{\varepsilon_0\}[D][B]dV\right)\{d\}$$
$$- \{d\}^T\left(\int_V [N]^T\{f_B\}dV\right) - \{d\}^T\left(\int_S [N_S]^T\{f_S\}dS\right) - \{d\}^T\{f_p\} \qquad (3.97)$$

When applying some basic rules of linear algebra for the multiplication of vectors and matrices and summarizing the displacement vector $\{d\}$, the following final form of the equation is obtained, which now has the same characteristics as the equation for the stiffness matrix from 3.81 from the elasticity theorem. Finally, the displacement vector for a finite element or the displacement vector $\{d\}$ for a body in the sum of many finite elements can be determined as

$$\underbrace{\frac{1}{2}\int_V \{\sigma_0\}^T\,[B]dV - \frac{1}{2}\int_V \{\varepsilon_0\}[D][B]dV - \int_V [N]^T\{f_B\}dV - \int_S [N_S]^T\{f_S\}dS - \{f_p\}}_{\{f\}}$$
$$= \underbrace{\left(\int_V [B]^T[D][B]dV\right)}_{[k]} \cdot \underbrace{\{d\}}_{\{d\}} \qquad (3.98)$$

3.5 Acoustics

In recent years, numerical acoustics has developed rapidly in parallel with the increasing performance of computers and permeates almost all fields of acoustics. Among the most widespread wave-theoretical methods of numerical acoustics are the boundary element method, the finite element method and the beam tracing method.

Generally, a distinction is made between problems of acoustics in gases and solid-state sound. It is obvious that the acoustics of gases are based on the fundamentals of fluid dynamics. In contrast, the theory of solid-state sound refers to the calculation principles that are also used for material structures [20].

A common method used in acoustics is the Fourier analysis. This method is mainly applied to perform spectral analyses of a sound wave, especially to generate or reproduce synthetic signals.

According to the Fourier theorem, a periodic signal $f(t)$ with the period T can be represented by a constant component and an infinite sum of harmonic signals $h_i(t)$ with different angular frequencies ω_i, which differ in their amplitudes c_i and phases φ_i. The angular frequencies of the suborders form multiples of the basic angular frequency $\omega_0 = \frac{2\pi}{T}$. For special periodic functions, the sum representation, also called trigonometric series or Fourier series, can be represented as follows:

$$f(t) = c_0 + \sum_{i=1}^{\infty} [a_i \cos(i\omega_0 \cdot t) + b_i \sin(i\omega_0 \cdot t)] \tag{3.99}$$

The quantities c_0, a_i and b_i are called Fourier coefficients. c_0 represents the mean value (direct component) of the signal $f(t)$. If $f(t)$ stands for a pressure $p(t)$ oscillating in time, c_0 corresponds to the mean value of the pressure signal. The representation of the Fourier series can be simplified if the following relationship is used:

$$a_i \cos(i\omega_0 \cdot t) + b_i \sin(i\omega_0 \cdot t) = c_i \cos(i\omega_0 \cdot t + \varphi_i) \tag{3.100}$$

$$c_i = \sqrt{a_i^2 + b_i^2} \tag{3.101}$$

$$\varphi_i = arctan\left(\frac{a_i}{b_i}\right) \tag{3.102}$$

Herewith, Eq. 3.99 becomes the so-called spectral representation of the Fourier series:

$$f(t) = c_0 + \sum_{i=1}^{\infty} c_i \cos(i\omega_0 \cdot t + \varphi_i) \tag{3.103}$$

A periodic signal $f(t)$ can thus be represented by a Fourier analysis with the following quantities [21]:

c_0 : Constant component (mean value of the signal $f(t)$);
c_i : Amplitude of order i;
φ_i: Phase of order i.

For a periodic signal, the transformation from the time domain into its spectral domain uses both an integral and a complex notation:

$$F(\omega) = \int_{-\frac{T}{2}}^{\frac{T}{2}} f(t) e^{-i\omega t} \mathrm{d}t \tag{3.104}$$

The back transformation from the spectral to the time domain is

$$f(t) = \int_{-\frac{T}{2}}^{\frac{T}{2}} f(\omega) e^{+i\omega t} \mathrm{d}\omega \tag{3.105}$$

The function $f(t)$ to be transformed is often not known, but can only be tapped at N discrete times with $t_k = (N-1) \cdot \Delta t$. In such cases the discrete Fourier transformation (DFT) is

used. DFT assumes that $f(t)$ uses a periodical continuation outside the interval. The Fourier coefficients are calculated according to the definition as follows:

$$F(n) = \frac{1}{N} \sum_{n=0}^{N-1} f_n e^{\frac{-2\pi i}{N}} \tag{3.106}$$

The inverse discrete Fourier transform (IDFT) is used for the reverse transformation from the spectral to the time domain is

$$f(n) = \frac{1}{N} \sum_{n=0}^{N-1} F_n e^{\frac{+2\pi i}{N}} \tag{3.107}$$

Based on Cooley et al., an algorithm was developed to reduce the number of complex arithmetic operations to calculate the spectral lines of the DFT by the factor $\frac{N}{\ln N}$ [22]. Due to the lower computational effort and the resulting shorter calculation process, the numerically favorable execution rule of the DFT is called Fast Fourier Transformation (FFT) in this context [23].

Figure 3.19 shows signals of different amplitudes and orders of a fundamental frequency f_{eigen} (here the orders 1, 3, 5, 7) and projects them on the time domain, where the superposition of all single orders can be recognized. At the same time, a projection onto the frequency domain takes place, which provides a breakdown of all involved signals.

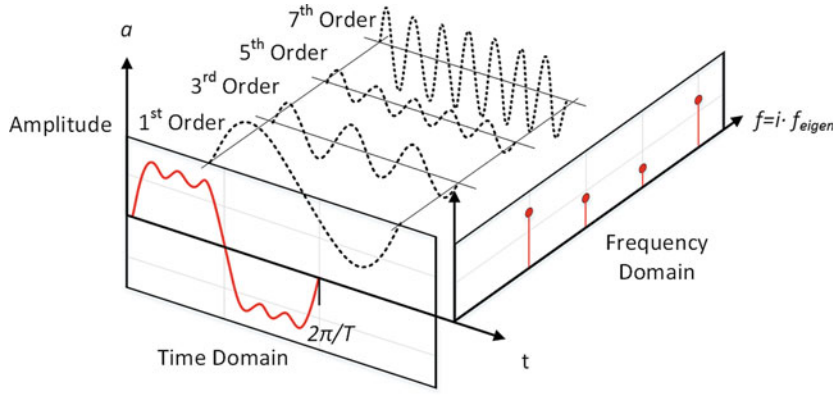

Fig. 3.19 Time and frequency spectrum by superposition of harmonic signals

Big Data for Powertrains

4

4.1 The Future of Powertrain Concepts

Tighter CO_2 limits as a result of climate targets, the Germany-wide diesel emission scandal, Brexit and, last but not the least, the trade conflict between the USA and China have paralyzed the automotive industry worldwide. All the signs are suddenly pointing to a new era and a colossal reshuffle. Manufacturers, suppliers and service providers are asking themselves what is the right strategy to get out of the situation as smoothly as possible.

Basically, the automotive industry reflects the transformation turn of digitization in all its far-reaching facets. As a pioneer of digitization and all the opportunities that this offers, the U.S. has taken on a brilliant role and demonstrated to the world the power behind modern corporate development and lean management style. Horizontal value creation chains are getting ever more popular and inexorably permeating today's corporate structures. Not only for modern companies but even more so for conservative ones it has become inevitable to overhaul old structures and adapt highly effective ones in order to remain viable in the highly competitive market. It is now the turn of the automotive industry to be put to the test, because it currently seems as if the cards are being reshuffled. The right positioning on the market today can prove to be very successful in a few years and a wrong positioning will lead companies to even greater problems.

Which positioning is the right one?

Digitization begins primarily in the mind. This means a change of thought patterns and, as a consequence, a change of an entire society. Ever-increasing personalization has led to a greater characterization of individuals. In this context, the term "granularity" of humanity is often used. Opinions can be expressed more easily than ever through social media. Collectively, they are able to influence and manipulate the opinions of others, even overshadowing expert opinions despite the lack of knowledge, thanks to media forces. As a result, never

A. Mirfendreski, *Powertrain Development with Artificial Intelligence*,
https://doi.org/10.1007/978-3-662-63863-7_4

before has there been such a large discrepancy of opinions among experts, society and, at the same time, politics.

Change means that there will be winners, just as there must be losers. For the sake of debate, let's say the combustion engine seems to have become obsolete because its potential is coming to an end and is damaging the climate. However, there are no short-term alternatives available, only medium-term visions. Is it possible to produce a high proportion of electricity from renewable sources worldwide to justify electric mobility through green driving? Are there sufficient lithium and cobalt deposits to cover the global battery demand? And can these raw materials be mined and sustainably disposed of in a resource-oriented manner and under fair working conditions? Doesn't it make more sense to leave the entire transportation infrastructure as it is and switch to synthetic and biologically produced fuels in order to continue to operate our valuable combustion engines? These are questions that every car manufacturer must answer for itself in order to set the strategic course for its future.

Where are we heading?

The world sales for automobiles had reached an interim peak of 85 million in 2018. The EU commission has passed very challenging CO_2 limits by 2030, with great consequences for all car manufacturers and their employees. Compared to the current level of 118 gCO_2/km, newly registered vehicles may only emit 95 gCO_2/km from 2021 and 59 gCO_2/km from 2030 onwards. In addition to the agreed CO_2 values of the EU Commission, Fig. 4.1 shows the CO_2 emission limits of other countries, which were passed in June 2019 and published by the International Council on Clean Transportation (ICCT) [24].

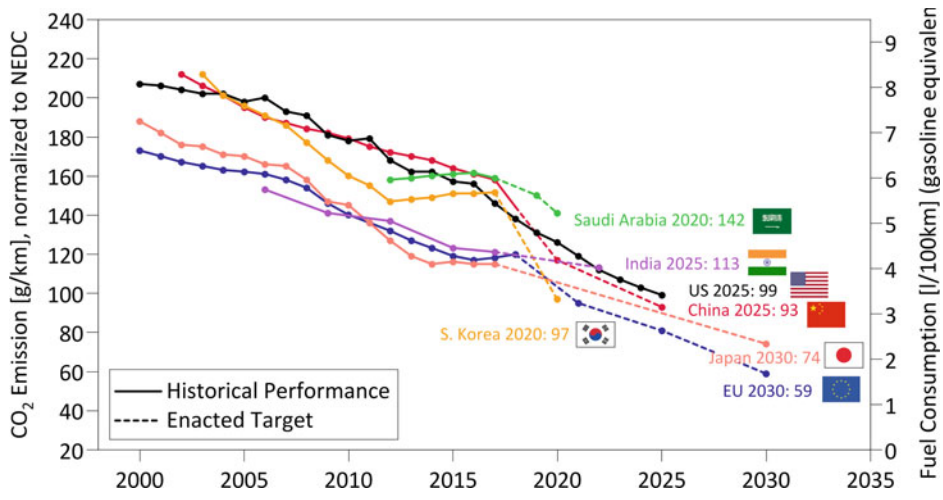

Fig. 4.1 Emission limits according to the European exhaust standard [25]

Despite the ambitious climate protection laws and efficiency targets set by the German government, mobility will stay important for all social classes and remain an expression of personal freedom. Climate protection will inevitably entail higher costs for the population, so it is important to carefully examine and weigh up the advantages and disadvantages of all types of powertrains and energy sources. Today, a large number of renowned studies provide possible scenarios of tomorrow's mobility, which serve as important guidelines supporting understanding which CO_2 targets can realistically be achieved. Which driving concepts can make a significant contribution to this and how do political decisions affect the new car fleet for vehicle customers?

All presented scenarios show that even assuming a value of 95 gCO_2/km as the EU limit in 2020, it is possible to halve the CO_2 emissions of the car fleet down to 45 gCO_2/km without switching to new forms of transport. High-quality fuels (including synthetic fuels and biofuels) in combination with innovative combustion engines enable efficiency improvements in the fleet, both by conventional powertrain systems and by the wide range of hybrid variants. The increasing proportion of electric driving, the growing shares of alternative powertrain systems such as the fuel cell, should help to achieve the defined targets. A major requirement for a growing share of electric mobility on the market is the provision of low-CO_2 electricity, i.e. an electricity mix with a steadily increasing portion of regeneratively generated energy.

The renowned studies selected in the following are intended to serve as guides showing where the automotive landscape is heading in the future: 1. "The Passenger Car Market until 2040" by the German Aerospace Center (DLR), 2013, a study from the perspective of a mineral oil company; 2. "Passenger Car Scenarios until 2040" by Shell from 2014; and 3. "Climate Protection Contribution of Transport until 2050" by the German Federal Environment Agency (UBA), 2016.

New registrations

For new registrations, DLR proposes a moderate "trend"-scenario with a target value of 70 gCO_2/km by 2040, in which conventional engines will hold higher market shares in the long term. The assumptions made here are stable environmental conditions, moderate change in consumer preferences, steady technological progress, a gradually changing fuel mix and a further decreasing emissions target path. Access to automobility in terms of affordability remains an important criterion for this scenario.

In contrast to this, there is an ambitious "alternative scenario", which, starting from the CO_2 target of the currently valid EU regulation of 95 CO_2/km in 2020, aims for an extrapolation to 70 CO_2/km in 2030 and to 45 CO_2/km in 2040. This scenario expects a massive change in environmental conditions, social and political upheavals of past trends, a noticeable change in consumer preferences, a rapid change in technological development, a significant shift in the fuel mix and a drastic reduction in the emissions target path. Achieving climates under this scenario comes with a higher cost to consumers.

In accordance to the DLR studies, Shell as well proposes a moderate "trend"-scenario with a CO_2 target of 70 gCO_2/km by 2040 and an ambitious "alternative"-scenario with

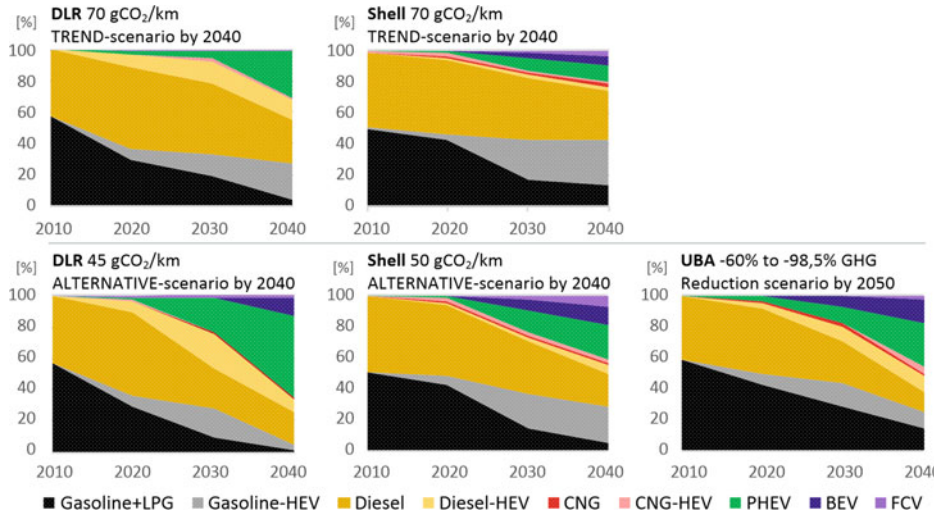

Fig. 4.2 Trend of new passenger car registrations along powertrain concepts in Germany until 2040 [2] [26–28]

a target of 50 gCO_2/km in 2040. This makes them suitable for a one-to-one comparison (Fig. 4.2).

The "Climate Protection Contribution of Transport until 2050" by the Federal Environment Agency is the third study used here for comparison reasons. It argues over the commitment of the Federal Government to reduce greenhouse gases (GHG) across all sectors by 80%–95% by the year 2050. If this target is projected to the transport sector, it means a reduction in GHG in the range 60%–98% must be achieved. Transport in 2050 hence must be almost greenhouse gas neutral. Only higher cross-sectoral targets there will give more flexibility to the transportation sector [26–28].

In both alternative scenarios of DLR and Shell as well as the UBA scenarios, hybrid concepts (HEVs) bring about significant changes representing a combination of electric and conventional propulsion. Due to the relatively simple convertibility of conventional drives to 48V mild hybrids, these concepts will be a good option for an interim solution in the short term until 2025. The possibilities of $P_0 - P_4$ topologies allow a high degree of flexibility depending on the base engine concept [29].

In 2030, hybrid vehicles (mild hybrids and full hybrids) alone will no longer be sufficient to reduce the fleet's average CO_2 emissions sufficiently. This means that the proportion of the distance traveled with electricity will have to increase, which can be achieved by plug-in hybrids (PHEVs) and Range Extender Electric Vehicles (REEV).

[2] LPG=liquified petroleum gas, HEV=hybrid electric vehicle, CNG=compressed natural gas, PHEV=plug-in hybrid electric vehicle, BEV=battery electric vehicle, FCV=fuel cell vehicle, GHG=green house gas.

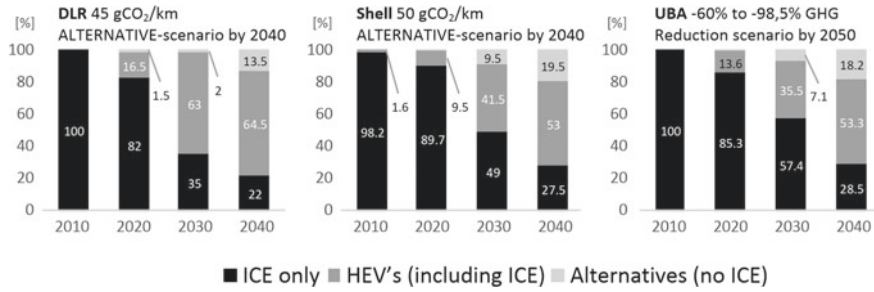

Fig. 4.3 Trend of the combustion engine as a proportion of all new car registrations [26–28]

The process of electrification will continue to be expanded until 2040. The PHEV share and the REEV share will clearly gain the upper hand compared to fully hybrid concepts. Pure battery-powered vehicles (BEVs) will continue to grow. At this point in time, the hydrogen fuel cell (FCV) continues to play a subordinate role in the market.

One question that still needs to be answered when it comes to the future of drive concepts is the role that the combustion engine will play. From the three ambitious scenarios of the presented new car fleet, a distinction is made between concepts relevant to the combustion engine and those not relevant to the engine; see Fig. 4.3. According to the DLR study, 86.5% of all powertrains will still have a combustion engine in 2040. The Shell study forecasts this proportion at 80.5% and the UBA study at 81.8%. What emerges from all three studies is that even with a drastic change in technology as a result of the climate targets, the combustion engine will keep significantly the upper hand even in 2040.

Vehicle stock

The new vehicles that are added in Germany every year make up about 7% of the total vehicle stock. According to the Federal Motor Vehicle and Transport Authority of Germany, the average age of all registered passenger cars in January 1st, 2019, was 9.5 years. The development of the vehicle stock is therefore lagging behind new registrations by this margin.

The car stock is derived from demographic and socio-economic developments and is determined by age- and gender-specific motorization concepts and age-specific car performance requirements. Socio-demographic factors and spatial settlement structures will also affect the demand for mobility as in motorization performance. Hence, these factors will have a great influence on fuel demand and the trend for the car stock. In addition, income and subsidizing effects of specific driving concepts and fuels can have a considerable impact on the automotive landscape [27].

According to the presented studies, the following graph shows the stock development until 2040. In the year 2040, according to the DLR study, 94.5% of combustion engines will still be operating on German roads. Shell and UBA both forecast this value at 89.5% (Fig. 4.4).

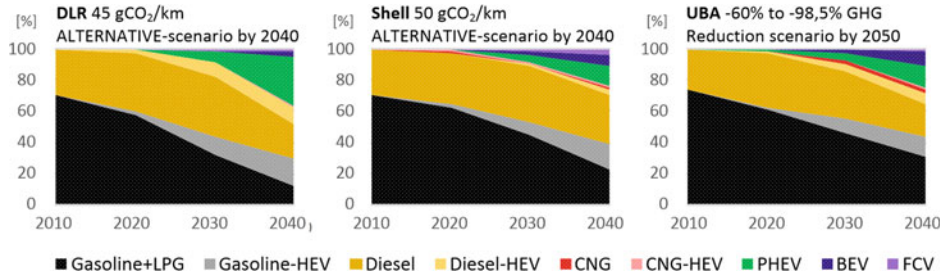

Fig. 4.4 Trend of passenger car stock along driving concepts in Germany until 2040 [26–28]

How do we prepare for these scenarios?

As a result of the targeted and versatile driving concepts, the development costs of automobile manufacturers will increase dramatically over the next years. Combustion engines have already reached a high potential regarding their efficiency and thus a minimum of CO_2 emissions. Further attempts at optimization are now only bringing marginal improvements at the same or even higher investment volume—but this does not mean that they are so easily replaceable. One thing, however, is certain—major investment trends for the development of internal combustion engines cannot continue as they have in the past decades. An investment basis resulting from more versatile driving concepts will only be profitable in the future if significantly leaner development processes and more efficient methods replace the current ones.

The right tools are available at the right time: artificial intelligence (AI). AI is the science of intelligent agents combined with the power of neural networks that primarily computer scientists have dealt with over the past decades. Their versatile fields of application have accordingly settled in the world of IT and have significantly advanced the digitization process since the1970 s. In the meantime, the concepts of AI have become versatile, reliable and highly efficient. How the topics of a digital IT sector can be transferred to industrial fields will be presented in the following chapters by means of work processes, concepts, methods and application examples.

4.2 The History of Simulation

Simulation as a development tool has significantly influenced the progress of technology since the1970 s. Irrespective of its field of application, it has been able to identify new optimization potentials, to compare and evaluate various system variants in a cost-effective and time-efficient way. It has also helped to define uniform development processes in a new way.

Only a few decades ago, powertrain development was test-based or prototype-based. This form of development was purely hardware-oriented and caused high costs over long periods. Each individual and new development stage that consists of compound systems (such as the

powertrain, which is a compound of numerous subsystems) could only be evaluated in its entirety once a finished prototype was designed. On the basis of this working principle, further development steps or improving measures could only be achieved on the basis of intensive observations, combined with a high level of experience and sound knowledge of theoretical fundamentals.

Nowadays, the manufacturing of industrial products, especially such as powertrains, is almost entirely virtual and model-based. From the first concept paper to the completion of a prototype, powertrains can be developed entirely virtually, so that development costs today have shifted almost entirely from a hardware-based to a software-based process. Almost 50 years ago, it would have been impossible to foresee this progress and today's development structures. Likewise, it is not easy for us to estimate how things will work 50 years from now. However, one thing is beyond question: What helps to anticipate the future is to understand the past and the present. According to this principle, it becomes interesting to deal with the historical aspect of simulation, to what extent it has taken not only the automotive industry forward but also the world.

Figure 4.5 shows the result of a study in which all simulation software products (tools) developed on the market since the 1970 s are listed numerically. The focus of the study rests on the product levels that are equally relevant for the automotive area, here subdivided into 3D-CFD, 1D-CFD/0D-CFD, elastohydrodynamics (EHD), chemistry/kinetics, FEM, multi-body simulation (MBS), acoustics/NVH and kinematics/chassis. Only conventionally available products are included in this illustration. The market entry of a software product is rated +1 and a market exit is rated −1. The graphic shows how the trend of the respective product level has developed since the beginning of the conventionalization of simulation from the early 1970 s until today.

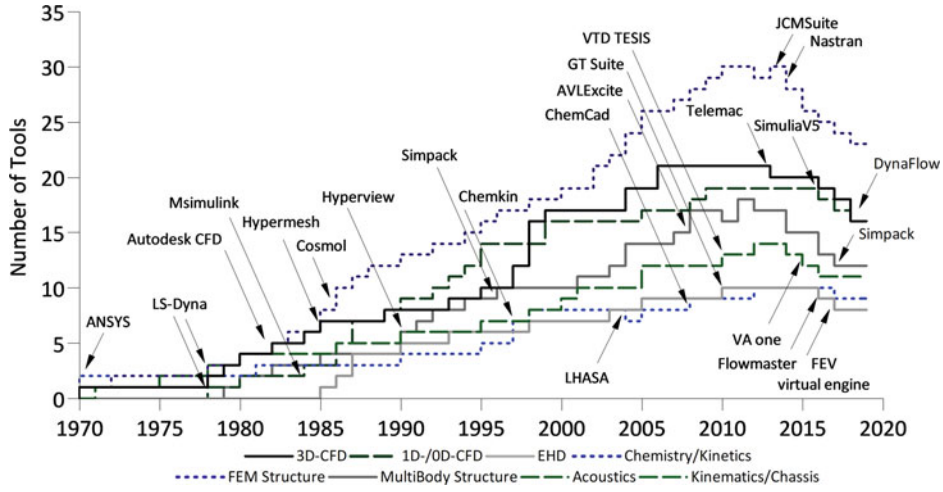

Fig. 4.5 History of conventional simulation tools for general applications

Until the end of the seventies, there are only a few products available. In the early eighties, software vendors had understood the potential of simulation-based development and correctly assessed a progressive increase in market demand, which led to a steep rise in supply. It is interesting to observe that despite individual delays, all product levels increased homogeneously, which indicates that a uniform implementation of all products into the complete value creation chain was recognized by customers and strived early.

In the 1990 s and 2000 s, the rapid increase took on. While software tools for chemistry/kinetics or EHD reached saturation early on, from the fact that a basic complexity could be achieved with very high predictive power, doors opened up for a deeper development potential for CFD (3D/1D/0D), FEM and MBS, so that product developers remained committed to satisfying the continuing demand for tools with higher precision and more complex requirements.

Around the year 2010, all product levels of the simulation were running into saturation and in the period between 2010 and 2015 a clear backward trend can be seen in all product levels. Fig. 4.6 allows a closer look at the simulation tools that are exclusively intended for the automotive market or at least target their core business there. The overall trend is almost identical. On a closer look, differences can be seen on the different levels between FEM and CFD (0D/1D/3D) as they grew closer together, which also underlines their capability for interactions.

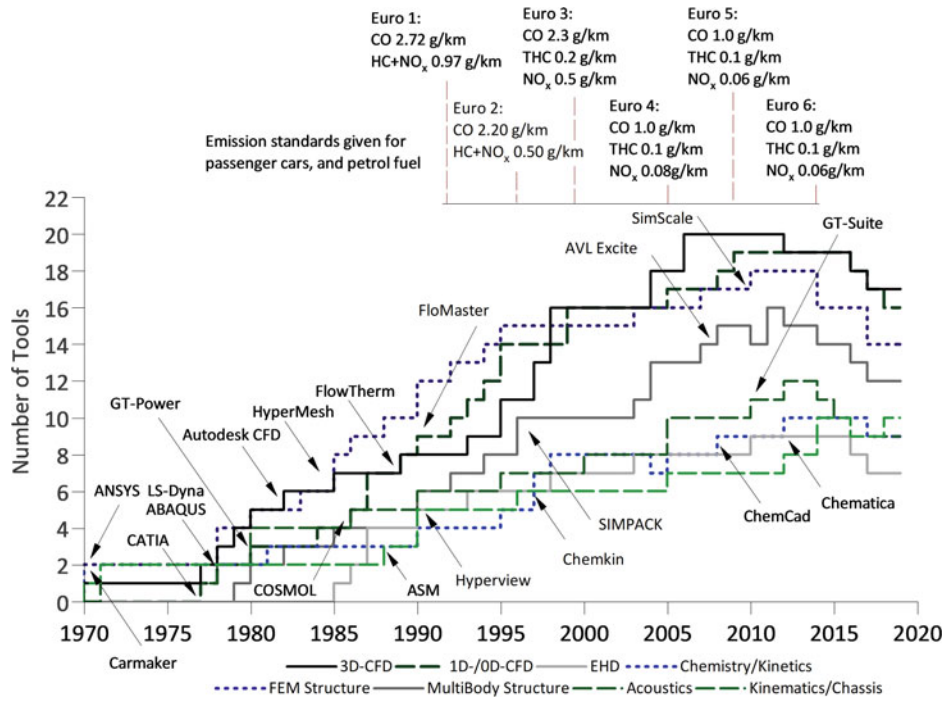

Fig. 4.6 History of conventional simulation tools for the automotive industry

Since 2013, the trend has been declining at all levels for which the following reasons are comprised.

1. **Centralization of development units and standardization of software tools**
Model-based development costs have increased significantly over the last decade. On the one hand, simulation software in general gains in complexity through continuous development, which leads to an increase in license costs. On the other hand, car manufacturers tend to use a high variety of software products, which is because usually different departments within a company often use different software products for historical reasons, which in principle cover the same product level. For this reason especially in recent years, it has been observed that companies have gradually centralized their pre-development units and standardized their software in order to save costs at this level. Nevertheless, the high performance of tools generates secondary costs, as they require centralized computing architectures and cluster systems. Last but not the least, there are high personnel costs for experts who have to bring or learn specific skills for the application of these software products.

2. **Change in the market**
Another reason why conventional simulation software is becoming less attractive for developers is that a declining sales market is expected in the future. The potential of the combustion engine with regard to improving efficiency is now largely saturated. The transition to electromobility and fuel cells does not demand the current variety of tools. As an example, structural calculation software (FEM/MBS) for a purely electric or fuel-cell-powered drive concept is losing relevance, as material stresses and loads play a much smaller role than before.

3. **A highly competitive situation**
The competition on the market for simulation software products has increased massively over the last three decades. Some products are well established within their level, others less. This has caused a strong economic gap, so that market-dominant suppliers repeatedly took over smaller and weaker products. Nowadays, it is almost impossible for small software suppliers to bring new products to the market, as they are under enormous competition and once established process chains in development units of car manufacturers can hardly be broken through advertising and marketing measures even at a great expense. These facts additionally contribute to the fact that the absolute number of products is decreasing.

Figure 4.7 summarizes the cumulated numbers of software products for general applications and specifically for the automotive sector. Looking at the emission limits according to the Euro legislation, from the introduction of the Euro 1 standard in 1992 until the

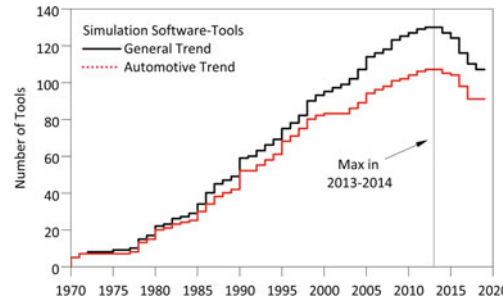

Fig. 4.7 Development trend of all simulation software products

introduction of the Euro 6 standard in 2014, the permitted CO content was reduced from 2.72 g/km to 1 g/km and the HC − NO_x limits from a total of 0.97 g/km to 0.1 g/km HC and 0.06 g/km NO_x. Including the Euro 5 standard, vehicle registrations were based on the NEDC driving cycle. Since then, the new WLTP[3] is being used as the basis for legislation; see Fig. 4.8 (left). China, which has the highest population density in the world, follows the EU's measures with its emission regulations. Eight years later in 2000, the first China 1 standard was announced. Since then, the country has caught up considerably with Europe and is now taking the lead with the early definition for the China 6b standard, which is comparable with the Euro 7 standard. Compared to the current China 5 standard, the CO and HC content of 1 g/km and 0.1 g/km, respectively, will be reduced by a further 50% and nitrogen oxides by a further 42%.

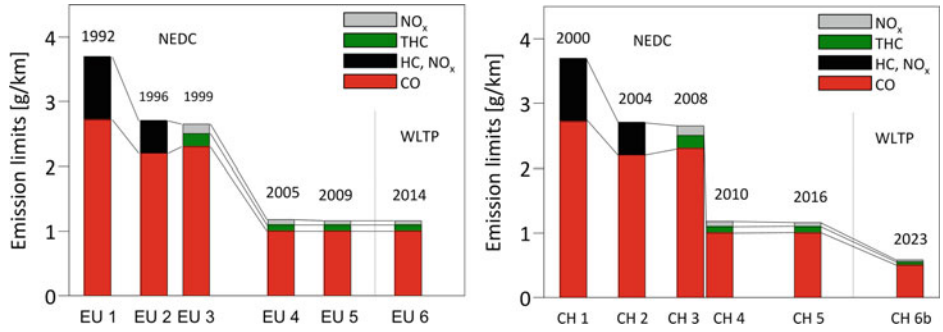

Fig. 4.8 Development trend of emission limits since the introduction of emission standards for the EU (left) and China (right) [30]

[3] Worldwide Harmonized Light Vehicles Test Procedure.

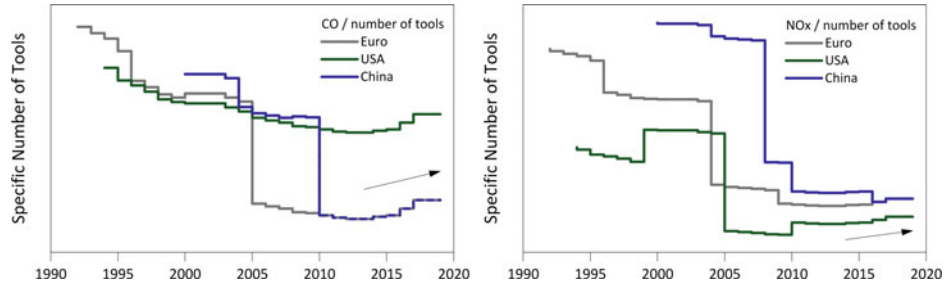

Fig. 4.9 Specific CO_2 (left) and NO_x (right) fleet development trend since the introduction of emission standards

When putting the market trend of the simulation tools in relation to the emission limits (here for CO and NO_x), one obtains a specific representation according to Fig. 4.9. The units [CO/number of tools] (left) and [NOx/number of tools] (right) give an indication of the extent to which simulation tools have helped us to reduce emissions using computer-aided and model-based methods in the context of powertrain development since the introduction of emission limits. Both graphs show how the specific value has been on a downward trend since the early1990 s. For all three legislations (Euro, US Ulev[4] and China), an absolute minimum is reached around 2013. After that, the specific emission values have started rising again.

To show the same specific trend for the CO_2 development, the number of the simulation tools is put into relation with the CO_2 limits in Fig. 4.10. Also here, it is evident that the specific CO_2 value reaches its minimum between 2014 and 2015 and has been increasing again since then.

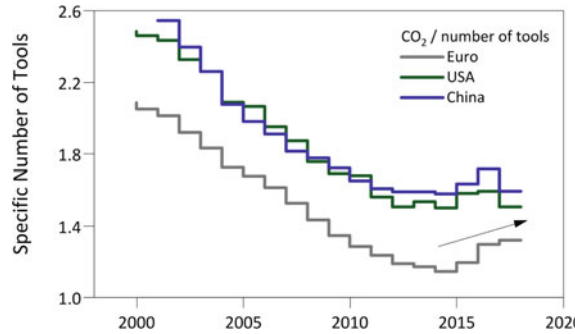

Fig. 4.10 Specific CO_2 fleet development trend since the introduction of CO_2 limits

[4] Ultra low emission vehicle.

4.3 Development Processes and Scenarios of Simulation with Big Data

As a result of the rapid development of data storages, starting with the simple floppy disk from the mid-1970s with a capacity of about 80 kilobytes and the market launch of recordable compact disks in the early 80s with several hundred megabytes suitable for series production, in the early phase of the digitization process it was well understood that the technological possibilities of storage and the availability of complex data volumes would strike new ways with inconceivable potentials. The term "Big Data" was first popularized in this context in 1990 by a US-American computer scientist named John Mashey.

Today, big data no longer stands for technological progress in handling large amounts of data solely, but for a breakthrough in new development methods for modern companies. It does not matter in which segment a company is positioned—the methods are universally valid and can be used in any field. However, the preparation (pre-processing) can vary greatly and play a decisive role in a successful implementation (Fig. 4.11).

From the possibility of generating large and indefinable amounts of data and making them storable, the real challenge arises, namely the systematic handling of these data. Big data is a far-reaching term and can be characterized by four properties for every conceivable amount of data:

- Data Volume describes the size of a data set.
- Velocity describes the speed at which data characteristics or the amount of data itself changes.
- Variety describes the expandability of a data set and the variability of a data source.
- Veracity describes a degree of average noise that naturally comes with real data.

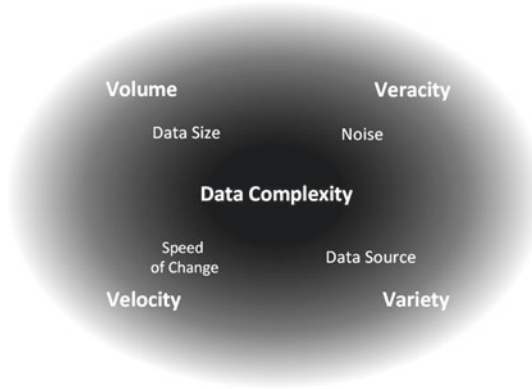

Fig. 4.11 Characteristics of data (Big Data) [31]

How can data be generated?

Until about the end of the1960s, when simulation tools were not yet firmly anchored in the processes of powertrain development, decisions for any development were purely taken based on testing results. Every development step was under close observation and without modern tools, as they are used today, directions and progress could only be achieved through a solid experience and a constant elaboration of theoretical foundations. The design unit, production and test bench operation were in a much closer interaction than today. This was necessary since the purely test-based development of systems and subsystems were requiring the production of new prototypes for every single development step. Only a validation of a manufactured system could provide a statement as to whether and what qualitative gain this development step brought about.

Figure 4.12 shows a general process chain for the development of a powertrain in a simplified form, as it was done before the age of simulation. A reference motor with the prototype designation P_0 is at the beginning of a new development stage. On the basis of defined targets (specifications), subsystems (component level) are optimized (R), adapted in terms of design (D) and manufactured (M). This can relate to cylinder and piston geometries, manifold inlet and outlet geometries, materials for higher load capacity, better thermal management or for weight reduction of mechanical components, ignition devices, the crank mechanism, valve train or any other form of system. The next step is to produce a modified

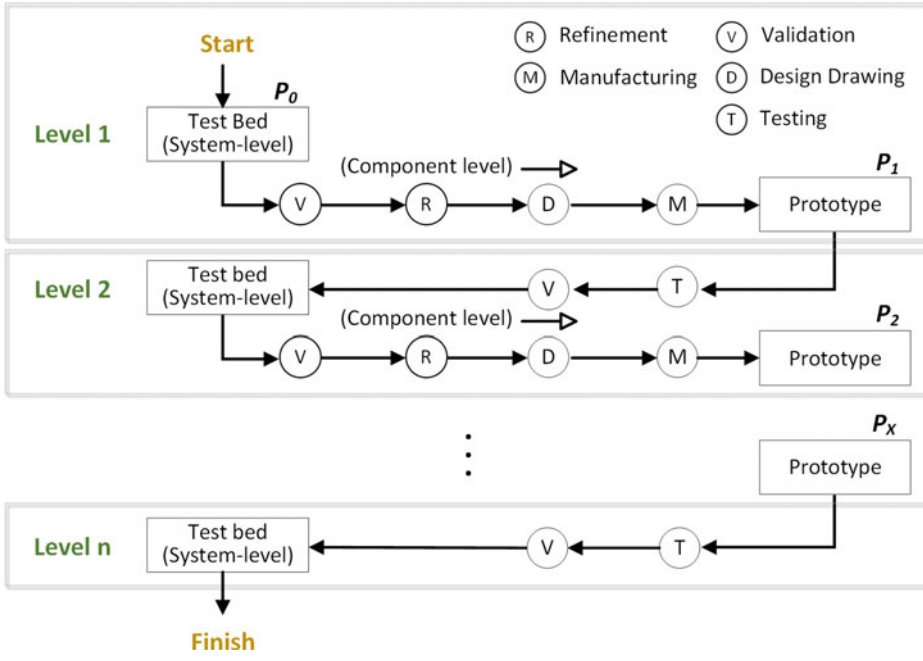

Fig. 4.12 Prototype-oriented/test-based development process of powertrains up to the1970s

system with the prototype designation P_1. In a closing loop, the new prototype is now tested (T)—a qualitative evaluation can be made according to a new validation loop (V). This process loop is repeated many times until the target of the specification sheet is reached by the prototype variant P_X and all subsystems are merged into a complete system (system level).

Nowadays, development departments of all automotive manufacturers strongly integrate simulation into their development routines. The theoretical foundations of some of the topics were presented in Chapter 3.

Since the beginning of the commercialization of simulation tools and their use in corresponding development phases of powertrains, such as concept design, material selection, construction, pre-application and application (see Fig. 3.1), development processes have changed dramatically. First and foremost, simulation had produced serious potentials that could not have been localized and implemented at comparable speed on a purely test-based approach. In addition, the avoidance of permanent production of prototypes resulted in significant cost savings of hardware.

A new process chain allows the virtual development of complete systems (system level) along continuous development phases (level) in a purely model-based approach. On the component level, the development comprises the chain of virtual calibration (C), optimization (O) and computer-aided design (D) of model levels ($M_1, M_2, \ldots, M_n$) and the subsequent data generation (DG) for the calibration of electronic control units. Only after the entire process has been completed the first prototype P_1 is produced, which immediately fulfills a large part of all the required specifications. Manufacturing is thus shifted to the very last step of the process chain (see Fig. 4.13).

Simulation is stronger than ever

Over the past decades, university research institutes, research and development units of automobile manufacturers as well as suppliers and external service providers have been intensively engaged in the field of simulation worldwide. This has resulted in a large number of publications that have gradually continued the success of virtual development. What can be designed surprisingly well with simulation approaches are methods and methodologies for advanced processes. Methods are single solution concepts, methodologies are the composition and process sequence of many single methods in a closed development framework.

Methodologies have now become overarching sub-disciplines in the field of virtual driving concept development, holding structures and strategies inside development units together representing the uniqueness of corporate cultures or even microcultures on a department level. Since all automotive manufacturers use the same or similar simulation tools by today, it is even more important to distinguish oneself by individual methodologies and create a unique development DNA.

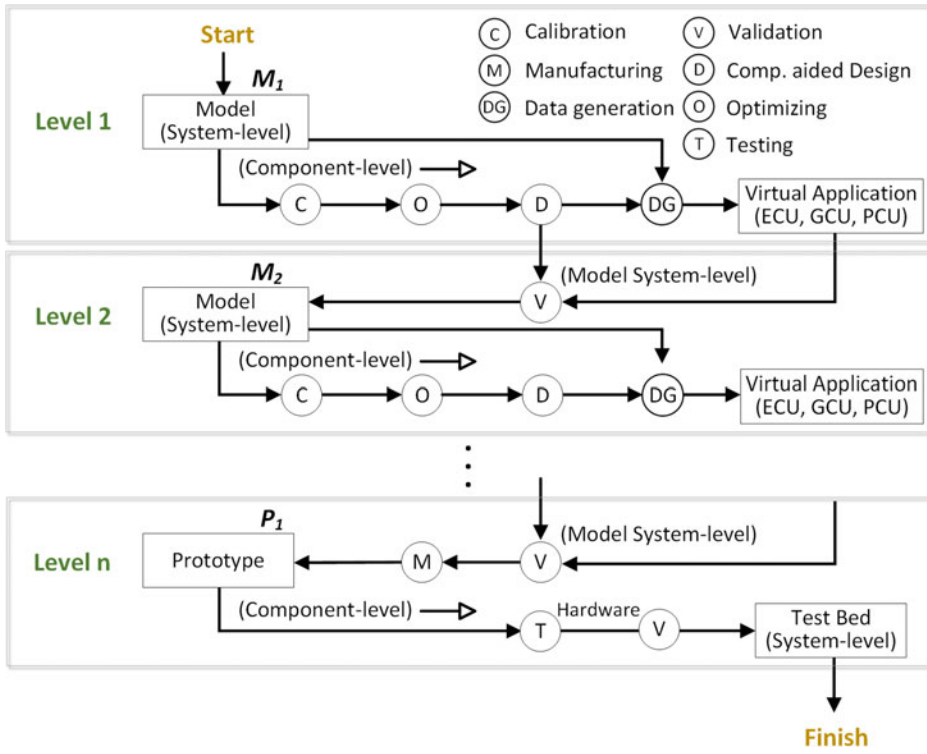

Fig. 4.13 Simulation-oriented development process of powertrains today[5]

Figure 4.14 (left) shows schematically how the quality and reliability of simulation tools have changed over time. As a result of the continuous development of model approaches, simulation tools are extremely reliable in terms of predictability and are close to reality, at least as far as qualitative trends are concerned.

In the past, simulation tools were used independent from each other on an individual demand. Therefore, it was essential to have realistic boundary conditions in order to make predictions of high quality. The graph on the right shows how simulation among powertrain development has evolved from an initially processless to a process-integrated tool since the 1970 s. Accordingly, the trend of test-based methodologies has declined. Today, test-based methodology plays a higher role at the end of the development process chain in the context of system validation.

As explained at the beginning of this chapter, big data provides the basis for the development of models that make use of concepts of artificial intelligence. Without the existence of large and, above all, diverse data sets, the highly effective algorithms of AI cannot be used. In order to make use of AI, the idea of generating data sets on real test benches would be an obvious one. However, this process would be extremely cost-intensive and not target-

[5] ECU=Electronic control unit, GCU=Gearbox control unit, PCU=Power electronic control unit.

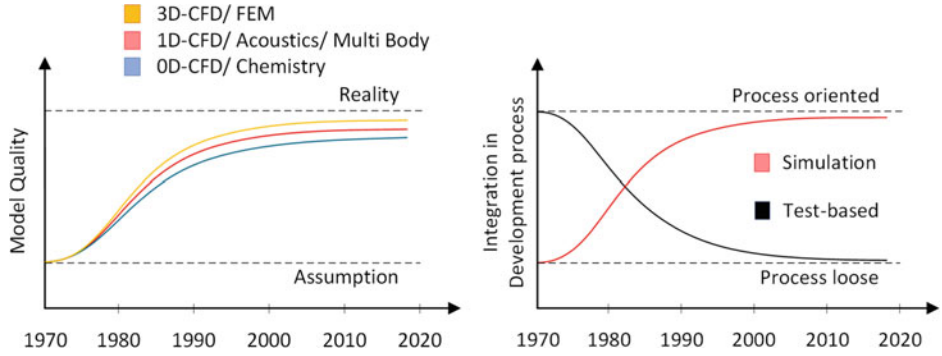

Fig. 4.14 Reliability of simulation (left), Historical change of development processes (right)

oriented, since real systems only generate data within the boundaries of systemic plausibility. An algorithm based on this data would be strongly restricted in its freedom and generate solutions which from the point of complexity cannot go beyond already known. What we expect from AI is not only new results, but above all new solution paths that leave the limits of systemic and human plausibility to create unexpected and unlimited solutions.

If we now try to implement a resource-oriented thought based on what is available to us, we would use simulation tools and models to generate massive amounts of data on a purely virtual basis in a short time. A possible basis for data generation is provided by the Design of Experiment (DoE). Fig. 4.15 compares both approaches, namely measurement-related data and simulation-related data generation. In principle, it is possible to use any simulation software as a data generator.

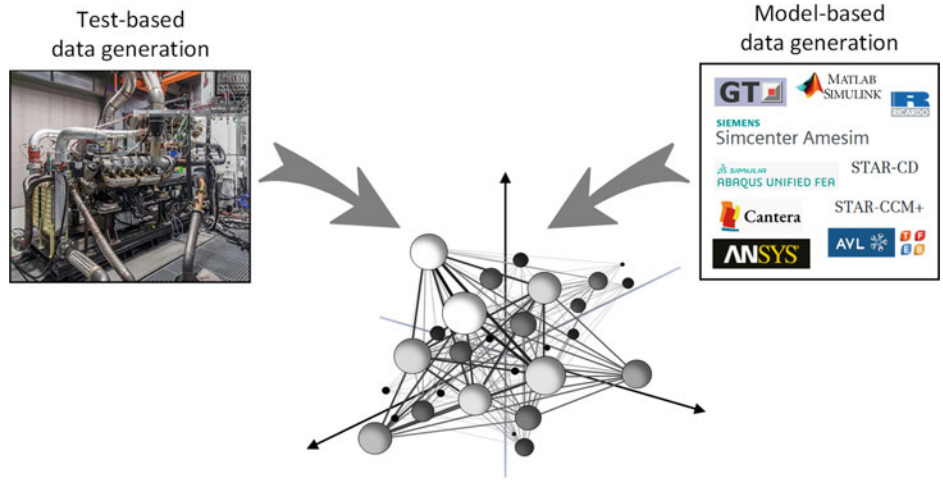

Fig. 4.15 Generating big data through real data (left) or through simulation software (right)

Advantages of AI-based powertrain development

The advantages that AI-based concepts can provide for the development of powertrains are obvious. While calculation in conventional computing systems are ordered serially, and lead to a lower data processing speed, an AI architecture processes in parallel and therefore gains an exponential speed advantage. Especially the associative operation allows finding creative and complex solutions to problems, which a normal computer code would not be able to solve due to its address-based principles. This results in many types of problems that could not, or only with great effort, be converted into an algorithmic form so that they could be solved by a computer. Also, unlike the processes of an AI system, conventional algorithms do not undergo a learning process and are not adaptive for recurring problems.

Figure 4.16 shows how AI calculation processes can be classified in terms of accuracy and computing time compared to classical methods of simulation. In general, the levels of simulation can be divided into differential equation methods and signal-based methods.

3D-CFD (see Sect. 3.1) presents the highest level of detail using the method of partial differential equations (PDE) for solving a problem. Solvers are computing both time discretely and space discretely for each individual node of a grid (mesh), and this is done several times per time step, depending on the order of the solver. 0D represents the lowest PDE-based level for which a spatial resolution is not executed (see Sect. 3.1.3).

The signal-based level is divided into white-box, grey-box and black-box models. White-box models are physical models that represent inputs and outputs based on theoretical (physical) relationships and are comprehensible for the user. Gray-box models, on the other hand, are hybrid models and known to combine a partial physical representation with additional

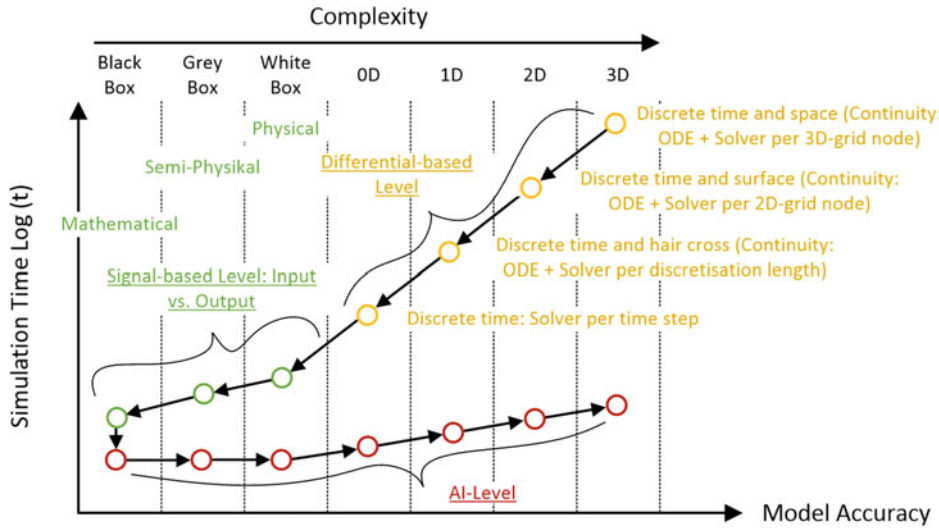

Fig. 4.16 Trade-off between level of detail and model accuracy: AI simulation compared to conventional simulation

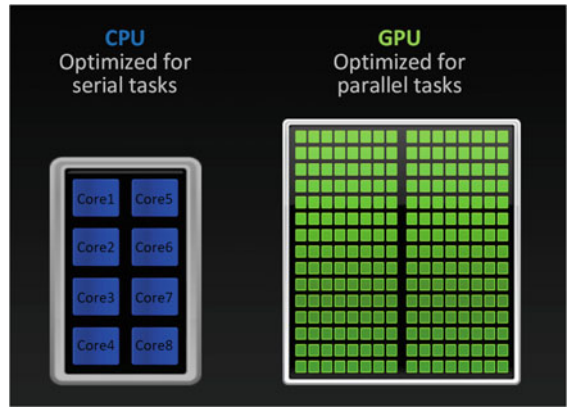

Fig. 4.17 Serial tasks versus parallel tasks

real data, which substitutes missing physical correlations through mathematical regressions. If no physical relations are known at all, so that correlations of inputs and outputs only have to be described by mathematical formulas, this can only be achieved by using large amounts of real data. The correlations remain intransparent for the user, which can be attributed to black-box models (Fig. 4.17).

While common central processing unit (CPU) chipsets in computers use multiple cores that focus on sequential processing of computational processes, a graphical processing unit (GPU) is suited for parallel processing. In contrast, it provides hundreds to thousands of smaller cores to process threads (or instructions) simultaneously. In combination with artificial intelligence and the parallel processing of neural networks, it becomes clear that GPUs are ideally suited for this purpose. The following graphic shows the result of a study in which the calculation speed of a CPU and a GPU are compared. For the benchmark, 4 neural networks were put to the test, with the increasing complexity of the architecture (Fig. 4.18). More details about network architectures are given in Sect. 5.5.4.

All PDE-based as well as signal-based layers can be simulated by AI. Hence, an AI level positions itself flexibly and, depending on the requirements, from simple to complex. When following the directions of the arrows, it becomes clear that even 3D problems at the highest detail level of simulation can be captured with AI, with a massive advantage in computing time.

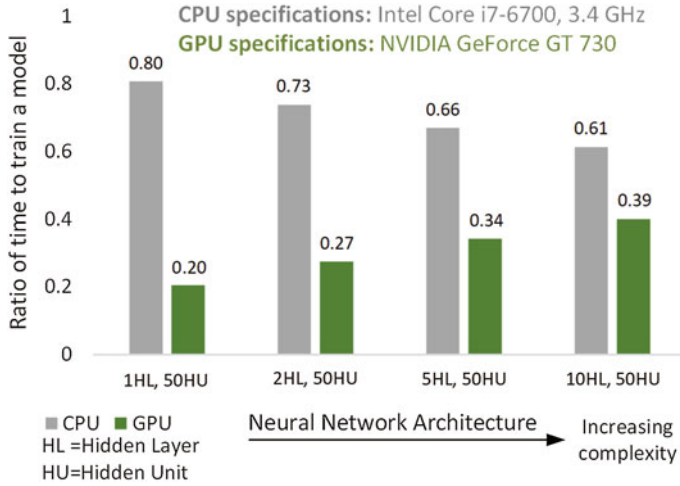

Fig. 4.18 Speed advantage GPU versus CPU

Exploiting the current trend toward new value creation processes

Operating speed is always directly related to costs. By applying AI model approaches, not only previous calculations but also methods and full methodologies can be integrated into existing development processes. This should enable not only a drastic increase in development speed but also a significantly leaner and more efficient process. In Sect. 4.2, the trend of the developed simulation tools until the1970 s was presented and discussed. The rapidly increasing demand for software until 2013/2014 (see Fig. 4.7), many of which are in competition with each other, has also confronted users with the difficult task of finding out which tools meet their requirements best and are integratable into their individual workflow. The consequences are clear. On the one hand, this leads to time-consuming and cost-intensive benchmarks. On the other hand, to high investment volumes such as for multiple licenses within identical application areas and high IT maintenance and network cost due to the diversity of softwares.

Following the idea, it becomes clear that the current trend together with the promising concepts of the AI interlocks ideally. A possible scenario that is presented here is that there will be a regression and reassortment of the software varieties. It is to be expected that software in the future will be limited to a core product that meets the requirements of the users in the broadest sense. In each discipline, whether 3D, 1D/0D, EHD, chemistry/kinetics, FEM, MBS, kinematics or acoustics, cost-saving measures can be taken by selecting the most efficient tool among a large variety for the respective needs and using it as a data generator from thereon. The development landscape will thus be composed of harmonious interaction of the strongest tool in its discipline (as a data generator), surrounded by many AI applications (AI gadgets) that use the input of virtual data. This rationalization process is referred to as gadgeting in the following (Fig. 4.19).

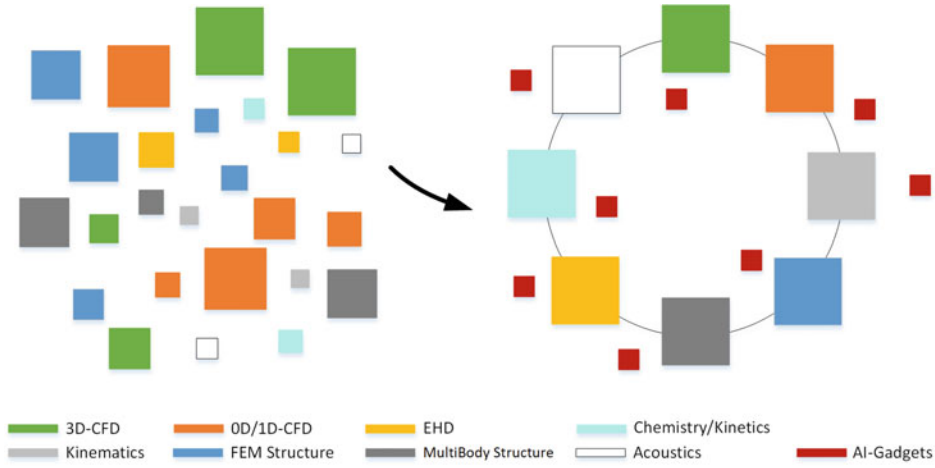

Fig. 4.19 Gadgeting process: Rationalization and reassortment of all simulation tools to the strongest tool in its respective discipline, extension of the development landscape with AI gadgets

In principle, this results in two interesting concept possibilities:

1. Partial concept: AI gadgets to support the calibration

A first concept possibility is to keep simulation tools as result- delivering systems. Additionally, they are used as data generators. The AI gadgets integrated into the structure have the function to set parameters of desired submodels in correlation with their initial results. In addition, the calibration effort (C) of models is automated so that a time-consuming para-

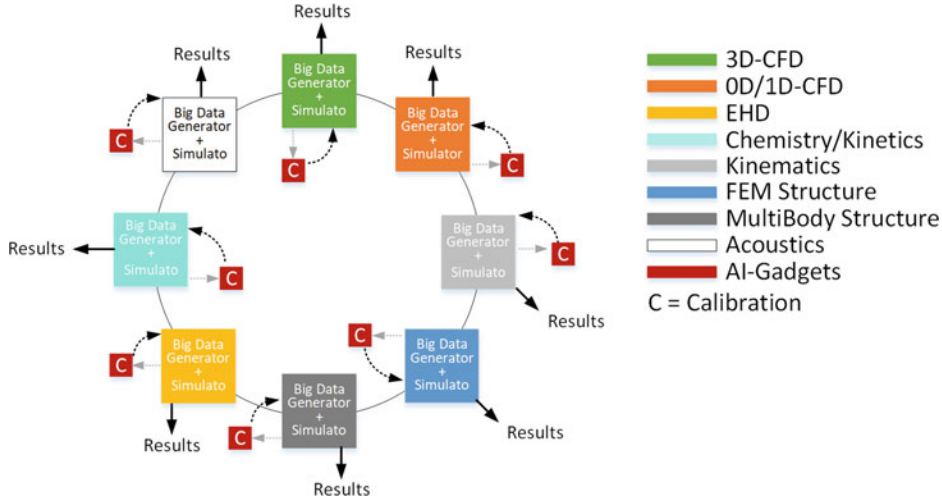

Fig. 4.20 Gadgeting sub-concept: AI gadgets to support the calibration

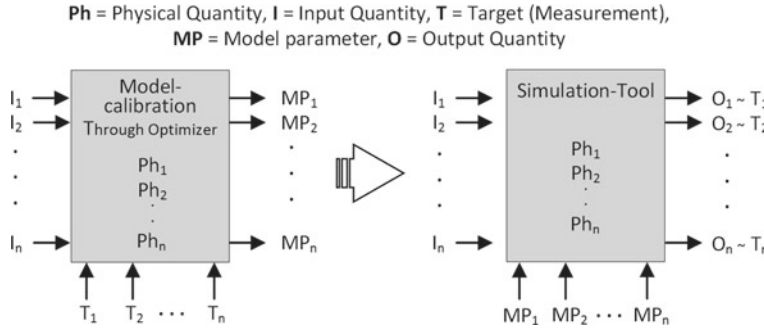

Fig. 4.21 Typical procedure of a model calibration (left) and applying a model as a data generator (right)

meter calibration to existing real data will not be necessary anymore. From there on, the correct parameterization is provided by AI gadgets. Fig. 4.20 shows how all systems interact in such a constellation.

To concretize the concept a bit more, it is shown in Fig. 4.21 how AI gadgets can be created to support model calibration. A typical two-step process chain is illustrated that is used to calibrate simulation models. In the first step (left), target values ($T_1, T_2, \ldots, T_n$) are specified, which usually originate from measured real data. By using optimizers, model parameters ($MP_1, MP_2, \ldots, MP_n$) are adjusted until the best combination is found which fulfills the target values at given input values ($I_1, I_2, \ldots, I_n$). In the second step, the results of the optimization (right graph) are used in the model, whereby it is now considered calibrated for the prediction of desired applications. After a tuning process, the resulting outputs should approximately match the target variables ($O_1 \sim T_1, O_2 \sim T_2, \ldots, O_n \sim T_n$).

The adaptation of a gadgeting process can be realized by a three-step procedure, (see Fig. 4.22). In the first step, parameters of the model ($MP_1, MP_2, \ldots, MP_n$) are varied cross-

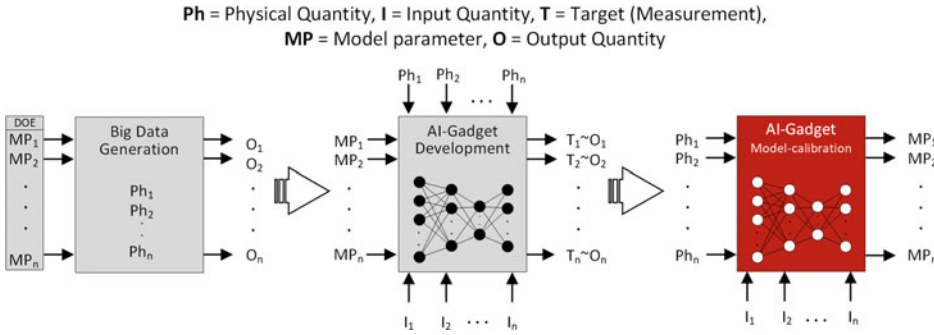

Fig. 4.22 Method for big data generation and creation of AI gadgets

wise over a DoE test space. The simulation tool acts as a data generator and generates result variables ($O_1, O_2, \ldots, O_n$) for each variation. In the second step, these variables are correlated with the physical input variables ($Ph_1, Ph_2, \ldots, Ph_n$), which are relevant for the considered model, and further input variables ($I_1, I_2, \ldots, I_n$), which are required by the model. By the approach of a suitable AI model, the aim is to generate the same target variables that corresponded to the model output in the first step. In the future, the AI model can be applied. Instead of performing a complete calibration again, the AI gadget is used, which initiates a reliable and fast prediction of the respective model parameters.

According to this idea, a modified process loop results. The delivery of results remains the responsibility of the simulation tools—the parameter calibration of all models, however, is done by the corresponding AI gadgets. If this procedure is integrated into the development, the following novel process loop results (Fig. 4.23).

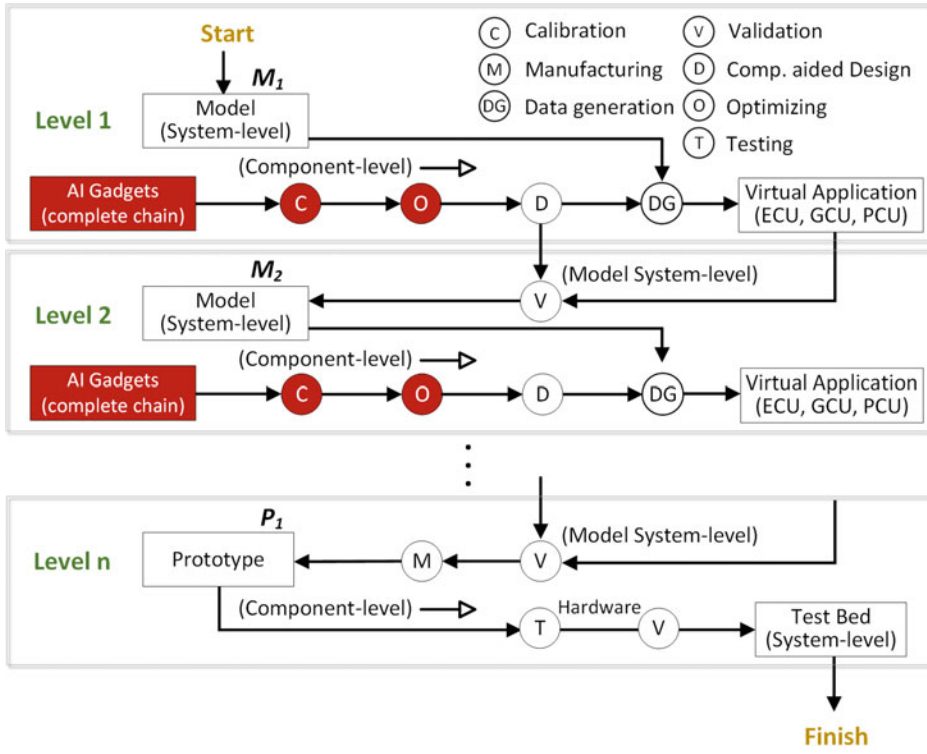

Fig. 4.23 Development of a prototype production: Gadgeting sub-concept

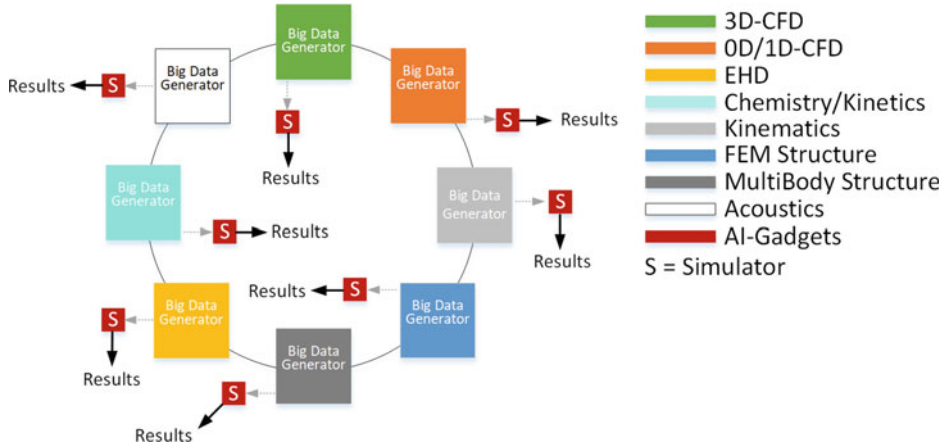

Fig. 4.24 Gadgeting full concept: AI gadgets as a result supplier

2. Full concept: AI gadgets as result supplier

The second and strongly extended process for using the lean structure of selected simulation tools is their pure use as data generators as shown in Fig. 4.24. For the generation of further results, the full concept is exclusively based on AI gadgets. Which powertrain concept is actually being developed plays a subordinate role.

A corresponding process chain within a development unit is illustrated in Fig. 4.25. In principle, it is conceivable that multiple AI gadgets can be interlocked and components can

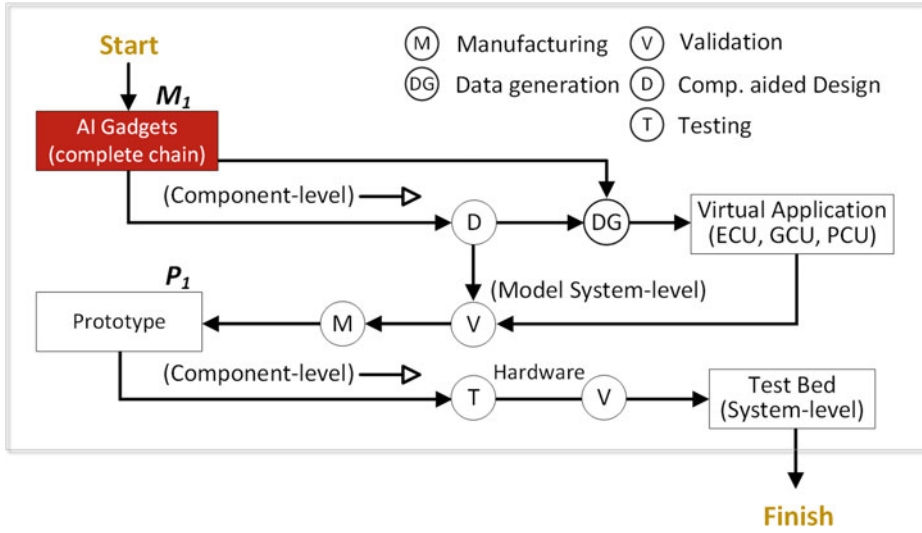

Fig. 4.25 Development process of a prototype production: Gadgeting full concept

be developed on a subsystem level in a single-step process. On the way to the first prototype (P_1), massive time saving is achieved. Finally, validation of the component level and the system level completes the development loop.

A number of topics are mentioned here, such as how gadgeting can be used in the development of combustion engines and so to concretize the novel process loop. Fig. 4.26 shows the most important submodels that are very typically performed using the means of simulation. Here, a boundary is drawn around the combustion chamber, which contains relevant submodels for the development of combustion processes. A typical loop within here encloses the topics (turbulence, charge exchange, ignition delay, combustion, wall heat losses, cyclic variations, knocking, raw emissions, exhaust aftertreatment and acoustics), here described as extensive effects. To be able to execute these models, boundary conditions are needed, which are represented by further submodels. These are characterized by intensive parameters.

In principle, it is possible to replace any individual submodel or even a group of submodels, which are usually determined physically, by the concepts of AI. Intensive parameters stand for quantities that have a direct and significant influence on the engine behavior — extensive effects, on the other hand, express the corresponding influence on a physical level.

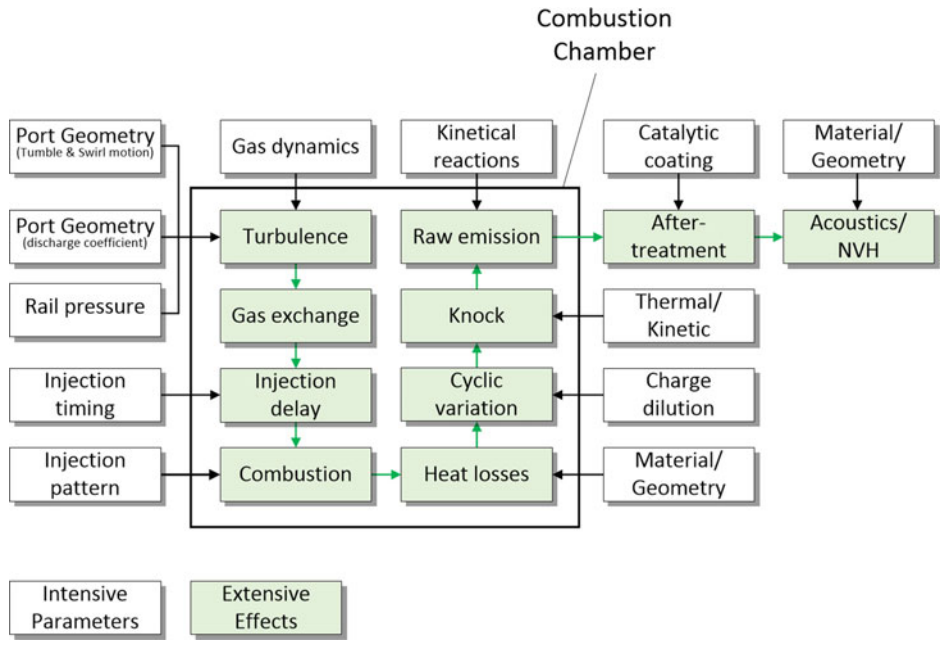

Fig. 4.26 Submodels in the development/simulation of combustion engines

During data generation (big data process), it is crucial which design of experiment (DoE) is selected to fill the design space. Additionally, each level of AI requires a different DoE method. There are basically four categories to be differentiated:

1. Space Filling Design
This experimental room design is suitable for both continuous (variable) and discrete (fixed) input parameters. The space filling design aims at filling the experimental space in such a way that all spaces are evenly covered, i.e. the distance between any two adjacent experimental points is maximized. In case of measurement outliers or areas of high sensitivity, this method is suitable to cover the experimental space evenly in the best possible way [32].

2. Robustness Design
This design variant is suitable for test spaces that require high robustness due to the interaction between controllable and uncontrollable noise. Control factors are used here, whose settings are made by the user or automatically and ensure that the noise of the test output is minimized.

3. Statistical Design
Statistical design of experiments provides an organized approach to generate data and optimize any process with multiple parameters. In a DoE approach, experiments can be run in random order while changing several variables simultaneously, rather than varying one parameter at a time while keeping all other parameters constant. The advantage of randomly selecting experiments is that each of them, as part of an overall population, has the same chance to contribute to the training of a model.

4. Optimal Design
Statistical designs such as the Full Factorial require an ideal and simple experimental setup, which is unsuitable for fulfilling multiple experimental objectives. The Optimal Design, on the other hand, is an approach that tries to take into account the entire observation space and to fully exploit the accuracy. It focuses on the minimization of a criterion related to either variance or other statistically relevant quantities. Two of the most common criteria are the D-criterion and the I-criterion. The D-criterion refers to the variance of factorial influences and the I-criterion to the accuracy of the prediction (Fig. 4.27).

Integration of AI-based development into lifecycle models
Lifecycle models set important quality and safety standards in the implementation of products within development processes. They serve as guidelines that support project monitoring and keep necessary development steps together so that they are not overlooked. Due to their phase-oriented basic framework, they provide decisive advantages in their application for the project management of product developments, not only for the project manager but also for the entire development team.

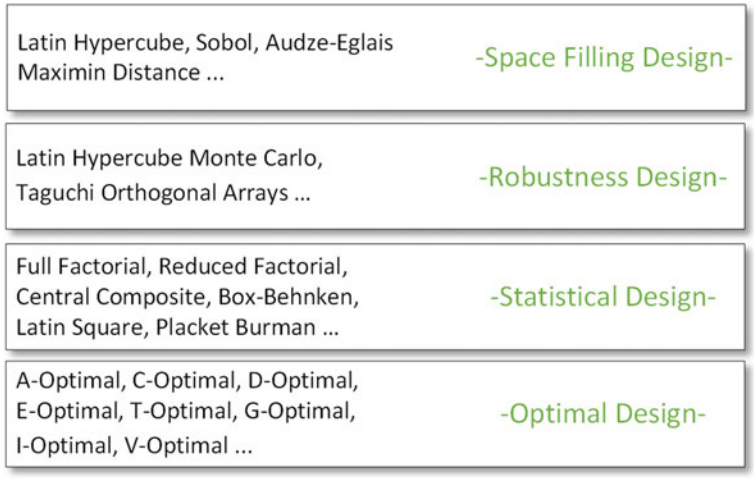

Fig. 4.27 DoE approaches for the creation of an experimental space

With the introduction of controlled development lifecycles, it could be proven that qualitative standards of product results could be raised in the medium and long terms. They demand a draft of system and software architectures in an upstream project phase and emphasize that all requirements for a system must be clearly defined before the start of an implementation. After the draft phase throughout the operational application, they serve as an orientation and contribute to realistic time and cost planning.

Especially in the automotive sector, the so-called V-lifecycle, which can be assigned to the classic lifecycle models, has become generally accepted over the last decades. Primarily in this sector, it is important to consider different components of products as well as software, mechanics, electronics or mechatronics as an integrated unit and not separately. The strict orientation of V-lifecycle models supports mutual links between different system levels (such as hardware and software) and emphasizes test, verification and validation phases to ensure the integrability to each new development stage.

The following diagram shows that the integration of AI can be very sensibly designed in the entire left half of the V. This includes the feasibility phase, the concept phase, design and implementation, starting at a system level all the way down to a component level (Fig. 4.28).

Every company has its own historically grown development DNA and individual product creation processes. In this respect, lifecycle models must be tailored to meet the internal, project-specific requirements. From a historical perspective, it can generally be seen that development NDAs between companies were much more different just a few decades ago than they are today. Due to international and open communication platforms as well as conferences, where internal development methods are disclosed, lifecycle models that hold together and standardize the core of complete development processes and, above all, a globalized employment culture where employees transfer professional experience from different

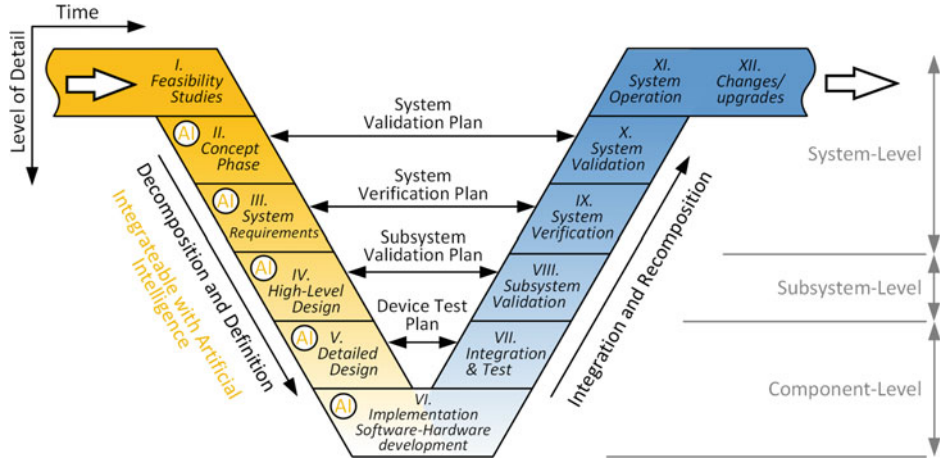

Fig. 4.28 Integration of AI into the V-development lifecycle for automotive applications [33]

companies to a new company, development cultures in the automotive industry are becoming more and more similar worldwide. In this respect, the transferability of lifecycle models has become easier and more flexible than ever.

Powertrain Development with Artificial Intelligence

5

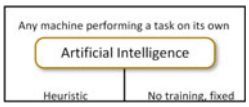

Artificial Intelligence (AI) is the science of transforming human learning, thinking and decision-making structures into mathematical models. Its goal is to enable machines to perform tasks intelligently and to detach them from an explicit path of programming a solution. The word AI was first coined by John McCarthy in 1956, who had the vision of giving computer systems a kind of decision-making power so that they work according to the model of human rationality. An intelligent system is defined as one that is able to perceive its environment and take measures to optimize any given situation on the basis of cognitive decisions. The variety of applications and imagination in the use of intelligent systems is great, and initially they did not primarily lie within the framework of technological developments but mainly in the medical field, such as neuroscience and psychology, as well as in disciplines of economics, linguistics and philosophy.

In the last few years, artificial intelligence has gained enormous importance. The availability of large amounts of data is the key basis for the application of AI. Since companies have been collecting large amounts of data of their business characteristics since the beginning of digitization, the majority of them are increasingly interested in using AI as a logical consequence. AI can help to decipher and interpret patterns within data and thus to extend development processes in an advanced way.

The original version of the chapter has been revised. A correction to this chapter can be found at https://doi.org/10.1007/978-3-662-63863-7_6

A. Mirfendreski, *Powertrain Development with Artificial Intelligence*, https://doi.org/10.1007/978-3-662-63863-7_5

5.1 Models of Artificial Intelligence

Artificial intelligence is a broad term and offers a wide range of possible applications. AI is often associated with the idea that machines or algorithms convey human thought patterns. It is important to realize that human thinking and its correctness can only be measured subjectively and does not necessarily have to correspond to rational thinking. An additional difficulty is that thought patterns or the solution of a thought process can trigger a behavior, whose correctness can only be judged subjectively. In this respect, a behavior as a result of a thought process can also be differentiated into a human and rational one.

Human thinking

The term thinking refers to all mental processes that combine imagination, memory, experience and a resulting process of cognition. Only the end product of thinking is consciously perceived as a result, rarely are the thought processes themselves accessible to one.

Thinking is a process that must generally be strictly separated from perception and intuition. Perception and intuition are not conceptual; in contrast, thoughts are propositional and tangible. If one examines the process of thinking, it can either be developed constructively or be triggered by an idea, a spontaneous feeling, a situation or by sensory impressions [34].

Thinking in detail is a current research topic in various disciplines. The complexity behind this lies in the construction of a thought structure, which can look very different depending on the discipline. In order to better understand the psychological, neural and biochemical mechanisms underlying a thought, brain researchers are studying the cellular level of thinking.

If a machine is attributed the ability to think humanly, then this refers in particular to the calculation process, which is comparable to the thinking process of a human. Thinking processes can be investigated and understood if they are related to the solution of a certain problem. In turn, solution paths can be manifold, which means that they have to be studied individually depending on the field of expertise and application in order to provide a tailor-made training for a machine. If a certain input-output pattern corresponds to that of a human, this is only the first proof that the thinking process could also correspond to that of a human.

A. Newell, J.C. Shaw and H. Simon developed the computer program “General Problem Solver” (G.P.S.) in 1959, which should be able to represent any form of problem definition by mathematical formulations. The focus for the developers was not to predict a correct solution for any given problem, but rather to design the solution path according to human logic in order to get to the same result. The interdisciplinary field of so-called cognitive science concentrates on bringing together computer models from AI and experimentally acquired techniques of psychology in order to determine precise test-oriented theories of the human mind [35].

Rational thinking

Making conscious decisions is an ability given to humans, which is only possible with the presence of imagination. An imagination of the effects of different or successive actions enables us to choose a preferred action from various options. In order to make such a decision, 1. a complex imagination in multidimensional levels and 2. target states are required, which make the effects of an action assessable. If an imagination corresponds to the actual effects and if, in addition, an effect is correctly measurable, it can be assumed that the original action is directly and functionally related to the solution. Both aspects are called epistemological and instrumental rationality.

Rational thinking is a skill that is not innate to humans, but must be learned and trained. Until then, our imagination seems to be afflicted with many shortcomings. It stands in contrast to irrational thinking. The ability to separate both thought patterns from each other is subject to a development process in our brain as it forms structures. The art of distinguishing conclusions that are correct in the majority of cases and therefore provide a good first estimation from cases that provide false results is called "heuristics". Since our brain learns through repetition, correct conclusions remain in our memory and overlay the cases in which we were wrong. On the other hand, if we reflect superficially, it is easy to overlook irrational thinking. This situation can lead to a situation in which one sees oneself in the right even if this is not the case. Human decision criteria are often based on experiences of many individual decisions from the past. Only the observation of past consequences, which have arisen from previous decisions, forms a sum of experiences, on the basis of which the following decision can be made. Thus, it can be said that human decisions are of statistical nature [36].

To know something means that it has been learned, and this in turn means that neuronal structures have been formed for it in the knowledge formation process. Knowledge can thus be directly related to complex functions in the brain. Unlike in an AI system, however, these functions are not activated by operators, but by biochemical processes and expressed through thinking. The reliability of biochemical processes can be equated to a probability thesis. According to this, probability is a property of the brain and a measure of the extent to which biomechanical processes can represent reality with the ability to abstract. Rational thinking is therefore also called thinking that is based on observable reality.

If one moves to the system level, systems are interpreted as rational if they deliver results "expected" by humans. Since the early sixties, programs have been developed in research, which are able to solve problems, which can be represented by logical notations.

Human and rational behavior

The British mathematician and logician Alan Turing is still considered one of the most influential theorists in computer science. In conjunction with his Turing machine, which was introduced in the mid-thirties, he succeeded in proving that machines can in principle succeed in reproducing complex relationships of reality on a mathematical basis. He postulated that cognitive processes can be reproduced as long as they can be broken down into algorithmic

relationships. As a result of his considerations, in 1950 he presented the Turing test, which is still known today and is considered a recognized measuring method for proving artificial intelligence. The test model was defined in the written communication between a computer and a test person. The computer tries to confront the tester as a thinking individual. Only once if a communication is completed and the respondent was unable to determine whether his communication partner was a human or a machine was the test considered successful. To achieve this, the machine must be able to fulfill the following levels of abstraction [37]:

1. The processing of a natural language to understand the information it contains;
2. A knowledge compilation to store the exchanged information;
3. The automated inference to formulate appropriate answers from the stored information;
4. Machine learning to determine customized answers from the information.

Developers have succeeded in imitating human behavior over short periods of time, both in written language via so-called chatbots and speech generators. If the test person is informed, however, that the communication partner is a computer, they can easily expose it by asking specific questions. In order to model rational behavior algorithmically, so-called "agents" are used, which take on a monitoring function in a learning and training phase. The agent is assigned the task of grasping its environment, understanding input and disturbance variables in relation to output variables and autonomously adapting changes in the system to achieve the desired result. Furthermore, it has the task to imitate rationality by means of its control criteria. But there are situations, where no logical solutions to a problem exist. Especially in these cases, the agent is required to design reflexive solutions and extend its "rationality" to arrive at a solution that is not explainable via logic. Thus, the agent acts beyond the laws of logical thinking, because unlike humans it does not need to prove logical conclusions to its decisions. The agent is able to present results, which our mind could not achieve due to its limitation of the human thought structure.

Singularity

In connection with machines that have a certain degree of maturity to imitate human thinking and rational behavior, the term singularity is often used. Technological singularity describes theories that provide an outlook into the future. It is mainly understood to be a specific point in time that machines reach, from which they are able to develop autonomously and rapidly by means of artificial intelligence. This point in time is predicted as a possible, historical revolutionary event, behind which the future of mankind is no longer foreseeable. For researchers, the estimation of an exact point in time is currently difficult, but it is possible that it will come about unexpectedly. This expectation is based on the observation that technology and science have developed ever more rapidly since the beginning of mankind and are subject to an exponential speed of development, especially in the last century [38].

Singularity is often associated with the idea that human-like robots, also known as trans-humanoids, live next door to us humans and are far superior to us in all our characteristics, speed, strength, intelligence, availability and efficiency. However, according to the current state of knowledge, this idea is based more on science fiction than a realistic prognosis. The initial singularity will rather take place on an algorithmic and a process-optimizing level than on a robotics level. Already today, state-of-the-art and intelligent algorithms are used in almost all technological development levels to make a process more efficient. If these processes can be made even more reliable and, above all, more autonomous in the future, this will primarily mean that the working world of technology, economics, finance and banking and other sectors will continue to be subject to topological change. Accordingly, AI will creepingly rearrange the interplay between algorithmics and the labor market. The question of the extent to which jobs are endangered by the takeover of computers has long been under discussion. While this has not yet been proven to be a case, a reorganization of job topologies and a change in operative work are already underway. It should be possible to extrapolate this trend further for the coming decades. The following figure schematically depicts the point in time of the singularity on the timeline of human intelligence development (Fig. 5.1).

The beginnings of machine learning and the path to artificial intelligence go back to the 1950s. A multitude of individual achievements has paved the way for AI to become a powerful tool. The special feature of AI is now that it is available to all users through software. Already today, we are experiencing a remarkable increase in the number of new companies that use AI technologies. This leads us to expect that in the coming decade, economic and social digitalization processes will face a significant next wave. The timeline Table 5.1 provides an overview of the most important milestones of AI from its initial founding to the present.

AI is identified by economic studies as the key technology of the future. Many of these studies have already dealt with market potentials and their effects on the most diverse economic fields. A study commissioned by the German Federal Ministry of Economics and

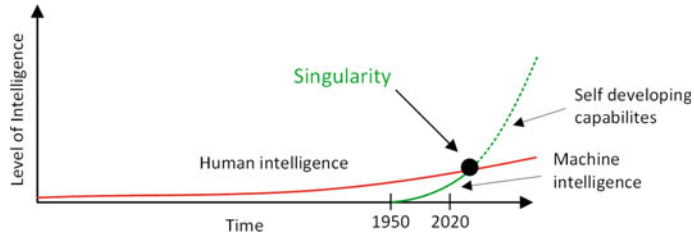

Fig. 5.1 Singularity [39]

Tab. 5.1 Milestones in artificial intelligence

1950	Alan Turing presents the Turing Test	1982	Dragon System introduces NUANCE, the development of the first commercial speech recognition system
1950	I. Asimov presents 3 laws of robotik	1986	Renaissance through neural networks by D. Rumelhart, G.E. Hinton and T.J. Sejnowski
1951	M. Minsky builds the first nuero computer called SNARC (Stoichastic Neural Analog Reinforcement Computer) with 40 synapses	1989	Carnegie Mellon University, Pittsburgh presents first autonomous vehicle based on neural networks
1955	First self-learning game „Checkers" is programmed by A.L. Samuel	1993	Computer POLLY gives tours on the seventh floor at MIT and interacts with visitors
1956	J. M. Carthy founds the word „Artificial Intelligence" as a research discipline on the scientific conference Dartmouth college, New Hampshire	1997	IBM DEEP BLUE beats the world chess champion G. Kasparov in chess
1956	A computer program named LOGIC THEORIST written by A. Newell, H.A. Simon and C. Shaw. It was the first program mimicing problem solving skills of a human being	1997	In Nagoya (Japan) the first robot world championship RoboCup is held with 37 participants
1959	MIT establishes an institute for AI	1999	Sony presents the first AI-based robot AIBO
1959	A. Newell, H.A. Simon and C. Shaw develop the computer program G.P.S (General Problem Solver) at the Carnegie Institute of Technology, Pennsylvania	2009	Stephen Wolframs develops the first semantic search engine called WolframAlpha
1961	The psychologist F. Rosenblatt implements perzeptron concept in the computer Mark I. Machine becomes adaptive through the trial error method	2009	Google builds the self-driving vehicle WAYMO
1961	First industrial robot „Ultimate" used in General Motors production line in Ewing Township, New Jersey	2010	Natural Language Generation (NLG) such as SARA are narrative AI tools presenting the ability to write documents
1966	The psychologist J. Weizenbaum develops the chatbot ELIZA, pretending to be a psychotherapist.	2010	Robust training of neural networs with multiple hidden levels becomes possible by G. Xavier and K. He
1968	First AI program for natural speech recognition named SHRDLU is presented by T. Winograd at MIT	2011	IBM supercomputer WATSON beats former Jeopardy champions
1969	Stanford Research Institute (SRI) introduces SHAKEY, the first intelligent locomotive	2015	Daimler presents the first autonomous truck on the A8 motorway
1970	Stanford University introduces MYCIN in LISP program, which analyzes blood infectious disease and suggests therapies	2015	Personal assistance systems such as Siri, Google Now, Alexa and Cortana are being commercialized
1971	The STANFORD-CART is presented as the first autonomous vehicle	2015	Open Source AI tools like TensorFlow, Azure, CloudML, Amazon AI, etc. are offered to users worldwide
1978	Facial action coding system (FACS) characterizes facial actions to express individual human emotions defined by P. Ekman and W.C. Freisen	2016	Google's Deepmind AlphaGo beats the reigning Go Champion Lee Sedol
1979	First AI expert system CADUCEUS for medical diagnosis specialized on internal medicine is presented	2016	NVIDIA Introduces the Supercomputer for Deep Learning and AI
1980	LISP based computers are available on the market	2045	Singularity of robotics predicted. The AI's intelligence is superior to that of humanity and can evolve independently

Energy uses intensive surveys of companies in Germany to determine the extent to which AI technologies are already being used in the manufacturing sector by small and medium-sized enterprises (SMEs) and large enterprises (LEs) in their respective value chains. For a total of nine value-added chains, an average of 15% of SME and 25% of LE stated that they already use AI technologies at least to a small extent [40] (Fig. 5.2).

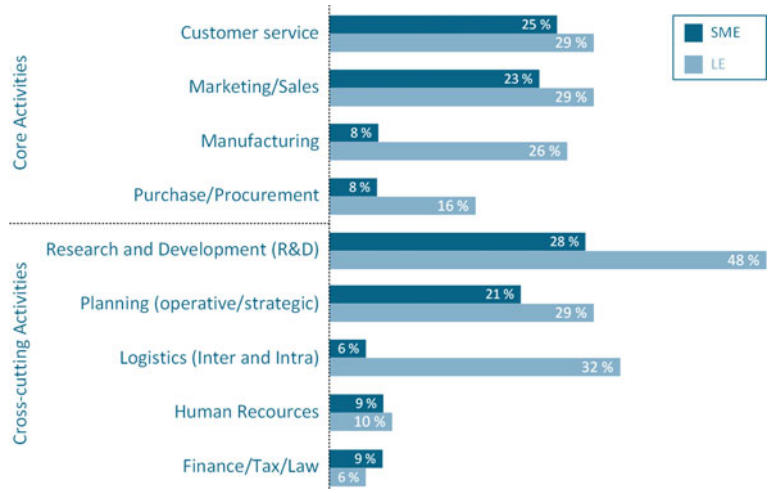

Fig. 5.2 Proportion of SME and LE that already use AI technologies, 2018 [40]

For a more comprehensive picture, the following diagram additionally considers the proportion of SME and LE cooperating with external service providers (Fig. 5.3).

A further representation permits the insight into the expectations of the SME and LE as a perspective outlook, specifically, how strongly it can be assumed that AI technologies will be used in individual processes of their value creation chains in the near future. The result clearly shows that all companies in the manufacturing or production sector foresee an increasing use of AI technologies in their processes (Fig. 5.4).

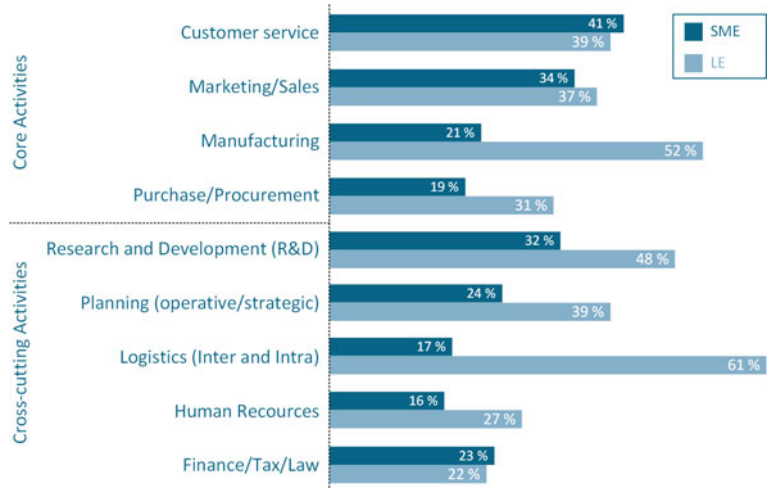

Fig. 5.3 Proportion of SME and LE which work with external AI providers, 2018 [40]

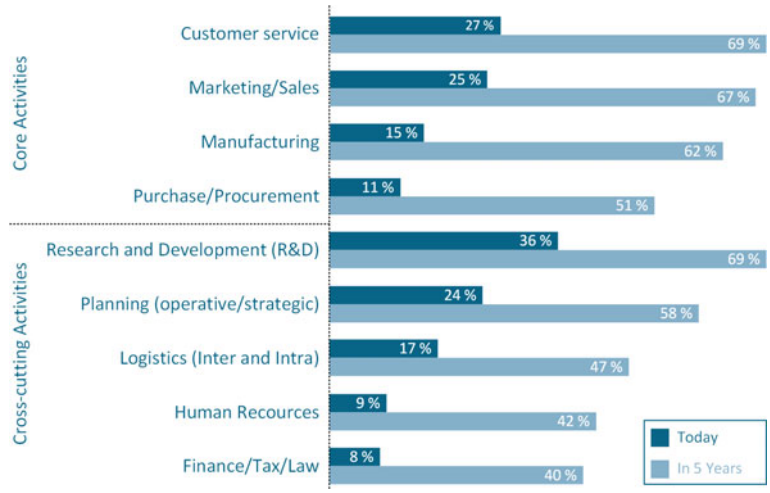

Fig. 5.4 Proportion of SME and LE that use AI technologies at least to a small extent today and probably in 5 years, 2018 [40]

5.2 Overview: Levels of AI

If models are discussed in general, a distinction is made between **deterministic** and **stochastic** models. If a recurring, identical input of parameters is followed exclusively by the same output, the model is defined and reproducible. This is a characteristic that applies to deterministic models. Here, the algorithm is clearly defined, i.e. all intermediate results that are generated are also identical. This is in contrast to non-deterministic models. As a rule, all realistic processes are not comprehensively tangible due to their complexity. Unpredictable disturbance and inaccuracies lead to dynamic input conditions, which have an equally dynamic effect on the result.

Especially in the simulation, one tries to achieve reproducible results. This is in contradiction to the fact that the goal is to reproduce stochastic scenarios. This is only possible if disturbance effects are neglected or combined in the form of assumptions and simplifications so that all boundary conditions are always identical.

The term artificial intelligence is popularly used in an inflationary way and meanwhile conveys the image that a process can be carried out by machine-learning and is therefore subject to a strong blurring. Even simple algorithms of mathematics, which were previously referred to as such, now enjoy an upgrading through the categorization of AI, which is correct as such, insofar as they follow certain basic principles of intelligent functions. Expectations

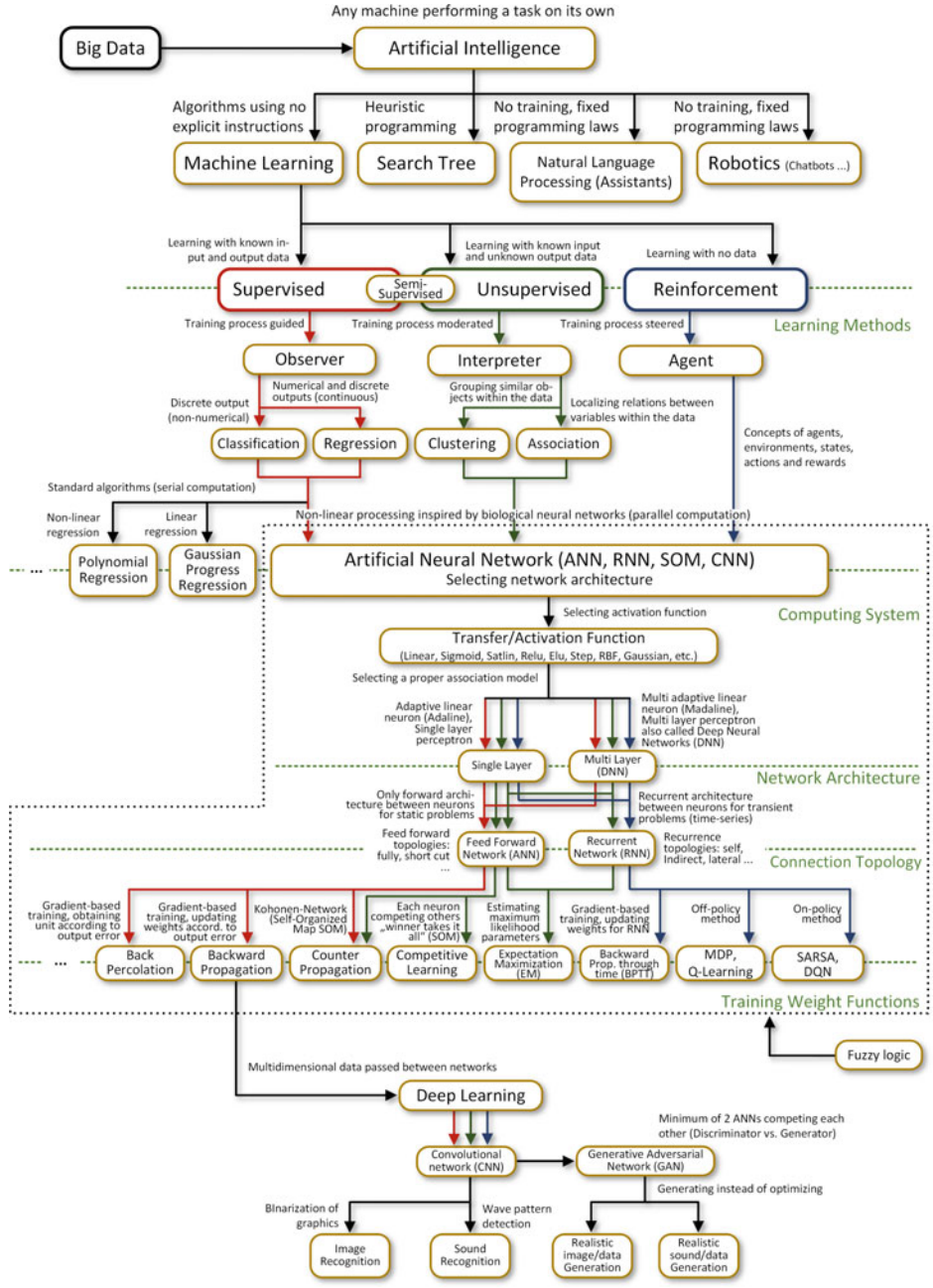

Fig. 5.5 Flowchart: Levels of artificial intelligence

of an AI model can vary greatly. Therefore, it is relevant to understand that we currently have various AI levels available, with varying degrees of model creation, individual degrees of complexity, and suitability for very extensive application fields. Looking ahead to this chapter, the flowchart shown above provides a detailed overview of the different levels of AI (Fig. 5.5). The chart also serves as a guideline, on which later contents in this book will continuously be referring to. Along the flowchart, all levels of AI are discussed in their basic features and general concept examples are presented, which are intended both to concretize the techniques and support the reader in stimulating his or her own creativity and to provide ideas for the development of his or her own application ideas.

5.3 Search Tree

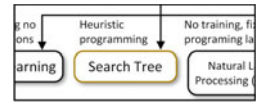

In the field of computer science, search tree functions belong to a long-established and important method of artificial intelligence. In an optimization process, search trees enable to transfer associative structures into an algorithm based on human decision-making. Among the most important are the A* (A-star) algorithms (Fig. 5.6).

A* algorithms are counted among the class of "informed search algorithms". The search for an optimum is formulated here in the form of weighted diagrams. From a starting node, the requirement is to find a path out of many possible ones that represent the lowest cost

Fig. 5.6 Search tree structure

function. Cost can be any target quantity such as distance, time, efficiency, consumption and battery state of charge (SOC). If the starting node of the search tree is defined, the path of least resistance (here cost function) is extended until a termination criterion is met. The selection of the correct path together with possible and innumerable alternative paths is done by a heuristic method. In this context, the teaching of heuristics is to use limited knowledge to draw conclusions about a system by an analytical estimation procedure.

At every iteration of a main loop, A* has to define which of its paths shall be extended. This is based on the cost of the respective path and an estimate of the necessary cost to extend the path to the target. In particular, A* chooses the path that minimizes $f(n)$ with

$$f(n) = g(n) + h(n) \tag{5.1}$$

Here, the variable n denotes the next node on the path, $g(n)$ the cost of the path from the start node to n and $h(n)$ a heuristic function which estimates the cost of the most favorable path from n to the destination [41].

The search depth is limited by the available computing time. On the one hand, this is proportional to the computational effort of the evaluation function and, on the other hand, it grows exponentially to the size of the search tree. Fig. 5.7 shows the schematic structure of a heuristic downward strategy (HDS). Starting from the right, the heuristic search performs as many investigations until it has optimized a subject into the fifth level. The idea with an HDS is not to provide the same amount of computing time to each subsequent node in the path but to investigate promising paths more intensively. For this purpose, all possible successor nodes x are sorted according to their neural evaluation $V_N(x)$. The evaluation function can take many different forms, which will not be explained in detail here.

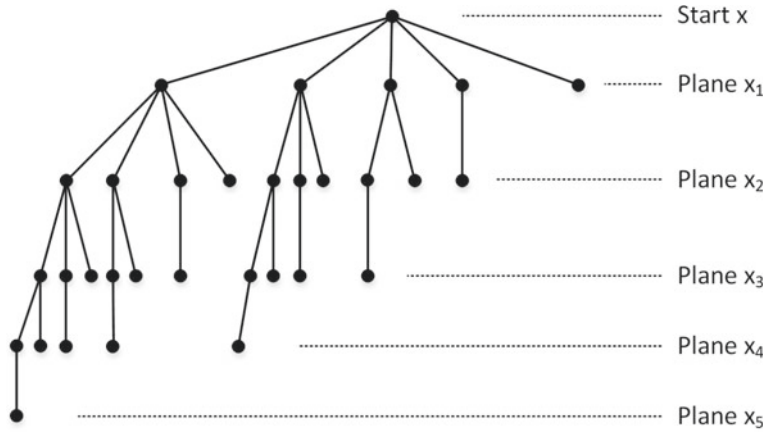

Fig. 5.7 Search tree through heuristic downward strategy [42]

$$HDS^1(x) = x_1$$
$$HDS^k(x) = f(HDS^{k-1}(x_1), HDS^{k-2}(x_2), \cdots, HDS^2(x_{k-2}), HDS^1(x_{k-1})) \quad (5.2)$$

The parameters $(x_1, x_2, x_3, \cdots, x_k)$ correspond to the successors of a node x in sorted order.

Similar to the way GPS systems work, such as those on the basis of updated driving data (weather station, traffic data) according to the heuristic search tree principle, multidimensional search trees can be nested together. Here, the result, i.e. the last node of a search tree serves as the start node of a new search tree. In GPS systems, this method of operation makes sense, since the consideration of all data over a desired route can become extremely large and the system would require a high computing time due to a massive amount of processes. The division into many different single stages can significantly reduce the workload, especially due to the continuous test procedure. Besides navigation systems, where search trees are used to determine the shortest route, they are also used in search engines. Their goal is to suggest the highest possible hits from a database when the user enters a search term. Further applications can be found, for example, in digital dictionaries, in the creation of complex database structures, for the prioritization of waiting loops or for compression algorithms of data formats such as JPEG and MP3.

The following are conceptual examples of how the search tree method can be used in the field of powertrain development (Fig. 5.8).

Example 1: Stationary application lean concept motor

This example shows how an ECU application can be performed on a lean concept motor using a search tree method. An optimization of parameters here is carried out on a stationary basis, i.e. after each working cycle on a warmed-up motor. There are a total of seven parameters objected to optimization: 1. air-fuel ratio, 2. valve timing on the intake side, 3. valve timing on the exhaust side, 4. wastegate position, 5. tumble position, 6. throttle position and 7. ignition timing.

The optimization by the search tree is done by this order and can go through several iterations until the result converges. The operating point will be predefined by a constant engine speed—optionally at controlled boost pressure through the wastegate position, which takes place in step 4 and/or additionally at controlled load, which takes place over the throttle position in step 6.

Each parameter is subdivided into 4 categories. The search tree gradually selects the optimal efficiency solution for each parameter variation and passes the best result to the next calculation step. In the first iteration loop x=1, the efficiency grows exponentially due to initially unfavorably selected starting conditions. In the second iteration loop, however, a fine-tuning process takes place, which reveals further potentials.

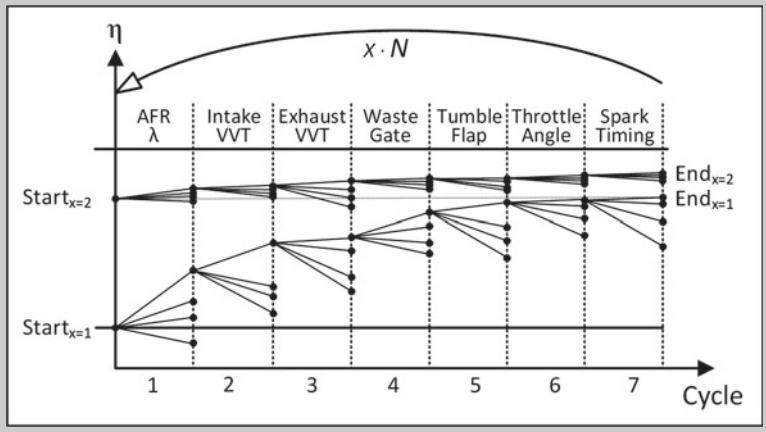

Fig. 5.8 Optimizing ECU application parameters for a lean concept engine using search tree

By anchoring the parameter sequence, this optimization method can also lead to instabilities, so that fluctuations prevent convergence of the calculation. In this case, it may be advisable to change the order of the parameters or to increase the number of categories to allow a finer approach to an optimal solution.[1]

Example 2: Operation strategy hybrid engine: Emission reduction in the warm-up phase versus loss of efficiency

The next example shows how the method of the search tree and the A algorithms can be used for transient warm-up optimization on a hybrid engine. Usually, low fuel consumption and low exhaust emissions are contradictory. To realize both at the same time is not possible, because the reduction of one causes the deterioration of the other.*

In a warm-up, for example, after starting an engine, it is import ant to warm up the exhaust system quickly by means of high exhaust gas temperatures so that the catalyst reaches its operating temperature (catalyst light-off), which is typically in the range $200°C–300°C$. *Only then does it start to convert pollutants such as* CO, HC *and* NO_x *efficiently. An internal measure that typically implements this is late ignition timing. When the exhaust valves are opened, an enthalpy flux at high temperature (unconverted energy to the crankshaft) is transferred. The exhaust gas heats the catalytic converter, and as a consequence, the engine efficiency deteriorates drastically.*

[1] The smaller the step size of the parameters chosen is, the more precisely not only local minima or maxima can be localized but also the interactions between the individual parameters can be decoded.

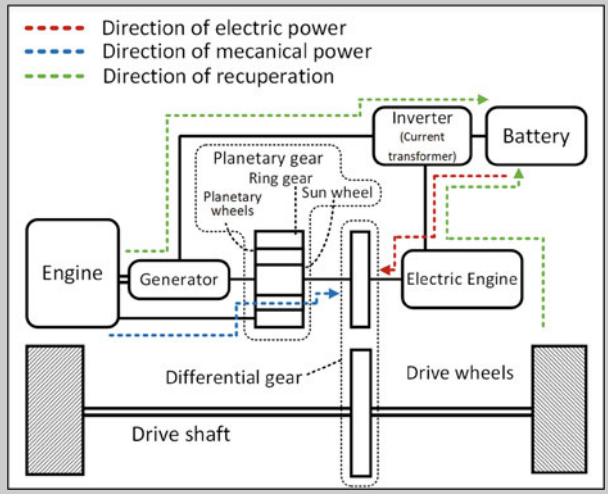

Fig. 5.9 Systemic representation of a parallel-serial hybrid powertrain

It is precisely here that the transient application of the search tree can provide efficient insights and suggestions as to how the hybrid strategy, i.e. the interaction between the combustion engine and electric motor(s) in a driving cycle, can be designed to find the best possible relationship between consumption and emissions. Fig. 5.9 shows the schematic structure of a parallel-serial hybrid drive [29].

The electrical path can be switched on or off through the parallel connection. The possibility of decoupling the electric motor results in a purely motorized, a purely electric or a mixed drive, which brings its individual advantages depending on the driving condition. The different torque sources can be added together by different types of transmission. In this example, not only a planetary gear is shown but also a direct coupling by means of spur gear or drive chain or by means of traction addition is conceivable. The battery can be charged either by increasing the load of the combustion engine (conversion of mechanical energy into electrical energy by the generator) or by recuperation, i.e. by using the braking energy. In order to use the braking energy, the electric motor takes on the function of a generator and feeds energy through the conversion chain from mechanical to electrical and finally to chemical energy and returns it to the battery.

In an experiment, for the first 200 s of the WLTC driving cycle, four different application strategies are provided to select from a search tree, which can alternate at each discrete time signal. The first strategy runs in an efficiency mode with an early ignition timing (SA) at knock limit, a closed wastegate in the acceleration phase and full support by the electric motor. The second strategy provides two intermediate solutions for all three parameters. The third strategy operates in a minimum emission mode, where the ignition timing is late, the wastegate position open and low electrical support to warm up the exhaust system quickly. The fourth operates in a recuperation mode, which starts charging the battery in braking and idling phases. During the transient run, the following integral is calculated using the sum of the effective engine efficiency and the catalyst efficiency.

$$\eta_{ges} = \int_{t_0}^{t} \frac{1}{2} \left(\eta_{eff} + \eta_{cat} \right) \tag{5.3}$$

The effective efficiency of the combustion engine is determined by the effective power P_{eff}, the fuel mass flow $\dot{m}_B$ and the lower fuel heating value H_u:

$$\eta_{eff} = \frac{P_{eff}}{(\dot{m}_B H_u)} \tag{5.4}$$

and the conversion rate of the catalyst from concentrations of the exhaust gas species at the inlet $K_{i,in}$ and at the outlet $K_{i,out}$ by

$$\eta_{cat} = \frac{\sum_{i=1} K_{i,out}}{\sum_{i=1} K_{i,in}} \tag{5.5}$$

According to the heuristic downward strategy, all four application strategies are executed in Fig. 5.10 at discrete sampling rates. After each new search tree, the variant with the highest cumulative efficiency η_{Ges} is selected, from where the next search tree is performed. By means of this, the strategy with the highest efficiency can be determined along the complete search path with a low computational load. It presents the best compromise between engine efficiency and fast heating of the exhaust system to reduce emissions.[2]

[2] The sampling rate can be selected more finely and more diverse parameters can be selected for the application strategies to ensure a more detailed breakdown for an evaluation than is shown here as an example.

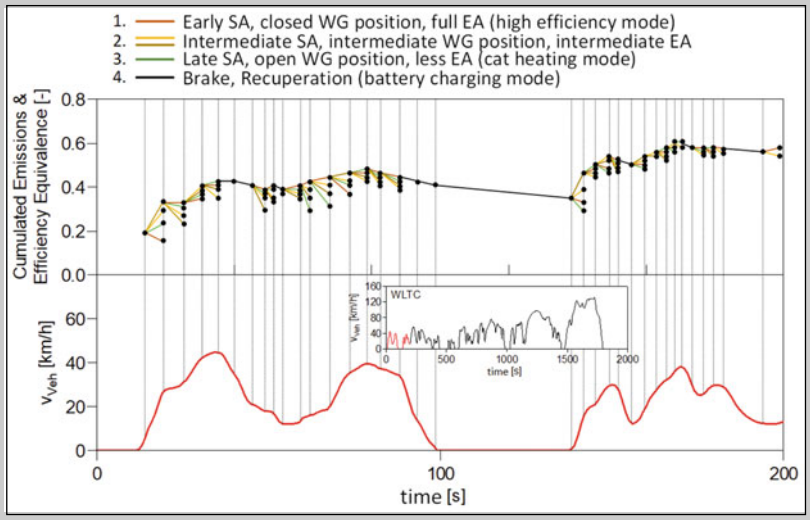

Fig. 5.10 Transient application of search tree: Optimization of a hybrid control strategy for the WLTC

5.4 Machine Learning

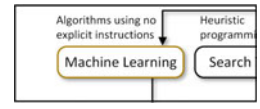

Machine Learning is a subarea of artificial intelligence. In contrast to explicit programming, it aims to enable systems to learn regularities based on data. The focus is on independent learning and the automated generation of a program code. In order to apply Machine Learning, large amounts of data are required. In this respect, the era of digitization and the resulting storage capacity and availability of enormous amounts of data (Big Data) is the actual driving force behind the development of Machine learning (Fig. 5.11).

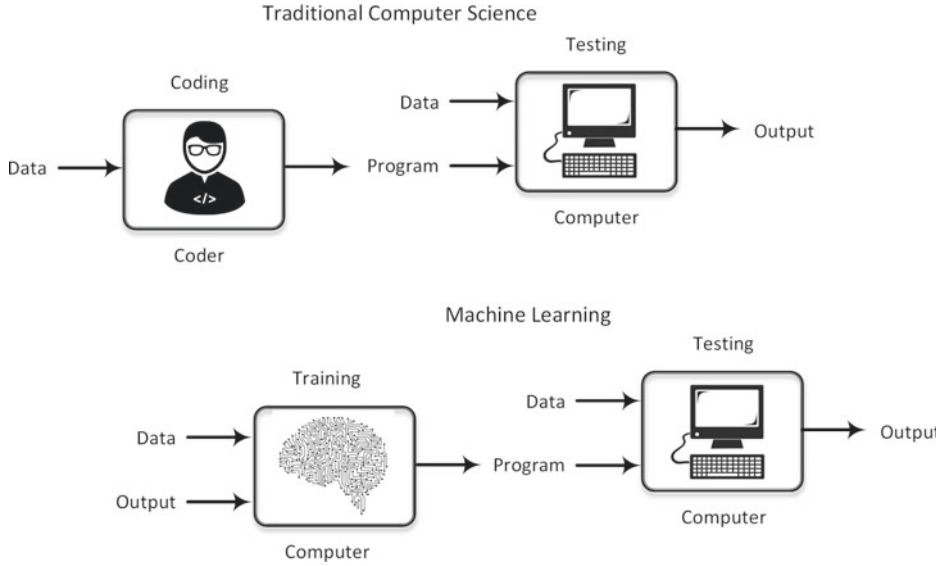

Fig. 5.11 Traditional programming versus machine learning

Machine learning includes many types of algorithms and training methods, all of which aim to generate statistical models that are able to analyze unknown data sets and make predictions based on their training data. Machine learning can basically be divided into three main learning categories: **Supervised Learning**, **Unsupervised Learning** and **Reinforcement Learning**, see Fig. 5.12 [43].

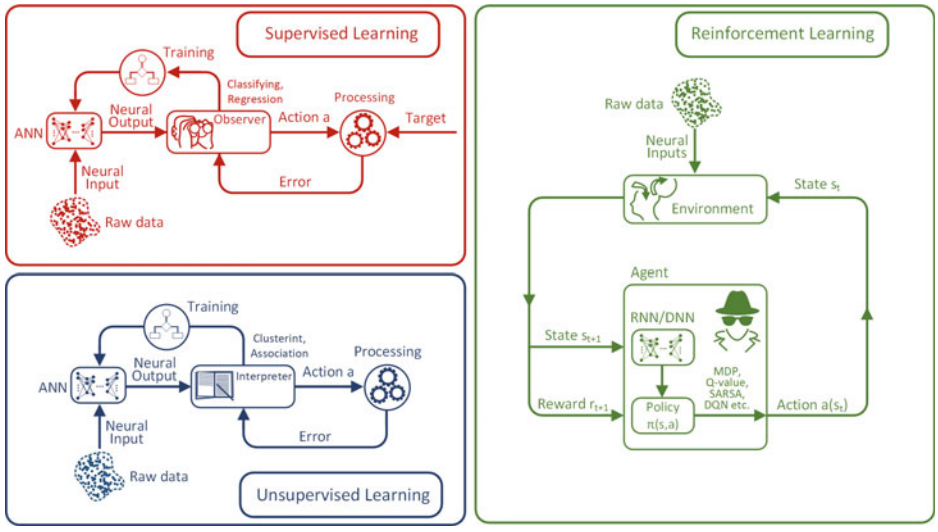

Fig. 5.12 Learning methods for machine learning

Only through the combination of machine learning algorithms and the system architecture of neural networks (see Sect. 5.5), both components combine to form a powerful overall system, which is today understood under the term artificial intelligence.

5.4.1 Supervised Learning

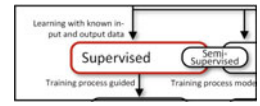

Supervised learning (SL) is one of the machine learning methods that requires a high level of interaction from the user during the training phase. For this method, both input data and output data in the form of target values must be known. Learning starts, as usual, with a set of training data selected from a larger data set. Part of the data is withheld from the training phase so that it can be used for a later validation phase. The learning method tries to recognize patterns between input variables and target variables within the data in order to transfer them into an analytical context. This can be done on the basis of different functions, polynomial approximation, Gaussian processes, or similar methods typically used in the field of powertrain development. These methods have proven to be particularly useful when real-time data generation is desired. Neural networks form a completely new basis of a model architecture, which can be used to design application paths with exponentially higher performance and process speed.

Classification and Regression

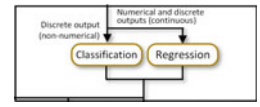

In order to analyze the significance of the data fed in, properties are first assigned to them. If data is discrete and can be categorized, a so-called **classification** is a suitable method in terms of the supervised learning method. If, on the other hand, a data set is numerical and continuous, the solution can be found by a **regression**. Fig. 5.13 illustrates both application types of supervised learning.

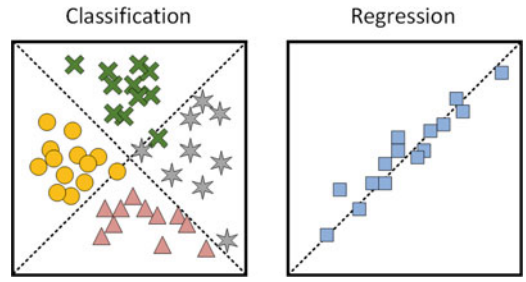

Fig. 5.13 Classification and regression of data for the supervised learning process

Observer

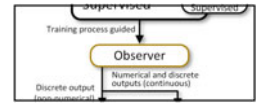

Machine learning focuses on the ability not only to reproduce results but also to steadily improve a solution path. The task of a learning system is to develop strategies to optimize behavior during the training phase. Within the framework of the supervised learning procedure, a so-called observer is used for this purpose. This observer is assigned the task to constantly monitor the error between the output of a model and the target. A simple form of strategic learning is to minimize an error between the target and the actual value. Fig. 5.14 shows schematically how the logic of such an SL procedure can be constructed in combination with an artificial neural network (ANN).

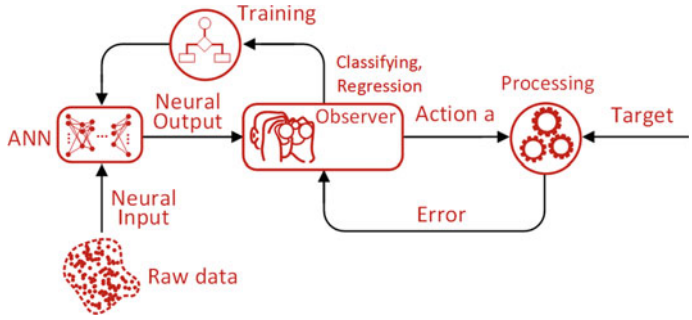

Fig. 5.14 Observer for the supervised learning process

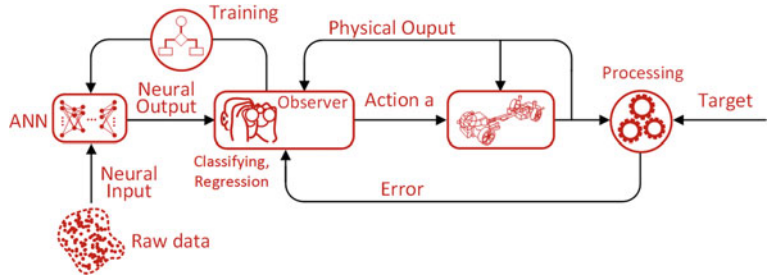

Fig. 5.15 Observer combined with a physical model

Often, it is desired to anchor parts of a calculation process in neural networks while retaining others on a physical level. This hybrid approach can be exercised by using the supervised learning method. The interaction of both systems proves to be very powerful, especially under the aspect that a physical mapping layer is transparent and comprehensible, whereas the ANN layer follows mathematical principles, and its decision-making is fundamentally unexplainable (Fig. 5.15).

Currently, the supervised learning method is widely used and is applied in economical sectors, for fraud detection, risk analysis for banking and financial sectors, product and job recommendation advertisements, Internet commerce, spam detection, speech recognition and many more.

The following examples are presented for possible applications within the powertrain development, where supervised learning is well implementable.

Example 3: Engine flow, combustion (classification)

An application from the field of fluid dynamics is the determination of the characteristics of flows. Based on physical evaluation variables, these can be classified either as laminar or turbulent or in possible subcategories. This is relevant, for example, to a) calculate heat transfer in the air path of an engine in order to draw conclusions about heat losses and thermal behavior in general, or b) to determine the transition from laminar to turbulent flow for fluids. The critical Reynolds number, which marks the transition between laminar and turbulent flow, depends not only on the geometry of the application case (tube inner flow, tube outer flow, plate flow, etc.) but also on the

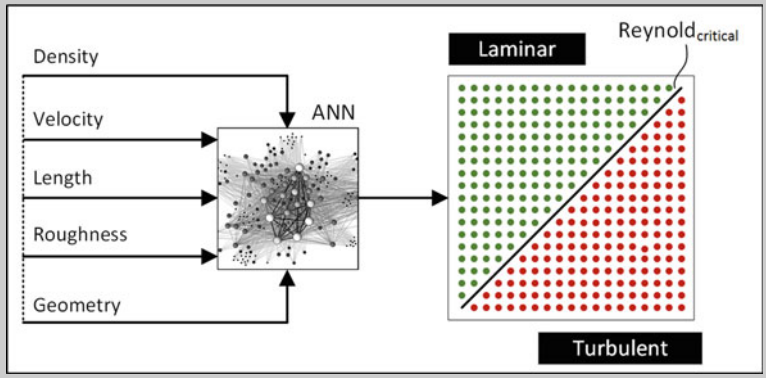

Fig. 5.16 Classification of thermokinetic data (Reynolds number)

choice of the characteristic length. The decision about laminar or turbulent or about subcategories (0 < Reynolds number < 200, 201< Reynolds < 400, . . .) is here delimited by threshold values in classes and is therefore suitable for a classification from the category supervised learning (Fig. 5.16).

Example 4: Thermokinetics (Regression)

A large part of all simulation tasks in the area of powertrain development deals with regression problems. Especially when calibrating models, the first step is often to map real data using models with a high prediction quality. In the following, a typical application is presented on how the combustion engine can be used as a combination of several submodels in an ECU system. The engine in Fig. 5.17 consists of the submodels "fuel", "air path", "torque" and " emission". Since a crank angle-resolved calculation of the variables is not necessary, the results can be generated faster than in real time.

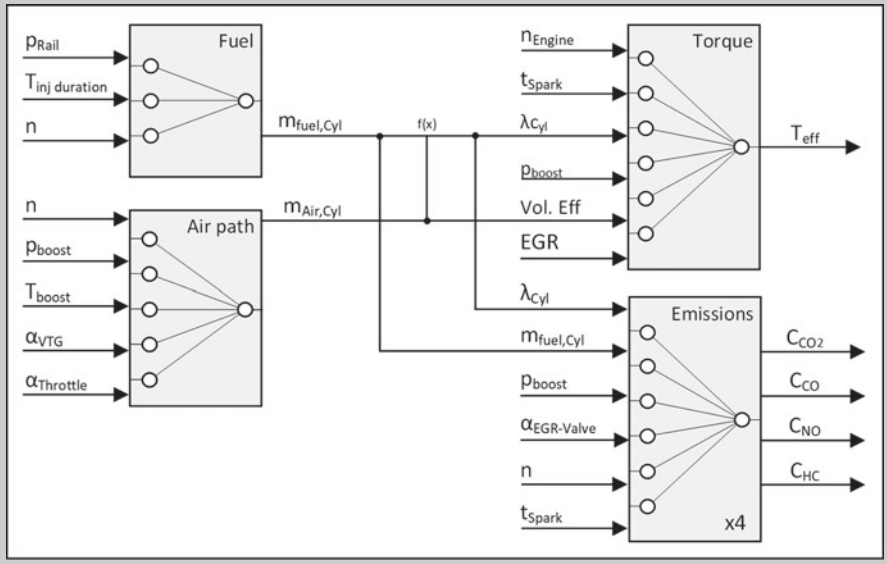

Fig. 5.17 Engine model of a control unit [44]

Fig. 5.18 presents the result of a regression analysis for the torque module (top right) based on 600 data points. The torque is shown as a function of the input parameters speed (n_{Engine}), spark timing (t_{spark}), air-fuel ratio (λ), intake manifold pressure (p_{boost}), air volumetric efficiency (Vol. Eff) and exhaust gas recirculation rate (EGR).

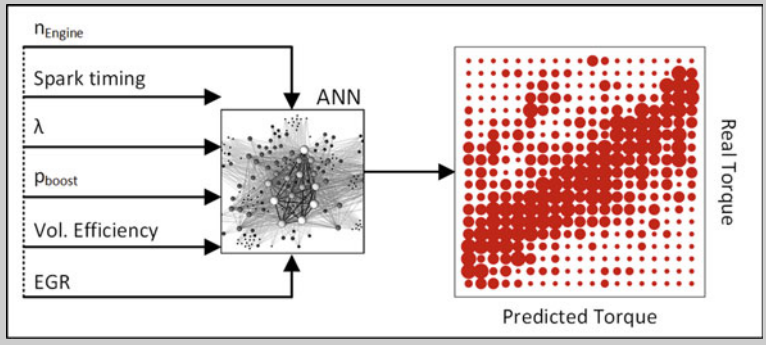

Fig. 5.18 Regression of thermokinetic data (Reynolds number)

5.4.2 Unsupervised Learning

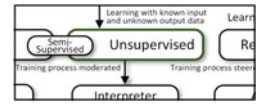

Unsupervised learning is a powerful method that is suitable when the amount of data to be examined is considerably large and, above all, not clearly identified. In principle, it can be composed of both discrete and continuous entries. The learning procedure is useful if the user lacks the coherence of data, if it is difficult to label the data or if the data does not contain any output variables. In contrast to the supervised learning procedure, the focus is not on forming a correlation between input and output data, but on characterizing features within the data. The strength of the learning procedure is based on the decoding of hidden patterns. The type of decryption is divided into two categories: The "clustering" and the "association".

Clustering and Association

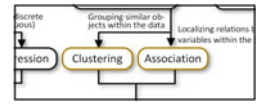

Clustering is, as the word implies, the grouping of objects that show similarities in their characteristics. The so-called associative rule learning goes one level deeper and localizes connections between existing parameters within the database. Unsupervised learning performs an iterative and autonomous analyzation process without any user intervention. Fig. 5.19 illustrates the processes of clustering and association.

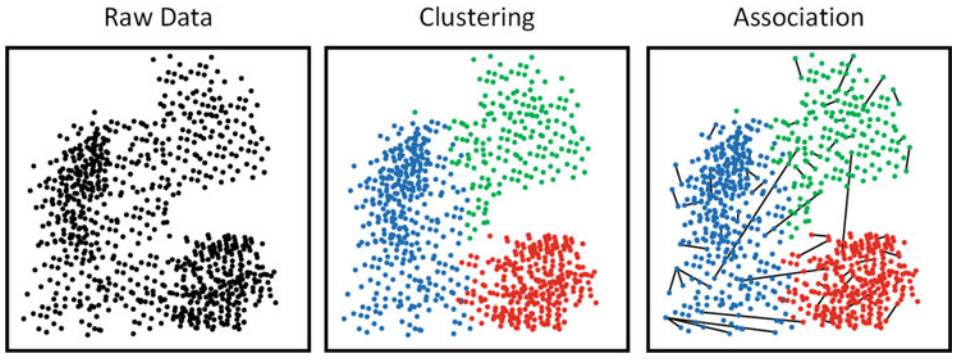

Fig. 5.19 Clustering and association of data for the unsupervised learning procedure

Interpreter

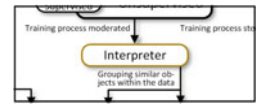

For the unsupervised learning procedure, an interpreter is generally used to process the Clustering and Association. The following diagram illustrates how the training loop is connected for such a procedure (Fig. 5.20, 5.21 and 5.22).

Ideally, an unsupervised learning process can also be used as a preliminary stage to mark unknown and unclassified data and then pass it on to a supervised learning algorithm (semi-supervised learning). Typical use cases for unsupervised learning can be found in the analysis and segmentation of customer behavior, market data, and sales data and so to optimize market activities. In healthcare medicine, the constantly growing volume of patient data is used to correlate disease findings with individual complaints and symptoms, resulting in training more reliable models that can be used to detect diseases at an early stage and provide timely treatment.

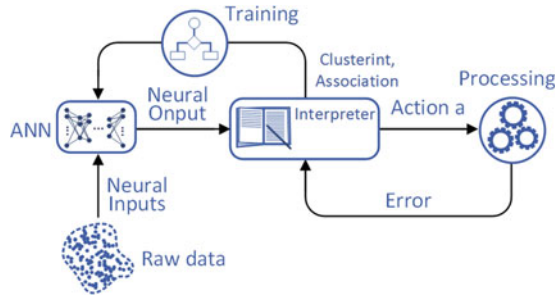

Fig. 5.20 Interpreter for the unsupervised learning process

Example 5: Pre-processing of measurement data/real data (clustering)

The handling of large amounts of data is one of the core issues that poses great challenges for engineers in many phases of powertrain development. In retrospect, as shown in Fig. 4.13, a model-based development process consists of recurring loops in which measurement data must be analyzed and post-processed. The process of selecting usable from unusable data can be very time-consuming and is often subject to the user's decision criteria. The clustering method of the unsupervised learning procedure proves to be extremely powerful for such applications. It is capable of grouping unmarked data and reliably identifying measurement outliers by a standardized process.

In the first step, data analysis can be carried out after inputting measurement data (here using the example of 10,000 data points and 10 variables each). The quantization error (QE) with the value range [0,1] describes the error between a data input and the value that a neuron outputs as a result after training. According to the error, the data is first broken down along a normal distribution. Using a threshold value, the user defines the aggressiveness with which the data selection should be performed. If a threshold with the value x is defined, the corresponding proportion of $(1 - x)$ data is sorted out of the data set (Fig. 5.21).

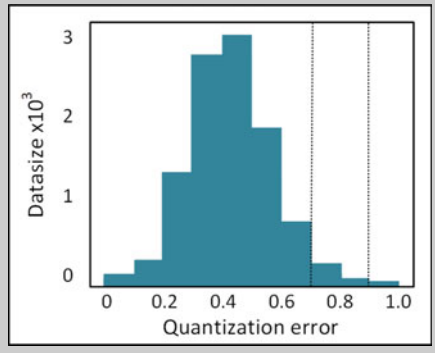

Fig. 5.21 Normal distribution of measurement outliers (quantization error) of a data set

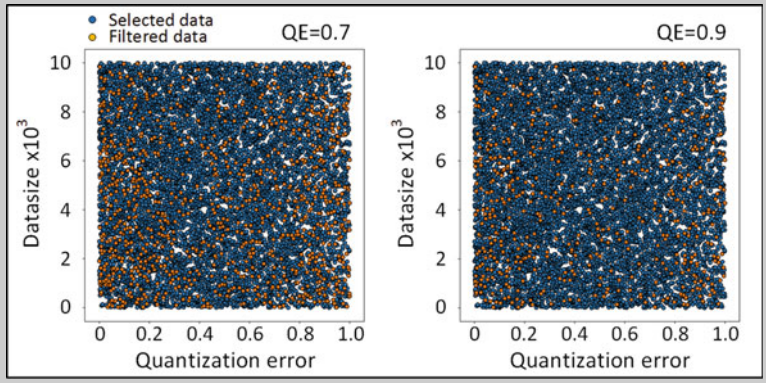

Fig. 5.22 Data selection for two different quantization error thresholds

Using the example of two selected threshold values (QE=0.7 and QE=0.9), the result of the data selection is given in Fig. 5.22.

Example 6: Interpretation of parameter studies—fuel cell efficiency (clustering)

The focus of data analysis is always the determination of influencing factors of specific input variables on one or more target variables. If there are many input variables that show a nonlinear correlation to a target variable and if these variables show additional cross effects among each other, the system is highly complex and cannot be easily interpreted without additional monitoring algorithms. Unsupervised learning can provide an enormous remedy for such cases. It is able to project data features of different kinds and especially their combinations to target values. If such a model is designed for a specific situation, it can provide fast and reliable statements regarding the data features in the future by entering new data sets.

Using the example of a fuel cell, a parameter study is carried out on the basis of a measurement series of 50,000 data sets. For this purpose 9 parameters, which determine the efficiency, are combined with a Latin hypercube DOE method (see Fig. 4.27). These are 1. temperature, 2. air mass flow, 3. air pressure, 4. humidity, 5. cathode resistance, 6. anode resistance, 7. capacitor capacity, 8. cathode stoichiometry and 9. anode stoichiometry. A self-organizing map (SOM) is trained using the Competitive Learning Procedure (see Sect. 5.5.3). As a solution, this map categorizes all possible combinations of inputs into three efficiency classes: high efficiency (1), intermediate efficiency (2) and low efficiency (3) (Fig. 5.23).

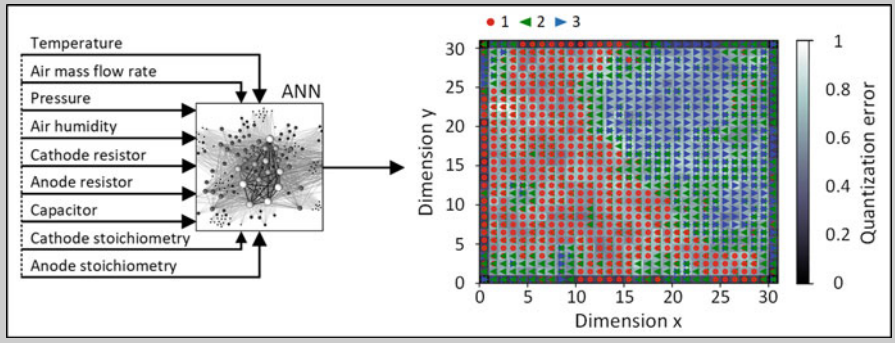

Fig. 5.23 Fuel cell: Grouping of efficiency classes

Example 7: Material Load Analysis Method (Clustering)

Another possible application of clustering is for failure analysis in the field of materials science. By entering a load type of a component (static or dynamic), the load time until material failure (fracture or deformation) and the fracture type (deformation-free, low-deformation or high-deformation) or the deformation type (plastic or elastic) and the characteristics of materials can be transferred into a data matrix. Clustering enables the introduction of an analysis procedure that allows component failures to be examined in more detail. For example, when screening a damaged component, clustering can tell which material with which specific alloys (Fe, Cr, Mo, Ni, Si, C, etc.) the component consists of (Fig. 5.24).

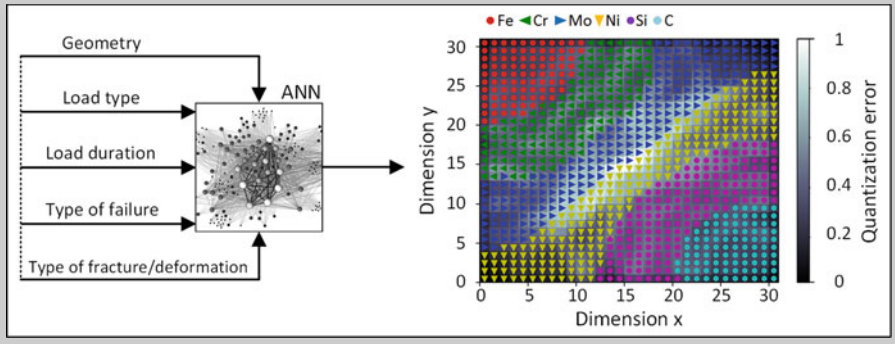

Fig. 5.24 Clustering to investigate a steel with nickel-chromium-molybdenum alloy after material failure

5.4.3 Reinforcement Learning

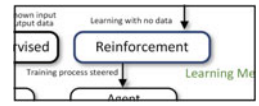

Reinforcement Learning (RL) is a further learning procedure next to supervised and unsupervised learning that is particularly characterized by its high performance and self-learning properties. RL uses a so-called "agent" as its main feature, which actively interacts with its environment, which has a set of states, independently searches for strategies (policies) and executes actions to maximize the accuracy of a model and is rewarded as a result of correct learning. While the supervised learning and unsupervised learning methods rely on existing real data during the training phase, the RL is highly dynamic and adapts to constantly changing data inputs. This is achieved through the interaction of the agent with its environment, which results in a continuous strategy adjustment and efficiency increase. Due to its self-learning properties, the system requires little to no real data and can still achieve resilient results.

When talking about artificial intelligence, users often have the idea that a smart algorithm is able to achieve the same solution faster and more efficiently than humans already achieve. If the user has a clear idea of what a result should look like, this leads to a strong limitation of learning. The challenge for AI would then be to find suitable ways to replicate the same solution. If, on the other hand, there are no concrete expected variables in a given situation that should be correlated by means of input variables, an additional degree of freedom results for the algorithm, with which solutions can be explored that go beyond the human imagination and which the user does not expect. Reinforcement learning is particularly suitable for this type of case.

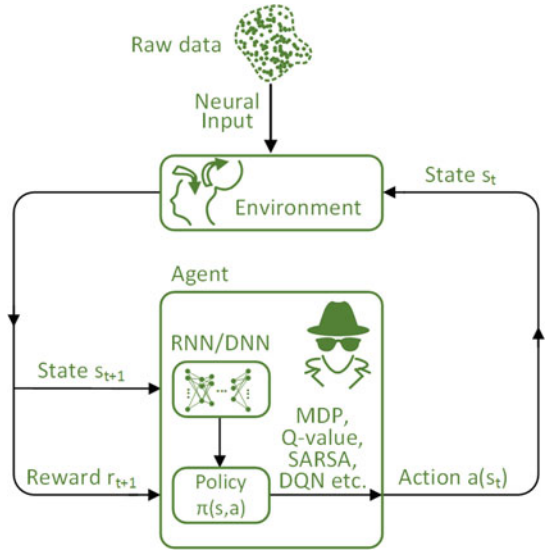

Fig. 5.25 Agent for the reinforcement learning process

Agent

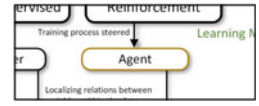

During data analysis, the algorithm receives feedback after each iteration loop from an agent, which here takes the function of a teacher. In contrast to the supervised or unsupervised learning methods, the algorithm does not only learn from the data analysis but also from an additional trial-and-error method, which gradually reinforces a mapping function for predicting a result. This has the advantage that a solution to a problem can be found via a smaller number of iteration loops (Fig. 5.25).

Example 8: Adaptive speed controller

Since September 1, 2019, the real driving emission (RDE) cycle is the certification basis for all new vehicles. Along with the worldwide harmonized light vehicles test procedure (WLTP), this should lead to more realistic consumption and emission parameters. Unlike previous certification cycles, the RDE cycle will not reflect an average real-life journey. Both the route and the load as well as driving style are flexible. This means that the route, speed and elevation profile are not fixed and can be set individually by any inspector.

One of the many fields for which reinforcement learning is suitable is the adaptive design of controllers with static control parameters so that they can always be dynamically adapted to the operating state for transient applications. Especially against the background of variable cycle profiles, adaptive control is particularly suitable for both model-based and test-based development of powertrains on the chassis dynamometer. This allows a wide variety of profiles to be run without the need for time-consuming and constantly recurring calibration of the control parameters. For a fast and reliable determination of corresponding consumption and emissions, this can result in a great time advantage.

The following figure shows a Fig. 5.26 simplified scheme of a virtual, static speed controller. In the first step, the desired driving speed v_{req} is converted into a desired torque T_{req}, taking into account existing gear ratios and existing driving resistances[3] *of the corresponding vehicle. With the previously calibrated control parameters of a PI controller (proportional component K_p and integral component K_i), the throttle is controlled by the accelerator pedal with the goal of minimizing the difference between ($T_{req} - T_{act}$).*

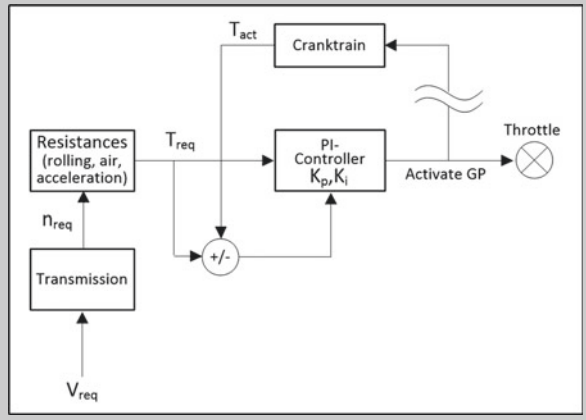

Fig. 5.26 Static control circuit for the vehicle speed of a cycle

[3] The driving resistance is usually divided into rolling resistance, air resistance, rotational acceleration resistance of all rotating parts and translational acceleration resistance of the total vehicle mass.

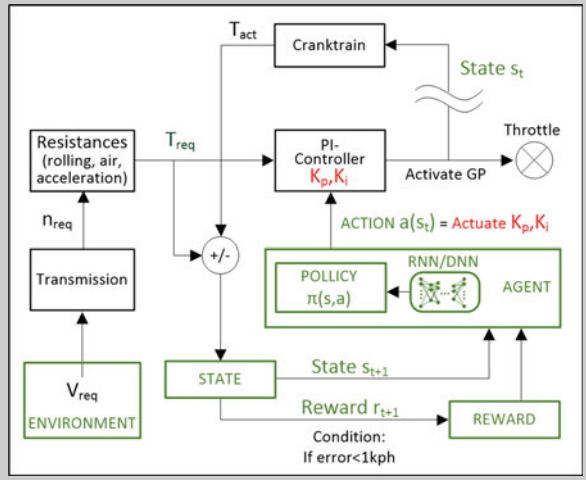

Fig. 5.27 Adaptive control loop through reinforcement learning

Since the control parameters are chosen to be constant, it must be assumed that even with good prior calibration, they will only work well in the range of the calibration. Due to the different operating conditions (speed and load) and the general variability of the RDE profile in testing mode, not all areas can be covered satisfactorily. If it is desired to use the reinforcement procedure, which automatically transfers an optimal set of parameters to the powertrain controller for each operating state, it is fundamental to define and implement the Agent, Policy, State, Reward and Environment functions into the control loop (Fig. 5.27).

In Fig. 5.28, the result of the above control loop is shown. The RL method needs a certain training time until it captures the control logic. From there, it is able to gradually adjust the given driving speed of the RDE profile with a small deviation (error ≤ 1 km/h). The ratio between the control parameters K_i / K_p is plotted below. For this purpose, a simple neural network architecture is selected. An increasing reward function describes the self-learning training effect.

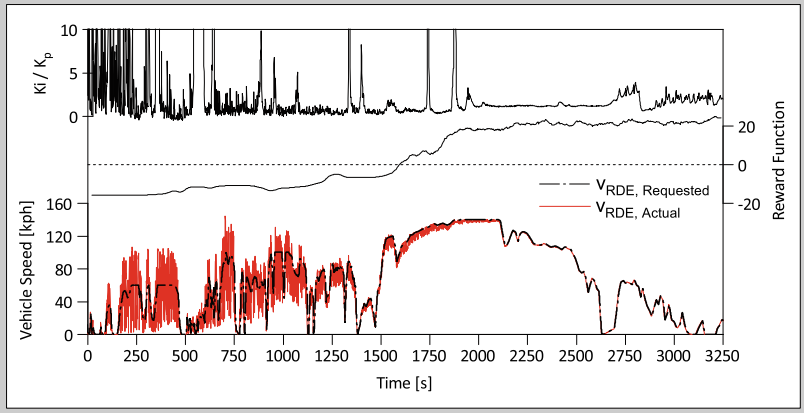

Fig. 5.28 Adaptive RDE speed control

Example 9: Vehicle chassis

A small company called Hackrod, based in California, is specialized in advanced chassis manufacturing for sports cars. The focus of their work is to free the limited design ideas of the human mind and to develop creative concepts based on digital training data and machine learning algorithms.

Using the RL process, the company succeeded in designing a chassis that is significantly more stable than a standard chassis, 30% lighter and therefore more cost-efficient. The net structure shown in Fig. 5.29 is asymmetrical, which is explained by the fact that the center of gravity of a racing vehicle including the driver does not necessarily have to lie on the axis of symmetry. The algorithm takes this into account and builds more heavily loaded regions with a correspondingly denser mesh than less-loaded ones.

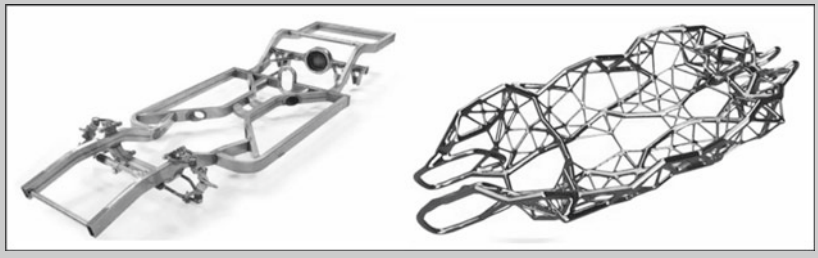

Fig. 5.29 Reinforcement learning applied to chassis design

5.5 Artificial Neural Networks (ANN)

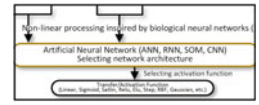

The elementary processing units of a brain consist of neurons. These are cells that exchange signals with each other through electrochemical impulses and thereby excite each other. The brain takes care of the reception, processing and response to stimuli, which are received by sensory organs and transmitted through signals. These signals are called receptors. They register all kinds of information such as light, temperature, sounds, thoughts, tastes and smells and transmit them to the brain via nerve tracts. There are about 100,000 neurons per square millimeter of the human cerebral cortex. One neuron has an average of 10,000 connections to neighboring neurons, so that a brain can have up to 10^{14} connections in total. The sum of these neurons forms a biological neural network (BNN) [45].

The processing and extraction of information in computer systems are different from that in a human brain. In 1945, the essential works of the mathematician John von Neumann were published, which formed the basic mode of operation of the computer architecture used until today. The so-called von Neumann architecture represents the individual components on which the mainboard of computers is built (Fig. 5.30).

While the calculation basis in computers is serially ordered, which leads to a lower data processing speed, processes in our brain are handled in parallel. Especially, the associative mode of operation of the brain allows creative and cross-topic approaches to solving problems, which is conditionally possible with a computer due to its address-based and 1D approach (Table 5.2).

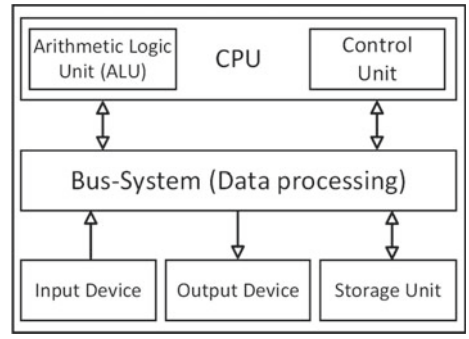

Fig. 5.30 Functioning of today's computer architectures based on Neumann [46]

Tab. 5.2 Data processing brain versus computer [47]

	Brain	Computer
Number of data processing units	$\sim 10^{11}$	$\sim 10^{9}$
Type of processing	Neurons	Transistors
Calculation configuration	Parallel	Serial
Data storage	Associative	Address based
Switching time	$10^{-3}s$	$10^{-9}s$
Number of possible toggle operations	$10^{13}\frac{1}{s}$	$10^{18}\frac{1}{s}$
Actual toggle operations	$10^{12}\frac{1}{s}$	$10^{10}\frac{1}{s}$

This results in many problem genres that cannot be transformed into an algorithmic form, or only with a great deal of effort, so that a computer can solve them. Unlike humans, computers do not experience a learning process and are not adaptive to recurring problems.

Based on human thought processes, a neuronal network of the cerebral cortex can be transformed into a model so that it becomes tangible through a mathematical formalism. Cell extensions of nerve cells (also called dendrites) emerge from a cell body, which serve to absorb stimuli and transmit them to neurons. Before they reach the neuron, they are inhibited or reinforced by synapses. The strength of the synapses can be described by so-called weights $w_{i,j}$, which can have any positive value $[0, \infty]$. A neural network basically consists of three layers, the input layer, the hidden layer and the output layer. Between the input values $I_1, I_2, \ldots, I_i$ and the output values $O_1, O_2, \ldots, O_o$, hidden layers can have any complex dimensions $L_1, L_2, \ldots, L_L$, which in turn can assume any number of neuron levels $N_{1,1}, N_{1,2}, \ldots, N_{1,N}$. The weights lie on the connecting line between two neurons, which is amplified or weakened by $w_{i,j}$, see Fig. 5.31.

A neuron is a processor that can assume a binary state. Either the state is deactivated or activated $I_{j,k} \in [0, 1]$. The product of the inputs $I_{j,k}$ with their respective weights $w_{i,j}$ forms a result that is measured at the threshold value Θ (bias). A neuron is then activated for following condition:

$$\sum I_{j,k} \cdot w_{j,k} > \Theta_k \tag{5.6}$$

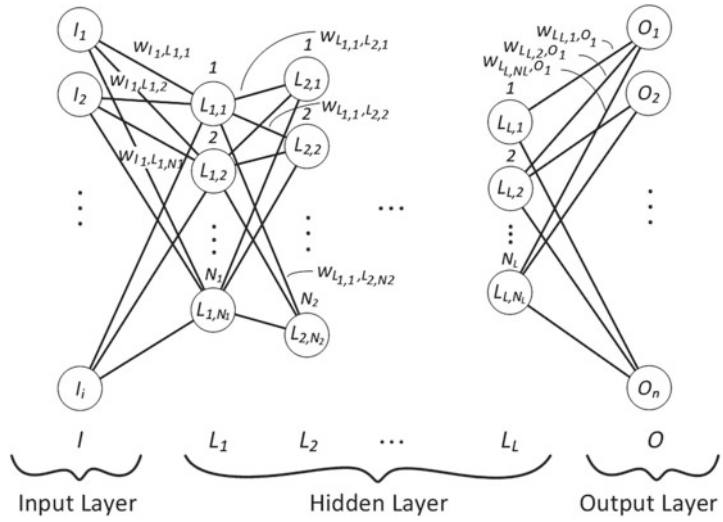

Fig. 5.31 Components of a neural network

Finally, a function s_k is introduced, which is the product of the input values $I_{j,k}$ and the weights $w_{j,k}$ plus the BIAS value:

$$s_k = \sum I_{j,k} \cdot w_{j,k} + \Theta_k \tag{5.7}$$

5.5.1 Activation Function

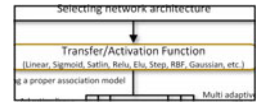

Activation functions are transfer functions that are used to calculate the weights. They are used to design nonlinear functional relations between input and output signals of neurons. An activation function is designated with F. After a signal s_k has been passed to a function F, z_k represents the result of the transfer:

$$z_k = F(s_k) \tag{5.8}$$

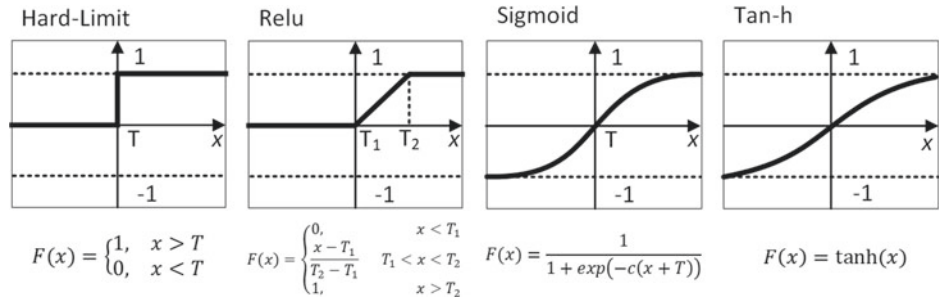

Fig. 5.32 Activation functions

The choice of a suitable activation function for a neural network can strongly influence the quality of the model. The right choice is subjective and depends on what kind of data is used and what properties it has. Among the most prominent functions are Hard Limit, ReLU, Sigmoid and tanh. If, for example, an output value is to be generated in a binary form, Hard Limit is suitable. If the right term from Eq. 5.7 assumes a positive value, then s_k is given the value 1, otherwise $s_k = 0$ [48].

However, due to the step response at x = 0, the system becomes non-differentiable. This can cause system oscillations depending on the application. If the differentiability of the transfer function is desired, a ramp function rectified linear unit (ReLU), a sigmoid function or a tanh function (tangens hyperbolicus) can be used. Furthermore, there are averted activation functions such as Leaky ReLU, exponential linear unit (ELU) or scaled variant of ELU (SELU), which can bring individual advantages for particular application problems.

The architecture of a neural network is composed of many parallel running computational processes. Each unit in the network performs a small part of the overall process. It receives inputs from neighboring units or external sources, calculates a new output value and passes it on to other neighboring units. An overview of all internal processes between a set of inputs and a neuron is shown in Fig. 5.33.

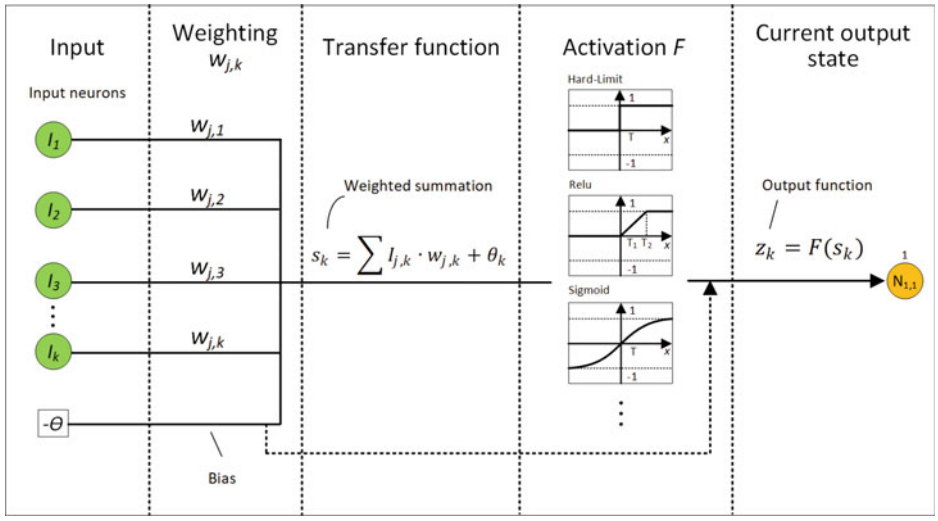

Fig. 5.33 Schematic representation of internal processes between two connected neurons [48]

5.5.2 Feedforward Networks (ANN) and Recurrent Networks (RNN)

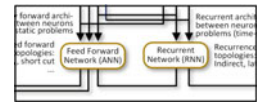

After the structure and function of a neural network were presented in Chap. 5.5, this chapter deals with possible network topologies. Topology means the variety of possible connection patterns between the individual neurons. A fundamental difference is made between a **feed-forward network** and a **recurrent network**.

In a feedforward network, as the name indicates, the flow of information points in a forward direction from input to output. Single-layer perceptrons belong to a subgroup of feed-forward networks. These include network structures that, unlike the one shown in Fig. 5.31, do not have hidden layers. The input layer is thus directly linked to the output layer. Multi-Layer Perceptrons on the other hand consist of at least one hidden layer. Since this allows realizing much more complex structures and interconnection logics between neurons, multi-layer perceptrons are one of the most common network types today.

To illustrate possible network topologies, Hinton diagrams are often used in this context, which show the connections between neurons in a matrix form. Fig. 5.34 (left) shows a simple three-level network with an input layer I_i, a hidden layer h_i and the output layer a_i. As shown here, one often encounters feedforward networks, where each neuron i is

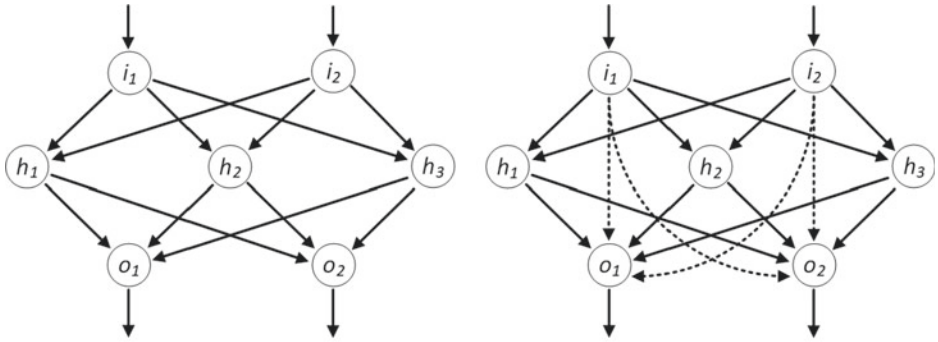

	i_1	i_2	h_1	h_2	h_3	o_1	o_2
i_1	0	0	1	1	1	0	0
i_2	0	0	1	1	1	0	0
h_1	0	0	0	0	0	1	1
h_2	0	0	0	0	0	1	1
h_3	0	0	0	0	0	1	1
o_1	0	0	0	0	0	0	0
o_2	0	0	0	0	0	0	0

	i_1	i_2	h_1	h_2	h_3	o_1	o_2
i_1	0	0	1	1	1	1	1
i_2	0	0	1	1	1	1	1
h_1	0	0	0	0	0	1	1
h_2	0	0	0	0	0	1	1
h_3	0	0	0	0	0	1	1
o_1	0	0	0	0	0	0	0
o_2	0	0	0	0	0	0	0

Fig. 5.34 Feedforward ANN with 3 levels: Hinton diagram with pure feedforward formation (fully linked network, left) and additional direct connections between an input and an output (short-cut connection, right) [47]

connected to all neurons of the next layer. This type of network is called a "Fully Linked Network" (left). Other feedforward networks allow so-called "short-cut connections", where connections can skip one or more levels (right).

In contrast to conventional feedforward networks, complex recurrent networks allow neurons to influence upstream and downstream levels and themselves through connections. This gives the system an iterative character, so that stability can only be achieved by certain iteration loops. The number of iteration loops depends on how well the starting conditions are chosen. The big advantage of RNNs is that they get a kind of memory by their iterative structure. This makes them particularly suitable for time-dependent data sequences (time series). Especially in the field of powertrain development, these powerful network structures allow solving transient problems.

In Fig. 5.35 (left), a network with a "Self-Recurrence" character is shown. This allows neurons to inhibit each other during the self-training phase until they are strong enough to exceed the threshold Θ and thus be activated.

If connections from a hidden layer are established back to the input layer, this is called "Indirect Recurrence". Unlike Direct Recurrence, here neurons can train their behavior as a consequence of downstream neural layers (see right graph).

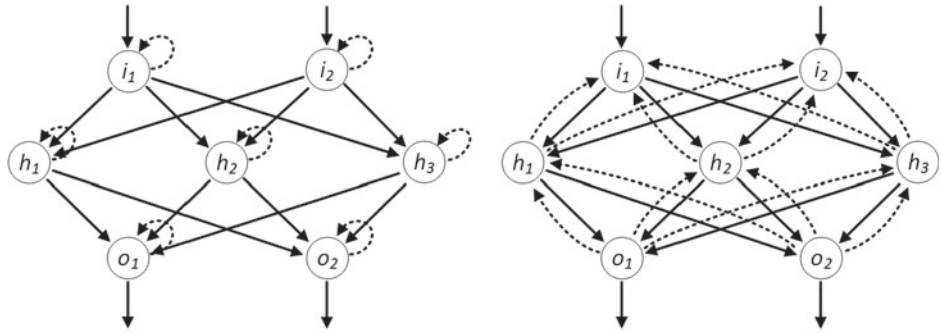

	i_1	i_2	h_1	h_2	h_3	o_1	o_2
i_1	1	0	1	1	1	0	0
i_2	0	1	1	1	1	0	0
h_1	0	0	1	0	0	1	1
h_2	0	0	0	1	0	1	1
h_3	0	0	0	0	1	1	1
o_1	0	0	0	0	0	1	0
o_2	0	0	0	0	0	0	1

	i_1	i_2	h_1	h_2	h_3	o_1	o_2
i_1	0	0	1	1	1	0	0
i_2	0	0	1	1	1	0	0
h_1	1	1	0	0	0	1	1
h_2	1	1	0	0	0	1	1
h_3	1	1	0	0	0	1	1
o_1	0	0	1	1	1	0	0
o_2	0	0	1	1	1	0	0

Fig. 5.35 Feedforward ANN with self-aligned recurrent loops of the neurons (self-recurrence, left) and externally aligned recurrent loops (indirect recurrence, right) [47]

To give systems an even higher degree of freedom in training, it is still possible to connect neurons within a hidden layer. This results in a direct competition between the neurons. In contrast to self-recurrence training, neurons inhibit others within the hidden layers to strengthen themselves and achieve an activation. As a result of this direct confrontation, only the strongest neurons succeed in activating, so that they prevail over the others according to the "Winner takes it all" principle. This form of topology is called "Lateral Recurrence" and is shown in Fig. 5.36 (left).

In contrast to the topology options presented, the "Completely Linked Networks" are at the outermost limit. These allow connections between all neurons. This leads to each neuron becoming an input variable, which is the reason why self-linking is no longer possible. As a result, previously defined levels can no longer be clearly separated from each other. In terms of training, this form of topology requires the highest effort, but depending on the application, it can quickly lead to a system being overtrained and, as a result, losing its ability to interpolate and extrapolate into unknown regions of a data set.

Especially at the stock exchange RNNs are widely used, because they are ideal for forecasting time-dependent sequences based on past scenarios. At the forefront of such an application is always the choice of a suitable network architecture and training of this network based on historical data. From now on, the method allows predicting a discrete time P_1 in the future (future prediction) based on the number of past time steps N_p of an

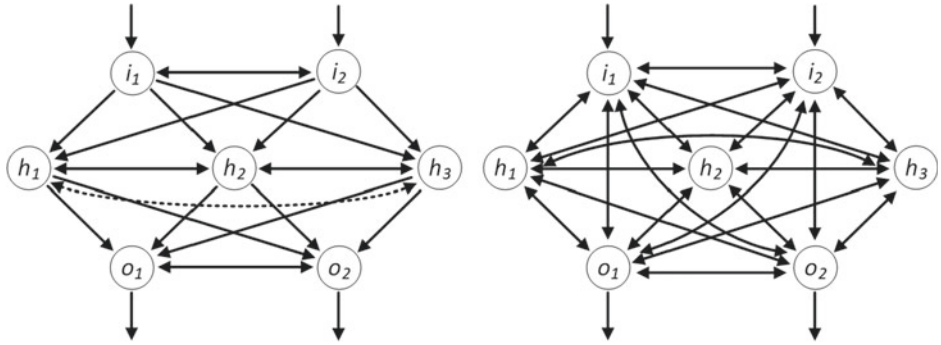

	i_1	i_2	h_1	h_2	h_3	o_1	o_2
i_1	0	1	1	1	1	0	0
i_2	1	0	1	1	1	0	0
h_1	0	0	0	1	1	1	1
h_2	0	0	1	0	1	1	1
h_3	0	0	1	1	0	1	1
o_1	0	0	0	0	0	0	1
o_2	0	0	0	0	0	1	0

	i_1	i_2	h_1	h_2	h_3	o_1	o_2
i_1	0	1	1	1	1	1	1
i_2	1	0	1	1	1	1	1
h_1	1	1	0	1	1	1	1
h_2	1	1	1	0	1	1	1
h_3	1	1	1	1	0	1	1
o_1	1	1	1	1	1	0	1
o_2	1	1	1	1	1	1	0

Fig. 5.36 Feedforward ANN with recurrent loops only within the layers (lateral recurrence, left), completely linked network (right) [47]

experience window (memory window). Starting from the current point in time, this time lies in the future by N_f time steps. The greater the value N_f is chosen, the greater is the probability that the prediction will deviate from reality. The loss can be counteracted by selecting a larger memory window N_p or by increasing the size of the RNN and training it again (Fig. 5.37).

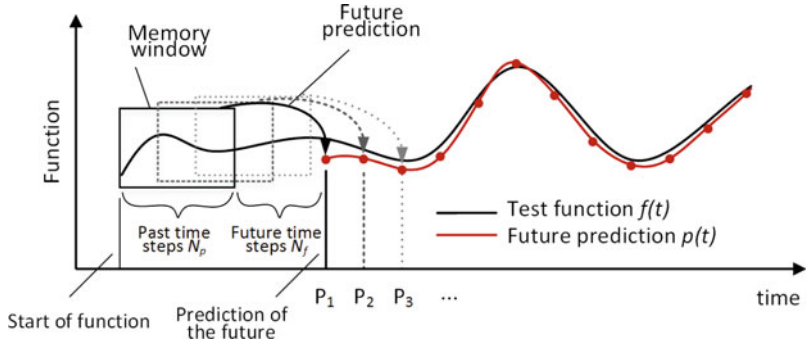

Fig. 5.37 Prediction of time-dependent variables: Definition of past time step and future time step

In addition to recurrent networks, there is a large number of other network structures that have recurring loops and are therefore particularly suitable for data that contains time sequences. These include the Long Short-Term Memory (LSTM) network or the Gate Recurrent Unit (GRU) network. Both types of networks are suitable for classifying, processing and predicting scenarios that lie in the future. Similar to recurrent networks, LSTMs and GRUs are considered deep learning methods due to their complexity and network depth (see Chap. 5.6).

RNNs can be perfectly applied for time-dependent sequences, for which individual RNN networks each consisting of a single neuron are combined to form a chain of modules. This gives them the character of sequential processing. Each module contains two weights, one anchored in the feedforward direction and one in the recurrent loop, which are usually activated by a tanh function (Fig. 5.38).

RNNs are capable of learning dependencies from the past and projecting them to a future point in time. In practice, however, studies by Hochreiter et al. [49] have indicated difficulties that may occur through the simplicity of the network architecture. LSTM networks are a more specialized form of RNNs that are capable of learning and predicting even long-term time dependencies. They were first introduced by the German computer scientists S. Hochreiter and J. Schmidhuber. Their applications are today widespread around the world. LSTMs also have this chain-like structure, but with a more complex processing unit, called LSTM cell. Instead of a single neural network layer, there are four of them interacting with each other through different operators: Two successive layers with a sigmoid activation function, a third layer with a tanh activation and another sigmoid layer (Fig. 5.39).

The key to LSTMs is the cell state $c_{(t-1)}$ (long-term state), which is the horizontal line that runs down the entire chain of LSTM cells in the upper part of the figure, being continuously updated through linear interactions. The sigmoid layers describe how much of each component should be allowed to pass, hence, they are controlling and protecting the cell state. This is why they are also referred to as gate controllers. Their outputs span values from 0 to 1, i.e. they close the corresponding gate with an output of 0, and open it with an output of 1.

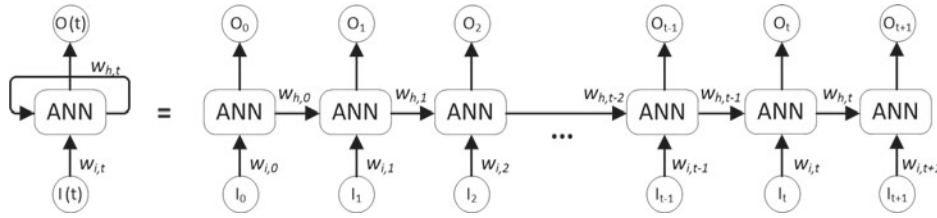

Fig. 5.38 Merging sequential RNNs for processing time-based events

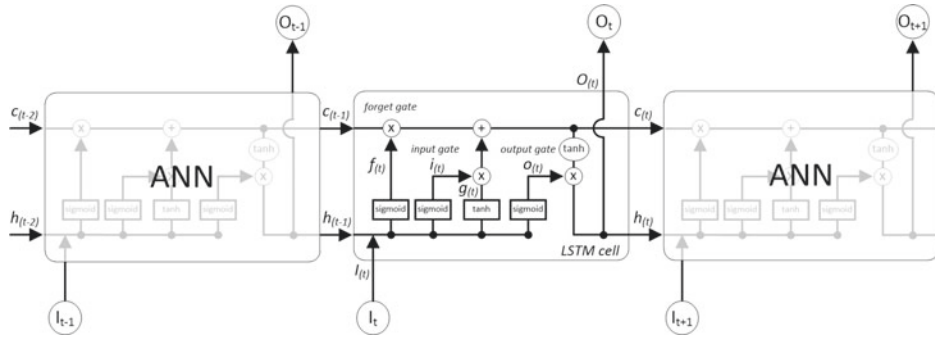

Fig. 5.39 Functionality of an LSTM cell [50]

More precisely, $c_{(t-1)}$ passes through a so-called forget gate $f_{(t)}$. This gate decides which parts of the long-term state are to be deleted. The input gate $i_{(t)}$, on the other hand, controls which parts of the tanh function $g_{(t)}$ should be overwritten and added to the long-term state. Finally, after another operation with the output gate $o_{(t)}$, it is determined which parts of the long-term state should be transported to the outside as a signal. The result is the short-term state $h_{(t)}$ which corresponds to the output of the cell at the time $O_{(t)}$.

In summary, an LSTM cell can learn to recognize an important input, store it in its long-term state, retain it as long as it is necessary and extract it again when needed. This explains why these cells perform amazingly well in capturing long-term patterns of time series.

The following equations summarize how the long-term state $c_{(t)}$ and the short-term state $h_{(t)}$ are calculated. Here, $w_{i,f}$, $w_{i,i}$ and $w_{i,g}$ represent the feedforward weights of the respective four layers to the input vector $i_{(t)}$. The weights $w_{h,f}$, $w_{h,i}$, $w_{h,g}$ and $w_{h,o}$, on the other hand, form recurrent loops back to the short time state $h_{(t-1)}$, (see Fig. 5.38). The terms b_f, b_i, b_g and b_o form the associated bias [50]:

$$
\begin{aligned}
f_{(t)} &= \sigma(w_{i,f} \cdot i_{(t)} + w_{h,f} \cdot h_{(t-1)} + b_f) \\
i_{(t)} &= \sigma(w_{i,i} \cdot i_{(t)} + w_{h,i} \cdot h_{(t-1)} + b_i) \\
g_{(t)} &= tanh(w_{i,g} \cdot i_{(t)} + w_{h,g} \cdot h_{(t-1)} + b_g) \\
o_{(t)} &= \sigma(w_{i,o} \cdot i_{(t)} + w_{h,o} \cdot h_{(t-1)} + b_o) \\
c_{(t)} &= f_{(t)} \cdot c_{(t-1)} + i_{(t)} \cdot g_{(t)} \\
O_{(t)} &= h_{(t)} = o_{(t)} \cdot tanh(c_{(t)})
\end{aligned}
\tag{5.9}
$$

Example 10: Predicting Emissions from the Real Driving Emission Cycle (RDE)

Emissions in real driving conditions are described as real driving emissions (RDE), unlike those measured under non-real test conditions on an exhaust roller dynamometer. Due to the fact that in real driving conditions, passenger cars certainly emit more exhaust gases than in the new European driving cycle (NEDC) test procedure, which has been used for vehicle registration in Europe since 1992, the European Union decided in 2015 to supplement the test procedure by the RDE test. The test procedure has been effective since September 2017 for cars, trucks and buses in everyday use. The great challenge of this test method is that, unlike other driving cycles, the distance and speed as well as the elevation profile are not fixed. The route that is driven during the RDE test consists of an urban, a rural road and a freeway section. The proportions are kept flexible within predefined limits, and the driving behavior during the test operation is not subject to any fixed specifications and can be individually adjusted by an inspector. These freedoms mean that it is difficult to accurately predict emissions using common models.

In the following example, a self-recurrent RNN is selected (see Fig. 5.35), which consists of 4 hidden layers and 30 neurons each. An RDE test cycle and associated measurements of carbon monoxide (CO) and nitrogen oxides (NO_x) recorded with a portable emissions measurement system (PEMS) serve as the basis for the observation. The first 4300 s of the test drive, representing 75% of the total test time, are used to train the neural network. For the remaining distance, a prediction of emissions shall be made. Alternatively, it is also possible to use a complete RDE measurement as a training basis and, based on this, to predict emissions for other RDE measurements (Fig. 5.40).

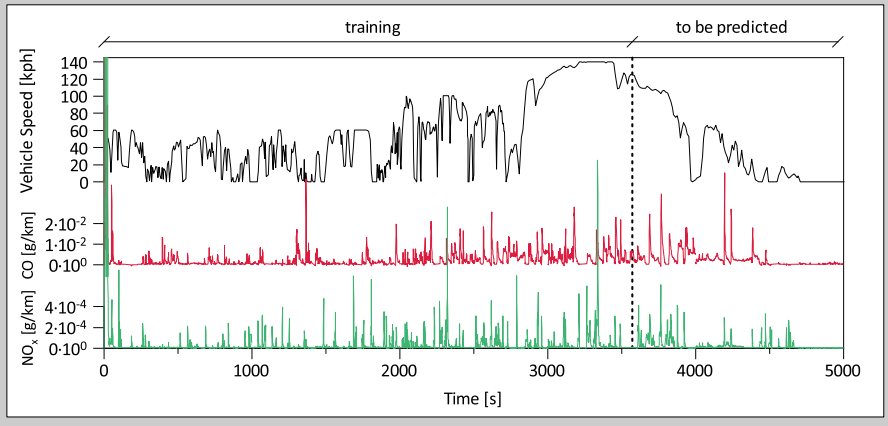

Fig. 5.40 Training and prediction of CO, NO_X emissions of the RDE test procedure

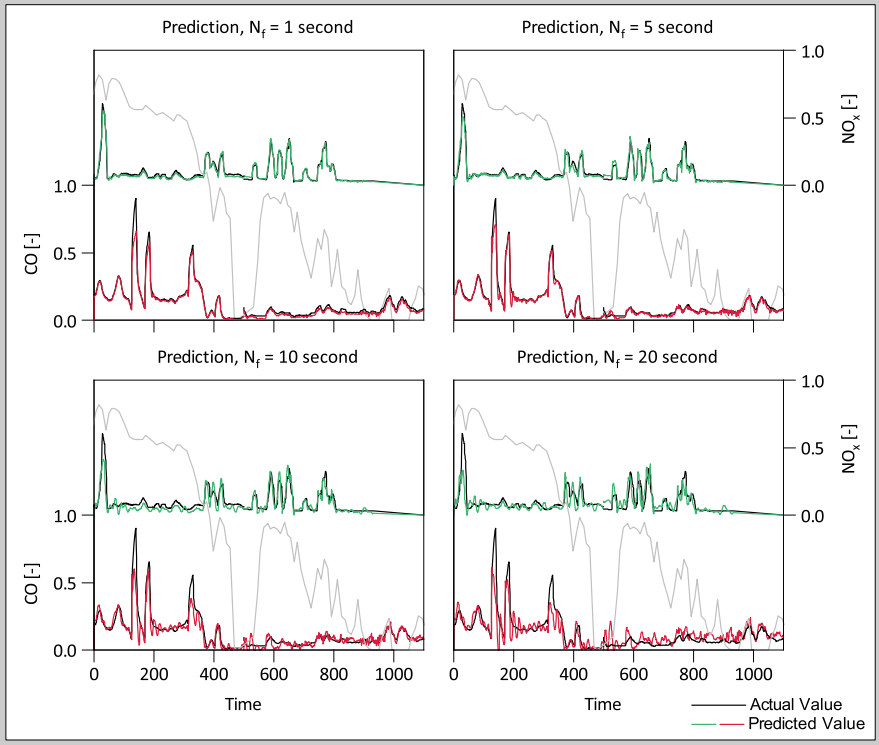

Fig. 5.41 Prediction of CO and NO_x in RDE for different future times steps N_f

When using RNNs, the user has the choice to define the time step size of the prediction. If a prediction lies far in the future (large N_f), it is recommended to counteract with an equally large N_p and/or a larger network architecture; see Sect. 5.5.4. The following graph shows the result of the predicted CO and NO_x on the RDE test for N_p=300 and $N_f = 1$ second, $N_f = 5$ seconds, $N_f = 10$ seconds and $N_f = 20$ seconds in the future. The quantities were normalized on the basis of the respective maximum value [0-1] (Fig. 5.41).

5.5.3 Training Procedure

Similar to biological neurons, which are inhibited or reinforced by their upstream synaptic connections, weights take over this task in artificial neural networks. During the training phase of an ANN, the weights are always adjusted. For this purpose, different training algorithms have been developed, of which only a few are suitable for multi-layered neural networks. Some of them are suitable for feedforward networks where the information flow

is unidirectional, others for recurrent networks where the information flow is backward, as presented in Sect. 5.5.2.

Detached from the nature of the network architecture, there are training procedures which are suitable if the output of the ANN is known (Supervised Learning; see Sect. 5.4.1), procedures for ANN with unknown output variables (Unsupervised Learning; see Sect. 5.4.2) and special procedures for self-learning systems (Reinforcement Learning; see Sect. 5.4.3). Which training method ultimately is the most suitable depends on the respective application.

In this section, some training procedures are presented. For an overview, please refer to the flowchart in Fig. 5.5.

Backward Propagation—Supervised Learning

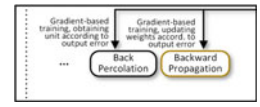

Backward propagation is one of several training methods to train artificial neural networks. The training is a supervised learning method, i.e. data that are subjected to training must be classifiable; see more details in Sect. 5.4.1.

At the beginning of a training process, all weights of a neural network are initialized. A good initialization is of central importance because it determines how many epochs (iterations) a network has to be trained to achieve stability. In addition, the final result can differ if the initialization is bad. One of the most important initialization methods are the ones of G. Xavier and K. He [51, 52].

After this step, the net now generates corresponding output data of the zeroth iteration. A deviation (error) from the expected output is calculated. The error is propagated backwards to the previous level. By adjusting the weights on this layer, the error is reduced by a gradient minimization method (gradient descent method). This process is repeated until the error falls below a certain limit. Once the smallest gradient is found, which corresponds to a global minimum, the training is considered to be completed.

The training process can be divided into three steps and is explained in more detail below using the example of a simple neural network (multi-layer perceptron) with two input signals (x_1, x_2), two hidden layers and an output signal y:

1. Forward Propagation
   Network training is an iterative process. In each iteration, the weights at each node are modified using new training data. Each training step starts with a new feed of input signals from the training set. Afterwards, the output signal values can be determined in each network layer for each neuron. The following pictures illustrate how a signal propagates through the network (Fig. 5.42).

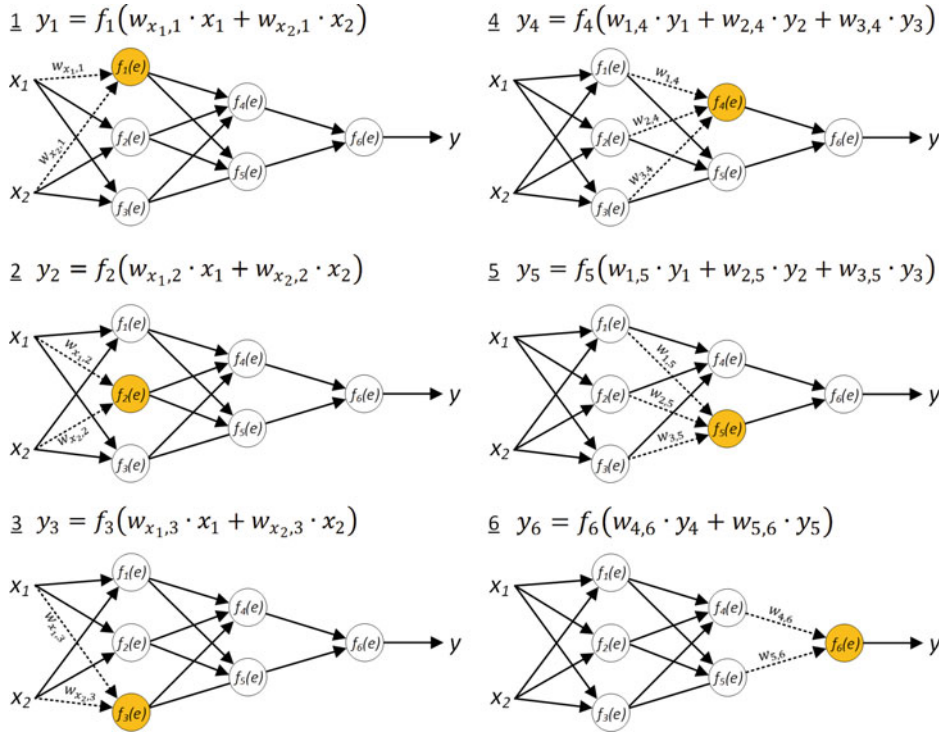

Fig. 5.42 Backward propagation training phase 1: Feedforward and derivation of individual neural outputs [53]

2. Calculation of the errors
   In the second step of the training phase, the output signal y of the network is compared with the target value, which is part of the training data set. The difference $\delta = z - y$ quantifies the error of the network.

   Any cost function C can be selected as a training basis for updating the weights.

$$C = \frac{1}{2} \cdot (z - y)^2 \tag{5.10}$$

   The coefficients $w_{i,j}$ of the weights used to retransmit errors are the same as those used during the calculation of the output value. It is therefore essential to select the same activation function for both the training process and the subsequent calculation process, otherwise the quality of the training results could not be reproduced (Fig. 5.43).

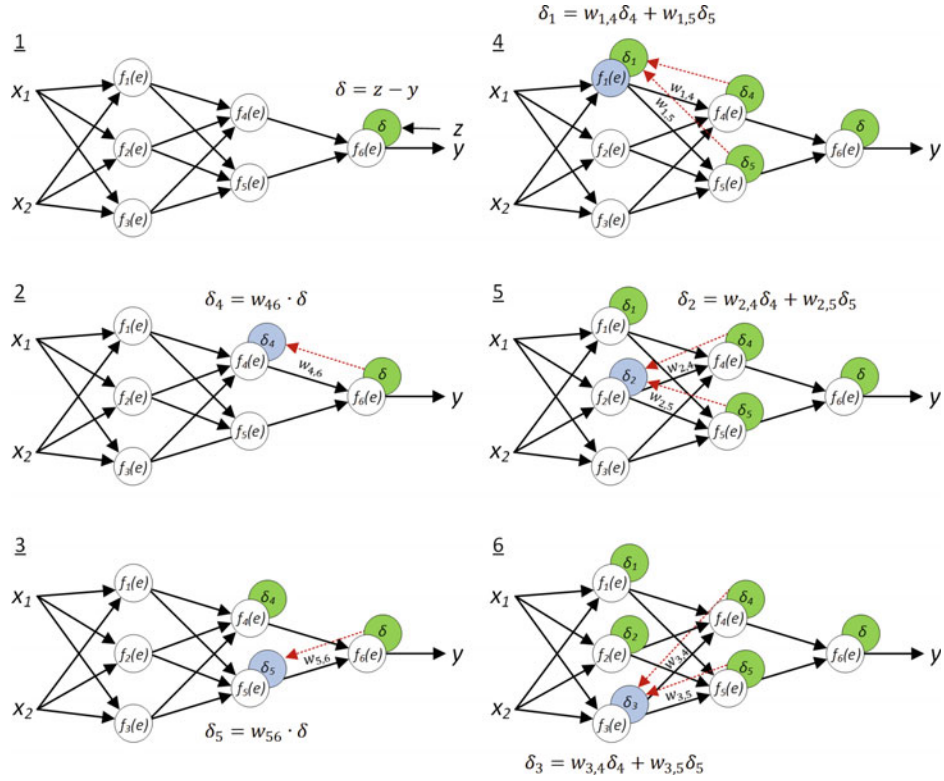

Fig. 5.43 Backward propagation training phase 2: Derivation of errors and gradients [53]

3. Update of the weights
   To adjust the weights, the partial derivative of the error function is performed:

$$\delta_k = \frac{dC}{dw_{i,j}} = (z - y_k)\frac{dy_k}{dw_{i,j}} \tag{5.11}$$

y_k describes the activation function as shown in Fig. 5.32. For the choice of a sigmoid activation function, y_k is

$$y_k = F(s_k) = \frac{1}{1 + e^{s_k}} \tag{5.12}$$

When inserting Eq. 5.12 in Eq. 5.11, the result is

$$\delta_k = \frac{dC}{dw_{i,j}} = (z - y_k) \cdot y_k(1 - y_k) \tag{5.13}$$

After the gradients are calculated, the weights are adjusted:

$$w_{i,j}^{*} = w_{i,j} + \Delta w_{i,j} \tag{5.14}$$

with

$$\Delta w_{i,j} = \eta \cdot \delta_k \cdot y_k \tag{5.15}$$

where η describes the learning rate of the backpropagation process by influencing the training speed in the network. There are two fundamentally different approaches to select these parameters. The first one is to give the training process a large starting value. While the weights are set, the parameter is gradually reduced. The second approach starts by teaching with a small parameter value. During the training, the parameter is increased while progressing and decreased again in the final stage. This makes it possible to determine the signs of the weights faster. This approach takes more time but reacts more robustly to a convergence criterion (Fig. 5.44).

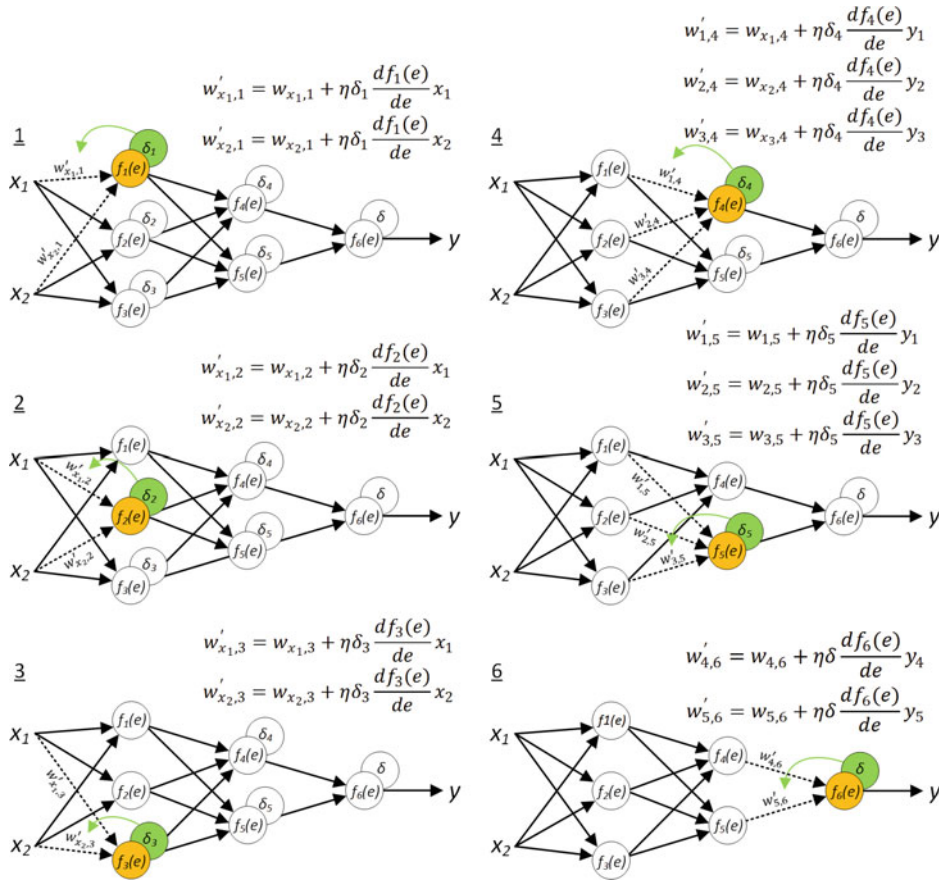

Fig. 5.44 Backward propagation training phase 3: Update of the weights based on the gradients [53]

Counter-Propagation—Unsupervised Learning

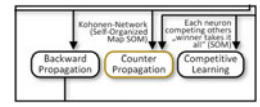

In 1987, the US-American computer scientist Robert Hecht-Nielsen presented a new form of training method for neural networks called "Counter-Propagation" (CPN). In contrast to backpropagation, this is an unsupervised learning method (see Sect. 5.4.2 for more details) and is especially suitable for feedforward networks. The counter-propagation has self-learning properties and is particularly designed for applications where a database is not classifiable, especially when input variables are dynamic, i.e. always changing, and output variables are unknown.

The counter-propagation training is typically combined with a Kohonen hidden layer. Kohonen networks are also called self-organizing maps (SOM), which are mainly used to visualize and analyze highly complex data. Each data point is assigned to a network node according to the similarity theorem and metric evaluation basis. This enables the method to "map" input variables directly to an output. The output layer is called the Grossberg layer.

In principle, a data mapping, i.e. a direct projection of an input signal onto a possible output can also be solved with the backpropagation method. However, the counter-propagation method promises a higher prediction and up to 100 times faster computation speed, especially for dynamic and variable data patterns. Particularly for applications where real-time is required, CPN is well suited.

Figure 5.45 shows a counter-propagation network with five layers, the input layers 1 and 2, a hidden layer 3 and the output layers 4 and 5. With a given vector pairing $\{x_1, y_1\}$, $\{x_2, y_2\}, \ldots, \{x_n, y_m\}$ the CPN tries to correlate an input vector $\{x_i\}$ with an input vector $\{y_i\}$ during the training phase. If a correlation can be described with a continuous function Φ, so that $y = \Phi(x)$ is true, the CPN learns to classify this solution for each vector $\{x\}$ of the training space of the same characteristic. If an inverse correlation is detected such that the vector $\{x\}$ is also a function of $\{y\}$ by $x = (\Phi - 1) \cdot y$, the CPN learns to map inversely. In this case, it is a "full counter-propagation network", otherwise it is a " forward-only counter-propagation network".

The training concept is based on a two-step process. First, an unsupervised learning method is applied. The Kohonen layer (Hidden Layer) works according to the "Winner takes it all" principle. According to this principle, the strongest neuron prevails in competition with the others by exceeding the threshold value (bias) and thus gets activated. The Kohonen level literally provides a classification. The activated node carries out a "supervised learning" method in the Grossberg layer (output level) and generates the output signal. In this respect, the training method is also categorized as semi-supervised learning.

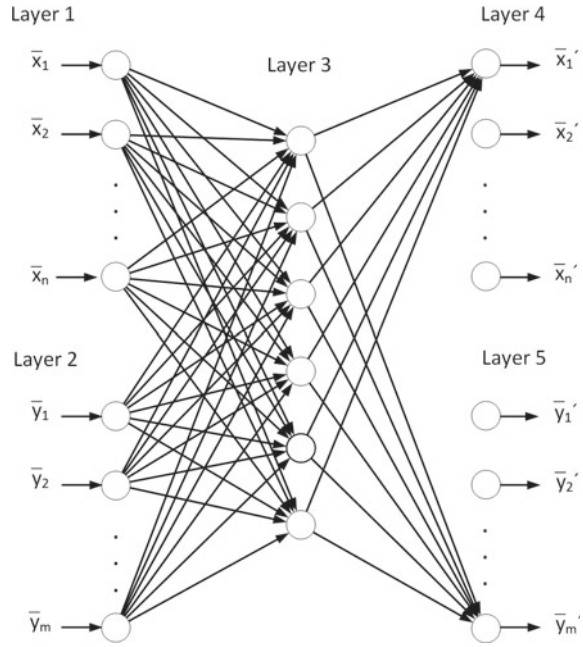

Fig. 5.45 Neural network for counter-propagation training [54]

Competitive Learning—Unsupervised Learning

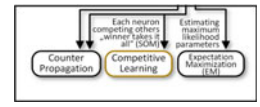

Among the best known competitive learning concepts are self-organized networks (Self-Organizing Maps: SOM). SOMs represent another form of artificial neural networks, which were presented in 1982 by the Finnish engineer Teuvo Kohonen. They are one of the most prominent unsupervised learning methods, which aim to reduce and discretize the dimension of complex data inputs to a 2D output plane (2D map). SOMs differ from common ANNs as the training of the weights is not performed by a gradient descent method (backward propagation), but by competitive learning. Each neuron works "self-organized", i.e. it competes independently with its neighboring neurons, which is according to the "Winner takes it all" principle. The weight of a neuron is rewarded if it produces results that are most similar to a randomly selected vector.

Based on common signal processing concepts, a so-called quantization error (QE) provides a measure of the average distance between the data points and the map nodes on which they are mapped. Kohonen proposed QE as a basic quality measure for the evaluation of self-organizing maps. The value for a map is calculated using the following equation, where n represents the number of data points in the training data and $\Phi : D \rightarrow M$ represents the projection of the input space D onto the feature map M of the SOM [55]:

$$QE(M) = \frac{1}{n} \sum_{i=1}^{n} \| \Phi(x_i) - x_i \| \tag{5.16}$$

Another goal of the SOM algorithm is to preserve the topological features of the input space in the output space. For this purpose, there is another important measure called topographic error (TE) that describes how well the structure of an input space is represented by the map. TE calculates for each input the best and second best matching neurons of the map and based on this, evaluates its position. If the nodes are adjacent, it means that the topology for that input has been obtained. Otherwise, this is evaluated as an error. The total number of errors divided by the total number of data points results in the topographic error of the map, where $\mu(x)$ denotes the best matching value for the data point x and $\mu^{'}(x)$ denotes the second best [55]:

$$TE(M) = \frac{1}{n} \sum_{i=1}^{n} t(x_i) \tag{5.17}$$

$$t(x) = \begin{cases} 0 & \text{if } \mu(x) \text{ and } \mu^{'}(x) \text{ are neighbors} \\ 1 & \text{otherwise} \end{cases}$$

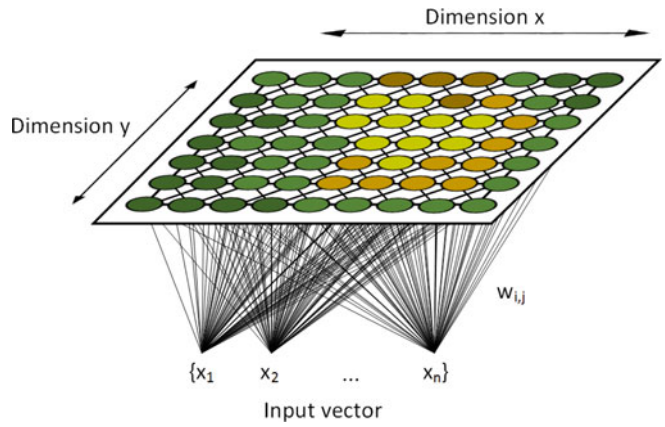

Fig. 5.46 Projection of data onto a 2D feature map (Self-Organized Maps: SOM) [56]

Each neuron acquires its own x-y coordinate on the feature map (color map). Through the simultaneous training of the neighboring neurons, the feature map grows gradually, which is the result of the clustering process. In this respect, each data point is assigned to a certain characteristic by representing a color class (Fig. 5.46).

MDP, Q-Learning, SARSA

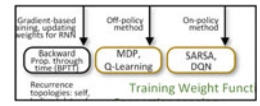

1. To describe the reaction behavior to environmental influences, so-called Markov decision processes (MDPs) can be used as a general framework for reinforcement learning. An MDP consists of a set of finite environmental states s, a set of possible actions in each state $a(s)$ and a reward function $r(s)$. The goal of an MDP is to calculate the optimal policy $\pi(s, a)$ so that a corresponding action can be taken for any possible state. This action is being rewarded, if it brings a success. The goal is to maximize the rewards as much as possible. However, since real environments can be highly dynamic, it is difficult to predict their reactions to changing input data. In such cases, the use of model-free RL methods is more appropriate, since they are better suited to predict unexpected effects.

2. Q-learning and State-Action-Reward-State-Action (SARSA) are two frequently used model-free RL algorithms. While Q-learning is an off-policy method in which the agent learns its environment based on a policy, SARSA is an on-policy method that learns it mainly based on its current action and secondly by the help of additional policies.

The weight for a step from a state t by Δt steps into the future is calculated with $\gamma^{\Delta t}$, where for γ $(0 \leq \gamma \geq 1)$ applies. This has the effect that earlier received rewards are valued higher than rewards received later. γ can also be interpreted as the probability of success after each time step Δt. Before the training begins, Q is initialized to any random value. Then the agent selects an action a_t at any time t, observes the reward r_t and assigns a new state $s_t + 1$. After this, Q is updated [57]. Both Q-learning and SARSA are based on the following equation:

$$\underbrace{Q(s_t, a_t)}_{\text{new value}} \overset{\text{updating direction}}{\leftarrow} \underbrace{Q(s_t, a_t)}_{\text{old value}} + \overbrace{\alpha}^{\text{learning rate}} \cdot \overbrace{\underbrace{(\underbrace{r_t}_{\text{reward}} + \underbrace{\gamma}_{\text{discount factor}} \cdot \underbrace{max\ Q(s_{t+1}, a)}_{\text{estimate optimal future value}}}_{\text{new value}} - \underbrace{Q(s_t, a_t)}_{\text{old value}})}^{\text{temporal difference between current and learned value}} \tag{5.18}$$

The methods are easy to implement but not generally applicable, because they are not able to estimate values for unknown states. This can be overcome by more advanced algorithms like deep Q-networks (DQN), which use neural networks to estimate Q-values. However, DQNs are more suitable for processing discrete and low-dimensional action spaces.

Reinforcement learning is widely used where training is based on variable input data and unpredictable output data, such as in the area of autonomous driving. The environmental influences that can occur while driving are complex and cannot be defined finitely. The situation is similarly complex in the field of "gaming", where virtual game partners are developed, or in the field of robotics.

5.5.4 Network Architecture and Performance

The architecture of a neural network describes its composition or dimension and is defined by the number of hidden layers (HL) and the number of neurons per hidden layer (Hidden Units: HU) that the network comprises. At the beginning of modeling, a network, searching for the optimal architecture, is one of the key aspects the user usually has to deal with.

The determination can be very time-consuming, therefore it is recommended to follow some general guidelines in order to get a possible orientation in advance. In principle, the optimal architecture is strongly related to the number of input variables of the model and the size of the data set used for training the network. Fig. 5.47 illustrates the dependency of the network architecture on its performance according to the amount of training data. Performance can also be understood as the capability of prediction, which can be expressed analytically either by the coefficient of determination (R^2) or by other standard evaluation quantities like mean square error (MSE) or root mean square error (RMSE).

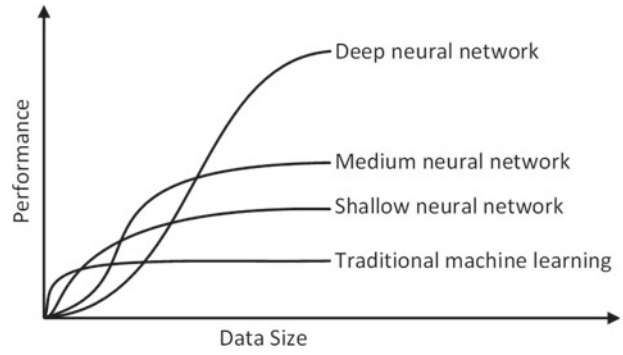

Fig. 5.47 Performance of an ANN as a function of data volume and network architecture [58]

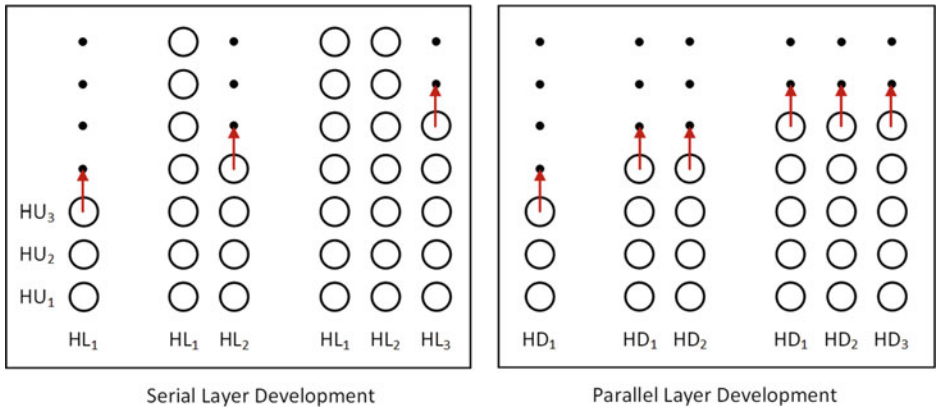

Fig. 5.48 Sequential construction of a neural network according to a serial method (left) and parallel method (right)

There are strategically different approaches to building a network. In the following, two sequential methods are presented: 1. a serial developing structure of HLs and 2. a parallel developing structure of HLs. For both methods, a maximum number of HUs must first be defined. In the serial setup, the HUs are developed one after the other, see Fig. 5.48 (left), while the performance of the network is always observed. When an HL is fully developed, the construction of the next HL level begins. In parallel setup (right), however, the number of HUs per HL is set up anew for each newly added HL. In principle, it is also possible to variably generate the number of HUs for each HL. This results in a permutative number of possible combinations, which leads to an exponential increase of arithmetic operations, which is why it is inadvisable.

Using the example of a set of 45000 training data points, 8 inputs and one output variable, the performance of a network during its development is shown. For this purpose, 75% of the data is used for training and 25% for validation. The coefficient of determination R^2 is shown as the evaluation variable, which represents the correlation between the real data and the results calculated from the model. For this example, a serial network reaches its optimal performance at about 3 fully trained HLs and 100 HUs. In contrast, the parallel development method finds an optimum at 4 HLs with 80 HUs. In principle, one can say that both methods propose similar architectures. Depending on the problem and the existing knowledge of a system, one or the other method can result in time advantages. In the search for an efficient network architecture, both methods should be weighed against each other (Fig. 5.49).

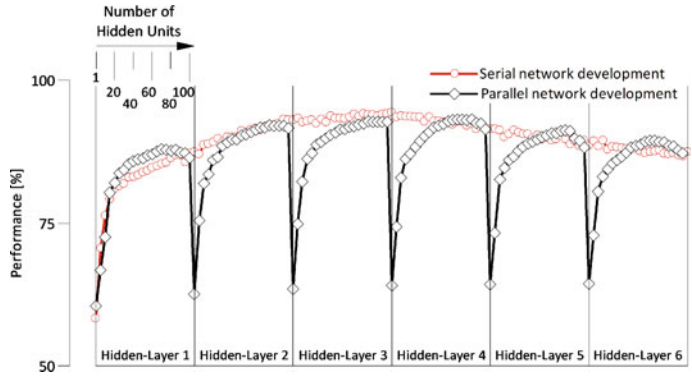

Fig. 5.49 Training of a serial and parallel network

The number of HUs reacts much more sensitively than the number of HLs for the increase in performance. The focus should therefore be more on the development of neurons than on a large number of HLs. As the number of HLs increases, the additional gain in network performance becomes smaller and smaller (Fig. 5.50).

Fig. 5.50 shows that the first HL is (are) considered the performance-defining pillar(s). If further HL levels are added, smaller potentials can be localized for large data sets (improving pillars). Any further levels from there represent only a slight increase in performance and

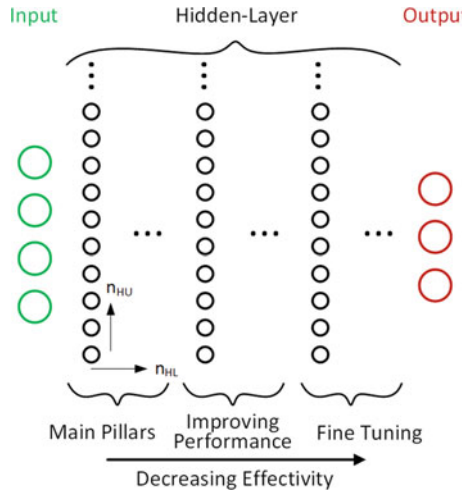

Fig. 5.50 Network dimension versus efficiency

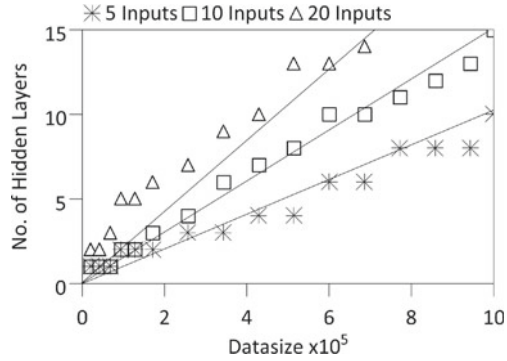

Fig. 5.51 Number of hidden layers to be selected depending on data volume and number of input variables

thus are identified as "fine-tuning pillars". The choice of a network structure is one of the sensitive issues, as it has an immense influence on the efficiency of a model. At the same time, sequentially enlarging the architecture according to Fig. 5.48 and approaching an optimum can be very time-consuming. In order to help the user to select a suitable architecture, the following illustration provides a rough orientation for the selection of the HL number. Depending on the data size and the number of input parameters, it can be described linearly (Fig. 5.51).

If the HL number was defined in the first step, the number of HUs remains as a further unknown variable. In the second step, it can be roughly selected for 5, 10 and 20 input variables using Fig. 5.52.

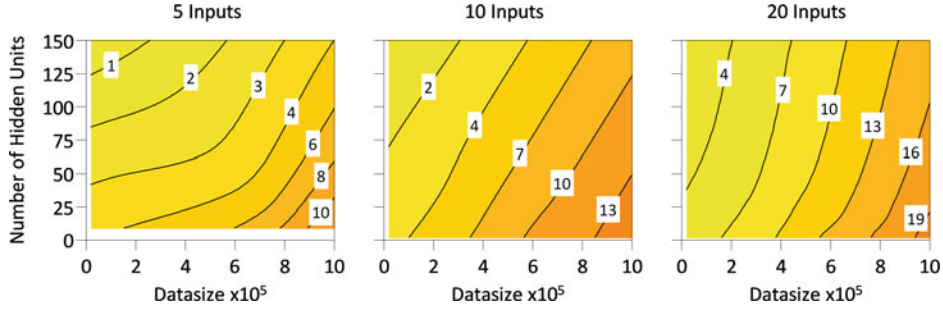

Fig. 5.52 Number of hidden units to be selected depending on the amount of data

Hyperparameter

In machine learning applications, there are a number of sensitive parameters that have a relevant effect on the performance of a neural network. Those that are used to control training and whose value, unlike other parameters, must be determined before a model is trained are called hyperparameters. The dimension of an ANN is therefore also counted as a hyperparameter.

The most important hyperparameters, which in sum have a decisive influence on the performance of an ANN, are listed as follows:

1. **Number of hidden layers and hidden units**
   As explained in the previous section, the dimension of an ANN plays a crucial role in the creation of a suitable model. The larger and more complex a data set and the more input variables it contains, the more likely a performance optimum of the ANN will shift toward a higher dimension.
2. **Dropout**
   Dropout is a technique used to increase network performance and avoid overfitting. By using a trial and error method, individual neurons are canceled out of the architecture, while the performance of the network is constantly checked. A dropout value of 20%–50% of neurons is recommended as a guideline. Especially for large networks, this method promises to uncover considerable potentials, and speed up the simulation time (Fig. 5.53).
3. **Activation Function**
   Activation functions are used to transfer nonlinear relationships of data into models. Depending on which characteristics and properties a data set has, it can make qualitative differences with which activation function a corresponding model is trained. As far as it has to be selected in advance of training, it is one of the most important hyperparameters. Further details were discussed in Sect. 5.5.1.

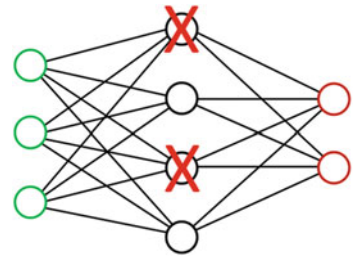

Fig. 5.53 Dropout of neurons [59]

4. **Weight Initialization**
   A sensible initialization of the weights at the beginning of a training decides on how many epochs a network has to be trained to reach its maximum performance. In addition, a good initialization can achieve a better training result than an unfavorable initialization. One of the most important initialization methods is that of G. Xavier and K. He, who estimate the best possible initial values of the weights based on an upstream analysis of the respective data [51, 52].
5. **Train versus Test Ratio**
   For a given data set before a training session starts, it is common practice to specify what proportion of the data set will be used for the training itself and which remaining part is used for the validation of the model (test). According to different sources, a ratio of 70%–85% is recommended between a training and a test data set. The selection of the portions shall be random. This value can be sensitive to the performance.
6. **Batch Size**
   If a data set is considerably large, the training process can result in an enormously high computing load. Especially for studies where a process is recurrent, progress can be inefficient in terms of time. One method that helps to reduce training time is to segment a data set into small packages (batches). Instead of feeding the entire data set once, the batches are then transferred sequentially to the network. The weights are updated after each input of a new batch. A default value for the batch size is 32, and for larger batches multiples of this number can be selected (Fig. 5.54).
7. **Learning Rate**
   Learning rate determines how fast the weights of a network should be updated. A low learning rate slows down the learning process, but is robust with respect to oscillations and more stable with respect to convergence. A higher learning rate can speed up the learning process significantly but runs the risk of oscillating. This parameter is typically chosen depending on the batch size. The higher the data set or the batch size, the more reasonable it is to choose a higher learning rate to counteract the slow learning process. It is also common to set a learning rate that degrades during the training. If a plateau is reached during optimization, the reduction of the learning rate can lead to higher robustness and initiate a fine-tuning process.

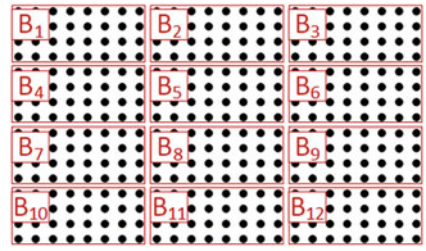

Fig. 5.54 Subdivision of a data set into batches

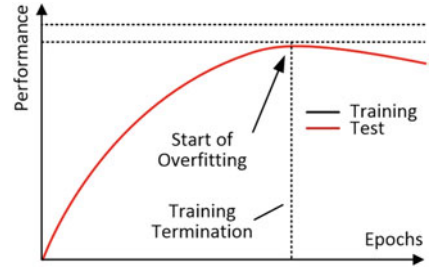

Fig. 5.55 Training/Test versus epochs

8. **Number of Epochs**
   The iteration of a training step (see Figs. 5.42, 5.43 and 5.44 using the example of the backward propagation procedure) is called an epoch. As a rule, so many epochs should be performed until the validation quality of the test data reaches a maximum. The training process should therefore be terminated by a termination criterion. If the training accuracy increases during further training while the validation accuracy of the test data remains the same or even degrades, it is a sign that overfitting is taking place (Fig. 5.55).

A manual determination of optimal hyperparameters by a trial and error method is enormously time-consuming and inefficient. Due to constantly growing challenges, AI users now have modern and reliable algorithms called Automated Machine Learning (AutoML) at their disposal, which highly automates upstream screens and the search for hyperparameters. The degree of automation promises to adapt the techniques of machine learning on a high level even to non-experts.

AutoML algorithms support from the input of raw data all the way to the complete development of predictive models and help users to shift their tasks more and more to overarching topics rather than having to deal with detailed tasks such as pre-processing of data, feature extraction and feature selection, algorithm selection and hyperparameter optimization. AutoML algorithms use optimization methods such as the Manual Search, Grid Search, Random Search and the Bayesian Optimization, which will not be discussed in detail here.

5.5.5 Fuzzy Logik

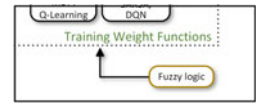

The term fuzzy logic was first published in 1965 by the Azerbaijani mathematician and computer scientist Lotfi Aliasker Zadeh at the University of California, Berkley. The basis

for this, however, lay in much earlier studies of the1920s by Jan Łukasiewicz and Alfred Tarski known through the so-called Łukasiewicz logic.

This topic deals with the handling of data that are subject to a certain fuzziness. In contrast to the concept of Boolean logic, where quantities are rounded to 0 and 1 to categorize fuzzy quantities, fuzzy logic allows assigning any value between 0 and 1 to a quantity, which is the basis of the concept of partial truth.

Fuzzy logic is based on observations of human decision behavior. Often these are made on an inaccurate and non-numerical background information. On the one hand, the information can be strongly founded and validated or it can be based on a conglomerate of unconscious experience values, which manifest themselves as a so-called "gut feeling". The intermediate stages are vague and not differentiable—this is exactly the area that fuzzy logic tries to represent numerically and quantify on a mathematical basis. The concept of fuzzy logic has a wide range of applications, especially in the field of control (electronics) and artificial intelligence.

Using a simple example of the subjective sensation of test persons who feel a liquid of different temperatures (in this case water) on their skin, the following diagram gives an example of how statistical sensation can be classified into individual categories using fuzzy logic. It can be seen from this that when control strategies of this type of subjective parameters are used, a range is obtained whose weighting is taken into account by fuzzy logic. In this example, 72% of the test persons perceive a water temperature of 39° C as hot and 28% as warm. In reality, dependencies cannot be represented by simple, linear relationships, as shown in Fig. 5.56.

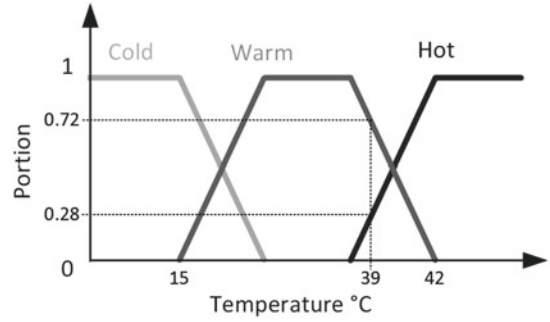

Fig. 5.56 Temperature sensation in a group of test persons

Combination of fuzzy logic and artificial neural networks

In the past, intelligent, hybrid systems combining fuzzy logic and neural networks have proven their high efficiency in a variety of real-world application problems. While neural networks, for example, are predestined to recognize patterns from a large amount of data and henceforth to expand their model predictivity in a self-learning manner, their decision-making is fundamentally inexplicable or incomprehensible. Fuzzy logic, on the other hand, can argue with the help of inaccurate information and present decisions in a comprehensible way, but it cannot determine the rules it uses for these decisions. As a result of the two-sided limitation, the motivation to combine both systems into an intelligent hybrid system becomes apparent. The computational process intended for fuzzy neural systems can be divided into the following three steps:

- The first step is the development of a "fuzzy neuron" based on the understanding of biological neural morphologies and subsequent learning mechanisms.
- This is followed by the integration of fuzzy neural models with synaptic connections, which include a fuzziness in the neural network.
- Finally, the development of learning algorithms for the adaptation of synaptic weights follows.

Basically, there are two possible ways to design fuzzy neural systems:

1. A multi-layer neural network controls the fuzzy mechanism; see Fig. 5.57 (left).
2. The fuzzy interface provides an input vector for a multi-layer neural network. The neural network is adaptive and is trained to calculate desired command outputs or decisions; see Fig. 5.57 (right).

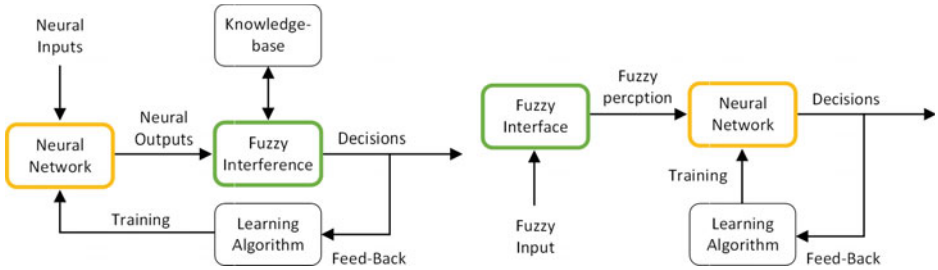

Fig. 5.57 Combination of fuzzy logic and a neural network as a hybrid system for 1. ANN as data supplier (left) and 2. fuzzy logic as data supplier (right) [60]

Example 11: Subjective driving behavior for the calibration of electronic control units

By definition, subjectivity describes the relationship of a subject to its environment. In a derived sense, a customer's decision to purchase a vehicle is based on subjective driving impressions. Particularly noteworthy here is the so-called "drivability", which is the sum of many individual technical components at the end of vehicle development. However, even the application engineer who is responsible for the application of electronic control units can influence the drivability of a vehicle to a certain extent.

For many years, many central research projects have been dealing with the development of suitable calculation methods for test procedures in order to transform subjective driving experience patterns into objective evaluation criteria. Finding a clear match is very complex, especially because a driving experience can vary according to country of origin, road conditions, age, gender and other factors. In [61]*, an approach is presented where objective parameters for the drivability are divided into 3 categories: 1. suspension comfort, 2. steering response and 3. load change behavior. They have proven to show a good agreement with subjective parameters. For a multitude of vehicle classes and subjective measurement data of drivers, the parameters provide information about trigger points in the vehicle, so that optimizing measures can be initiated concretely.*

If the three categories (suspension comfort, steering Response and load change behavior) are divided into 5 evaluation levels, a very useful application for the hybrid combination of fuzzy logic results: (Fig. 5.58)

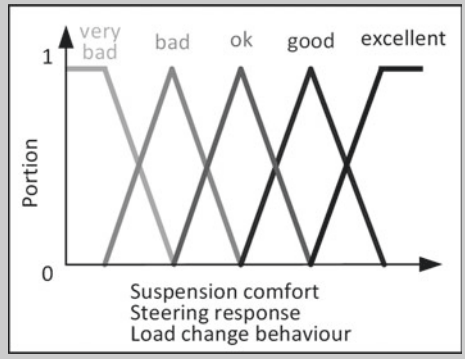

Fig. 5.58 Weighting of different load shares of a driving cycle using fuzzy logic

5.6 Deep Learning

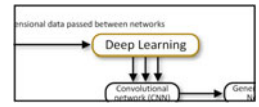

Deep learning is a special learning method for artificial neural networks, which is characterized by a much more complex structure than the networks discussed so far. Basically, an ANN is also called Deep Neural Network (DNN) by definition, if it has at least two hidden-layer levels. Besides DNNs, the term deep learning also includes other forms of networks such as the convolutional neural network (CNN), which is mainly used for image and sound recognition [62].

For neuronal networks of the category deep learning, multiple learning methods can be used: Classification and regression of known input and output data (supervised learning see Sect. 5.4.1), clustering and association of non classified data (unsupervised learning see Sect. 5.4.2) as well as reinforcement learning, where an agent is in exchange with an environment as a source of interference (see Sect. 5.4.3). The method chosen depends entirely on the application case and should be carefully considered before starting to create a model.

5.6.1 Convolutional Neural Network (CNN)

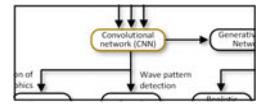

Convolutional Neural Networks (CNNs) belong to an extended form of networks that, similar to ANNs, are composed of neurons with learnable weights and a bias. The fundamental difference is the application of these networks: CNNs explicitly assume that the input consists of graphics. As a consequence, CNNs are composed of pure feedforward connections, (see Sect. 5.5.2). For the training of the weights, the backward propagation method is usually used (see Sect. 5.5.3).

Usual ANNs are unsuitable for scaling single neurons to a full pixel level of images. A simple graphic with 32X32 pixels and 3 RGB color codes per pixel would have 3072 connections (weights) in the hidden layer if an input neuron was completely connected by all combinations. If one assumes that a significantly higher number of hidden layers is desired to increase the performance of the model and that graphics can have much higher resolutions,

the total number of weights would exceed the computational load of any computer. Hence, a completely linked connection of all neurons would prove to be inefficient.

CNNs divide the 3D pixel color code of a complex graphic into many small segments called cascades. From now on, a neural network is divided into subareas—each subarea represents a cascade and is individually trained. This highly efficient approach allows the number of connections to be reduced abruptly. This has the further advantage that cascades of certain image areas can train special image features, which, when all cascades are combined, provide more detailed information about a graphic.

Image Recognition

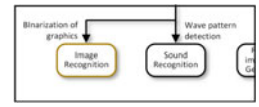

Image Recognition is an interdisciplinary field of science that focuses on training algorithms to examine digital images, videos or video sequences at a high level of detail. This includes methods for capturing, processing, analyzing and extracting multidimensional visual data from the real world. Image recognition can be interpreted as the decoding of symbolic information from image data, which in its inner core can be constructed of geometry, physics and statistics. In principle, the method of image recognition is comparable to a classification of the supervised learning process (see Sect. 5.4.1).

From an engineering perspective, this science is used to automate tasks that the human eye and brain cannot comprehend due to their complexity. A common problem of image processing is to determine whether image data contain specific objects, features or image sequences. For this purpose, the process of image recognition is divided into different cascades.

Using the example of image recognition, the transformation chain and the process of a CNN will be illustrated. For this purpose, an optical measurement of a 6-hole injector nozzle of a DI gasoline engine (snapshot of an injection pattern) at 270° crank angle before top dead center is fed into the network.

In Fig. 5.59, the first layer of the CNN recognizes the number of injection nozzles, the second layer deals with the injection angles, another layer with the geometric limitation by the combustion chamber walls, another layer focusing on the turbulence decay of the injection, etc. Furthermore, optical measurements can be post-processed by the application of filters, for example, by illumination, so that further layers can better interpret characteristic features of combustion such as temperature distribution, combustion speed, emissions and soot particles [63].

In the shown cascade, after feeding it with images, the hidden-layer process begins which consists of a convolution process and a pooling process, taking place in alternating order

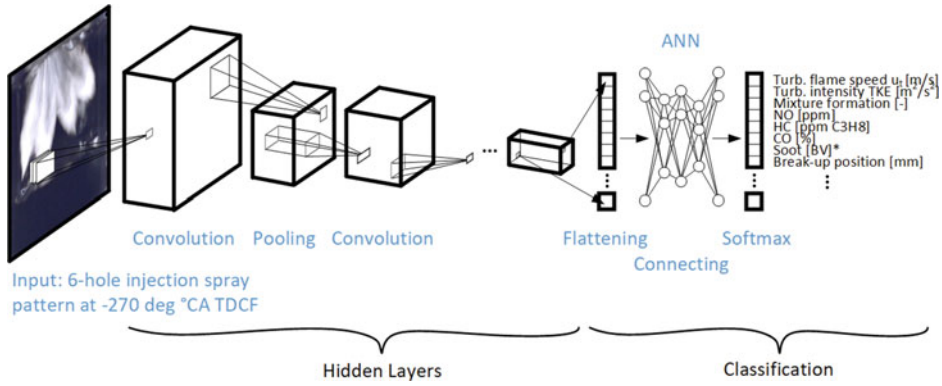

Fig. 5.59 Cascade structure of a CNN process[4]

to gradually break down desired features. Once this process is completed, the classification process follows. Here, the results of a matrix are transferred into 1D vectors and transformed into a softmax.

The Hidden-Layer Process

Convolution is one of the main building blocks of a CNN. The term derives from the mathematical combination of different sets of information to generate a function. By applying filters, so-called feature maps are generated. Each input node is subjected to matrix multiplication and the result is projected or summed up on the feature map. Especially for image processing, the matrices are composed of the 3D height, width and depth, and the contents correspond to the red-green-blue (RGB) color codes.

In the following, Fig. 5.60 shows the projection of a pixel-code area, which is projected through a convolution filter onto a result matrix.

In a hidden-layer process, the input is subjected to numerous convolutions, with each convolution using different filters. This results in different feature maps. Finally, all feature maps are combined as the sum of all convolution layers into an output matrix. As in all neural networks, activation functions are used to design nonlinear functions between inputs and outputs. A common activation function that is chosen is the ReLU function; see Fig. 5.32 in retrospect.

Since the size of a feature map becomes smaller than that of its input matrix due to a convolution, an intermediate step must be initiated to restore the original size. For this purpose, the padding method is used, and empty spots of the result matrix are filled up with zeros.

[4] BV=Blackening Number or smoke degree.

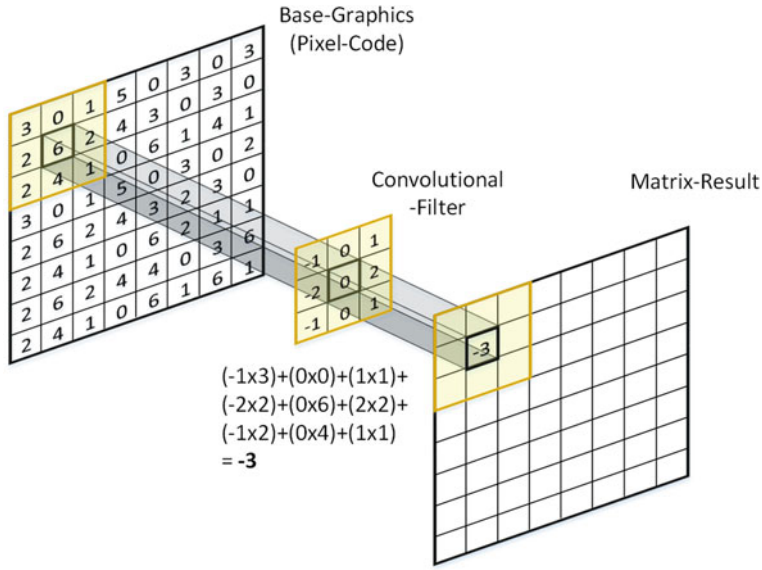

Fig. 5.60 Conversion of an RGB pixel code by a convolution filter (convolution process)

After convoluting and padding, the next process called pooling is performed. This has the function of smoothing the result matrix and removing possible irregularities or outliers. In addition, this process continuously reduces the dimension of the matrix, which reduces the computational load of the network. Different approaches for pooling are presented in the literature. Among the most important ones are Average Pooling (projection of the mean value), Max Pooling (projection of the maximum value) and RMS Pooling (projection of the quadratic mean value) as summarized here (Fig. 5.61).

The Classification Process

The main purpose of the classification process is to transform the results of the hidden-layer process into tangible quantities. According to Fig. 5.59, this section is divided into Flattening, Connection and Softmax.

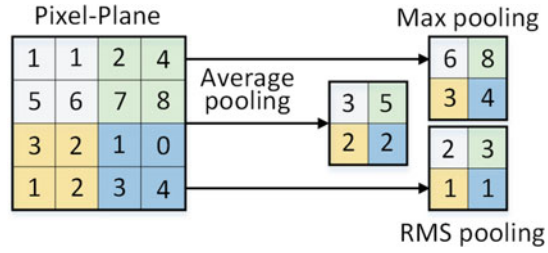

Fig. 5.61 Pooling method for data filtering [64]

The Softmax function comes from mathematics and has the function of normalizing absolute numbers of different features and units. The normalization process projects all numbers onto a range of [0,1] so that they can be interpreted as probabilities. Consequently, the result of a CNN process is a statistical analysis serving a probability statement. It is important that through such an intensive learning process, the network is able to decipher independently which functions have to be optimally placed on which level. In this way, each layer learns to convert its input data into a more abstract and coordinated representation. If a statistical analysis is not desired, the value range of the output can also be transformed back to the original unit.

Image recognition has become a far-reaching term that combines a variety of technologies. One of the more prominent applications is the principle of **Identification**. Here, it is of interest to identify individual features of an object in order to compare them with other features from a database, for example. The identification by scanning of QR codes, eyes (iris scan), fingerprints or handwriting is one of the most prominent applications.

Object recognition or **object classification** belong to the methods that aim to identify single or multiple defined objects or object classes within an image. Blippar, Google Goggles and LikeThat are examples of independent software products in this segment.

A subcategory of this, called **Shape Recognition**, deals with the investigation of class features in the narrow sense. In contrast to object recognition, nested layers are analyzed and distinguished, such as head, shoulders and arms in an image of a person or animal, to which the averted form **Face recognition** also belongs.

Graphics Detection is a method that scans images to identify special features. It is mainly used to analyze parts of interesting image data and to conclude concrete interpretations regarding the content. In medical applications, for example, this includes the detection of possible mutated cells or abnormal tissue from high-resolution CT or MRI images.

Content-based image retrieval is based on a fast search algorithm that is able to check a huge pool of images (example: circulating Internet data) for specific content. The search criterion can be to search for images with similarity to a reference image or by entering any search criterion (example: search all images from which animals are found).

In addition to the categories mentioned above, there are a number of other application-related possibilities such as **Pose estimation**, for estimating the orientation of certain objects relative to the camera (example: supporting a robot arm when retrieving objects from a conveyor belt for industrial applications), and **Motion analysis**, for detecting moving images (video recordings) [65, 66].

The following examples will give some ideas on how image recognition techniques can be applied to powertrain development in a goal-oriented way.

Example 12: Influence of injection characteristics on combustion and emissions

The image recognition is suitable for breaking down a large number of graphics into their characteristics in order to draw conclusions about their content. One topic from the field of powertrain development that is ideally suited for this purpose is the evaluation and processing of optical measurements using high-resolution low- and high-speed cameras. In order to use the cascade of the presented example from Fig. 5.59, it is shown here to what extent large data sets of injection cone images can be used to train neural networks. Three different injectors with the following geometries are the basis for preceding optical measurements, see Fig. 5.62.

The training phase of a CNN is carried out with a total of 750 images. Each injector is subjected to a series of measurements, with 50 discrete crank angle images. The operating load is in the range of 0–40% of the maximum possible load. The following pictures show the result of a measurement series. On the left side, a standard image is shown, and on the right side a special color filter is applied to emphasize certain image features in order to simplify later recognition process (Fig. 5.63).

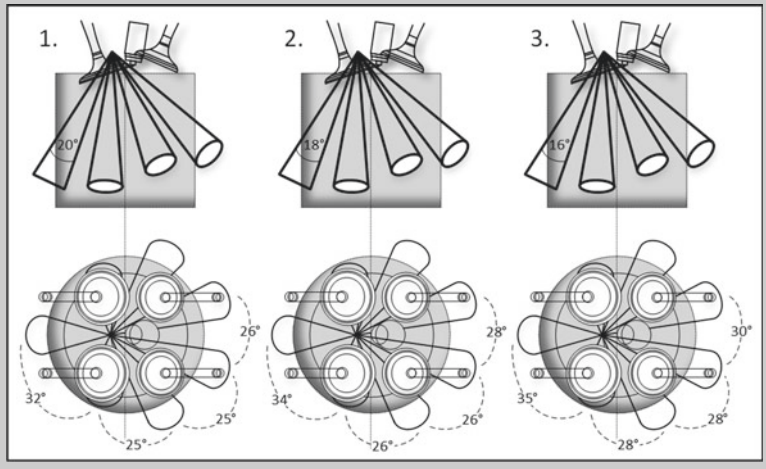

Fig. 5.62 Geometries of three different fuel injectors

The results of combustion from the resulting injection variations are shown here. Filters are also used here to enhance the visual characteristics, see Fig. 5.64.

Finally, for the training phase of the CNN, desired parameters such as turbulence, mixture and emissions which were determined by means of measuring devices, are put into relation with the images (Fig. 5.65).

Images not involved in the training are always used to validate the model. In principle, it is possible to reverse the procedure. In this case, the CNN would generate images of injection features and the corresponding combustion if the desired output variables are specified. The model is thus able to provide precise suggestions as to what the geometric characteristics of the injectors should look like in order to meet desired physical target values.

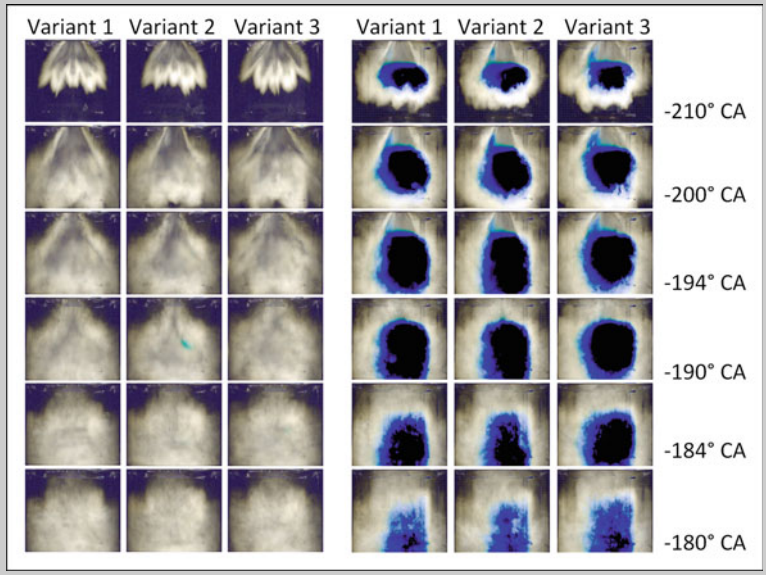

Fig. 5.63 Optical measurements of injection characteristics for different geometries

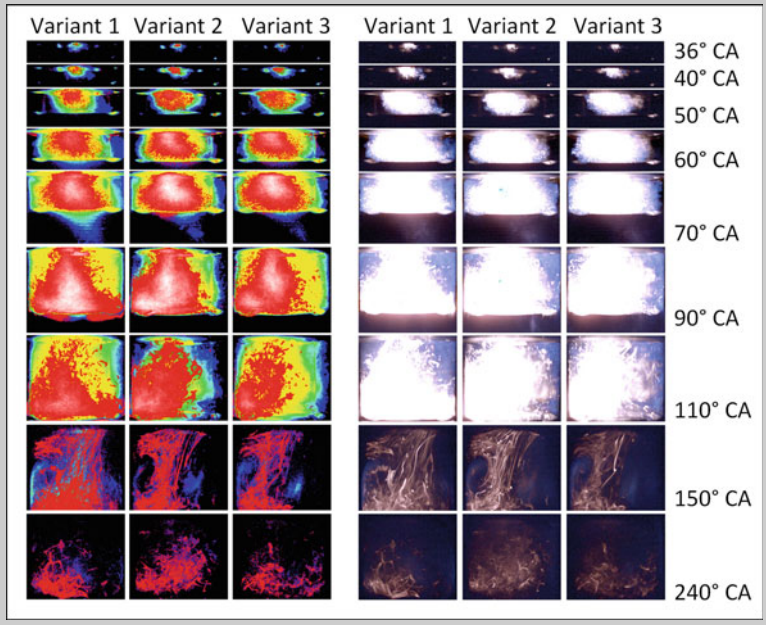

Fig. 5.64 Combustion optics: Application of fluorescence filters to enhance image features: diffusion flame (left) and soot formation (right)

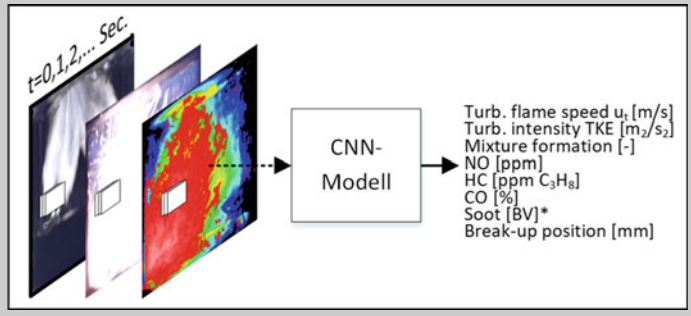

Fig. 5.65 CNN to predict specific quantities (turbulence, mixture formation, emission, etc.)

Example 13: Flow simulation

In this example, a CNN is developed to reflect 2D/3D flow calculations. The main focus is on the fact that it is in principle feasible to predict transient, i.e. time-dependent phenomena of Newtonian flows.

As long as a neural network is provided with the necessary inputs, it is in principle possible to implement shear rates proportional to shear stresses as well as the viscous behavior that obeys the equations of Navier-Stokes. If a high quality of agreement with classical 3D-CFD computation can be achieved, massive time and cost savings will result, particularly since the computational time reflects the bottleneck of development processes. In retrospect, Fig. 4.16 has qualitatively represented the savings of the calculation time that are possible with AI compared to conventional methods.

Using the example of a plate with variable dimensions in height, length and width, airflow is examined, which enters the plate at the entrance (top right) and exits on the bottom left; see Fig. 5.66. The state is changed by making a circular or elliptical incision in the plate. This incision is shifted on the coordinate system within the plate and, in the case of an ellipse, rotated randomly in order to train all possible effects of the deflection of the flow.

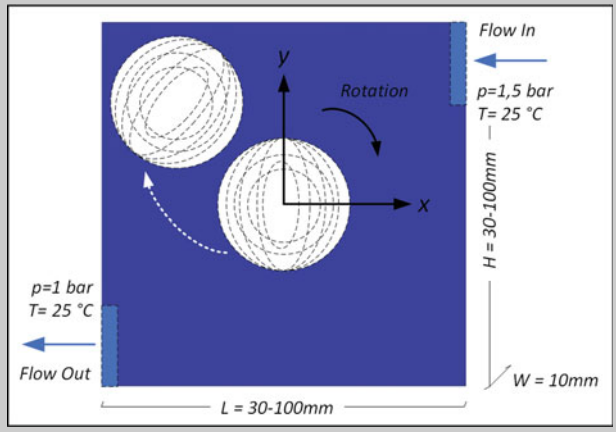

Fig. 5.66 Training phase of a flow through a plate with variable geometry (variable circular or elliptical incisions)

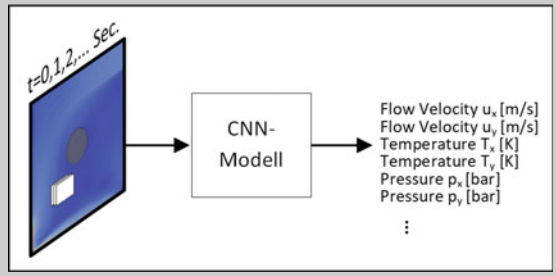

Fig. 5.67 CNN for generating time-discrete outputs of flow results

Then each variant is calculated by 3D-CFD simulation. The results of the calculation provide time-discrete snapshots, which are used for the training of the CNN (5000 images in total).

Figure 5.67 shows the principle structure of the model. With 3D-CFD, the CNN model is trained and time-discrete results for the velocity vector (u_x, u_y)*, the temperature vector* (T_x, T_y) *and the pressure vector* (p_x, p_y) *are determined. The 6D output vector* $(u_x, u_y, T_x, T_y, p_x, p_y)$ *reflects the flow state in each coordinate point.*

In contrast to the training phase, which consists of the generation of flow patterns of plates with a single incision, the validation phase also examines plates with two or more incisions. This helps to understand how flexible the CNN model is and how it is able to adapt to new and previously unknown planes. In the following, 3 different plates are presented for the validation, all with the dimensions $(x = y = 50mm, z = 10mm)$ (Fig. 5.68).

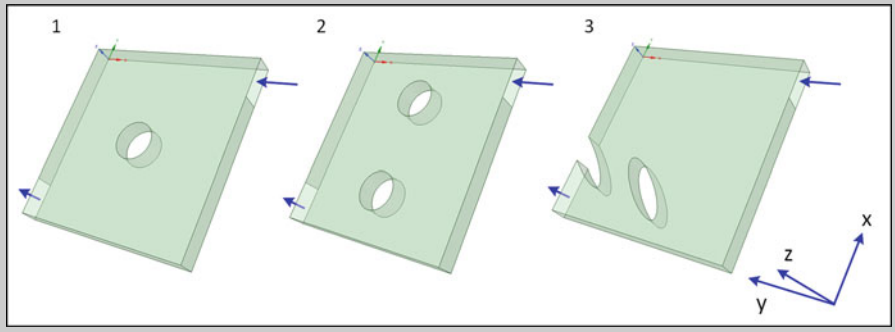

Fig. 5.68 Validation of the CNN model using flow-through plates with different incisions

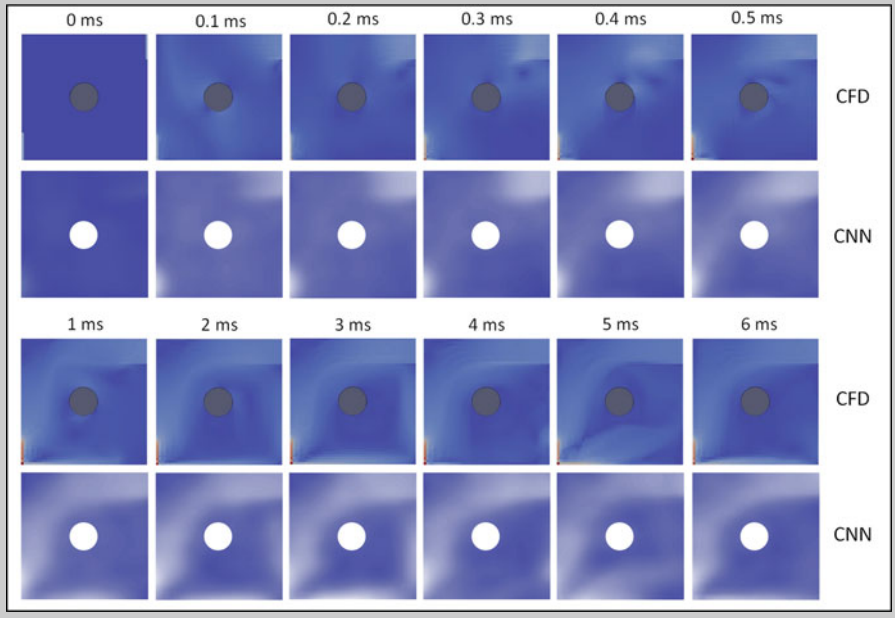

Fig. 5.69 Plate flow with central, circular incisions in comparison: CNN versus 3D-CFD

Figure 5.69 compares the result of the CNN model for plate variant 1 and a central hole incision with the 3D flow calculation (CFD). The CNN model generates transient flow images ranging 0ms–6ms. It is remarkable that it is able to reproduce recurring flow fluctuations (see 4ms–6ms) that occur in a phase before convergence is reached.

The example of plate variant 2 clearly shows that the interaction of the flow can be transferred to 2-hole incisions. Realistic images can also be generated here compared to that of CFD calculations (Fig. 5.70).

Finally, the validation on plate variant 3 shows that the flow can be qualitatively simulated even along complex and asymmetrical incisions (here elliptical shapes), one of which is adjacent to the plate edge. Here also, the effects of short-circuit currents, which are reflected in the snapshots ranging 0.5ms–3ms, are remarkable (Figs. 5.71).

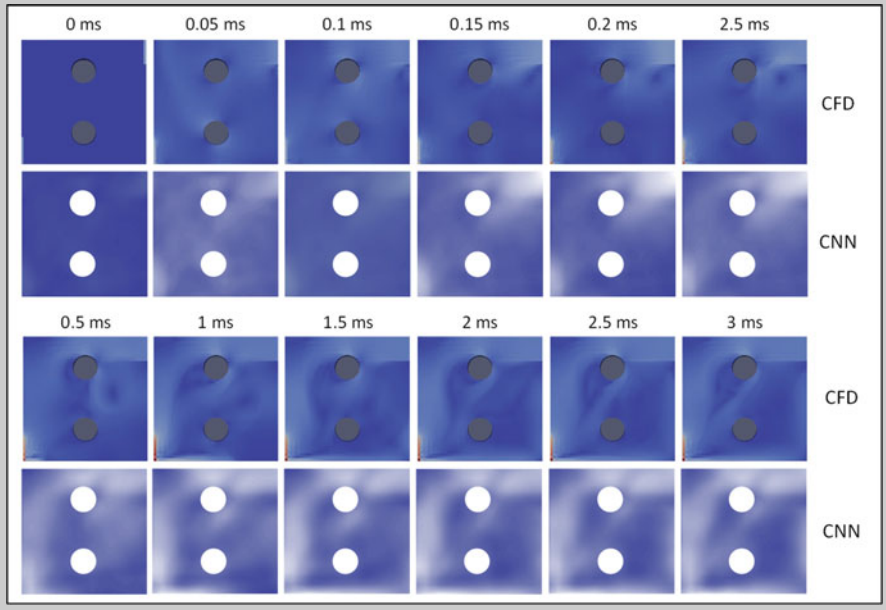

Fig. 5.70 Plate flow with two circular incisions on the transverse axis in comparison: CNN versus 3D-CFD

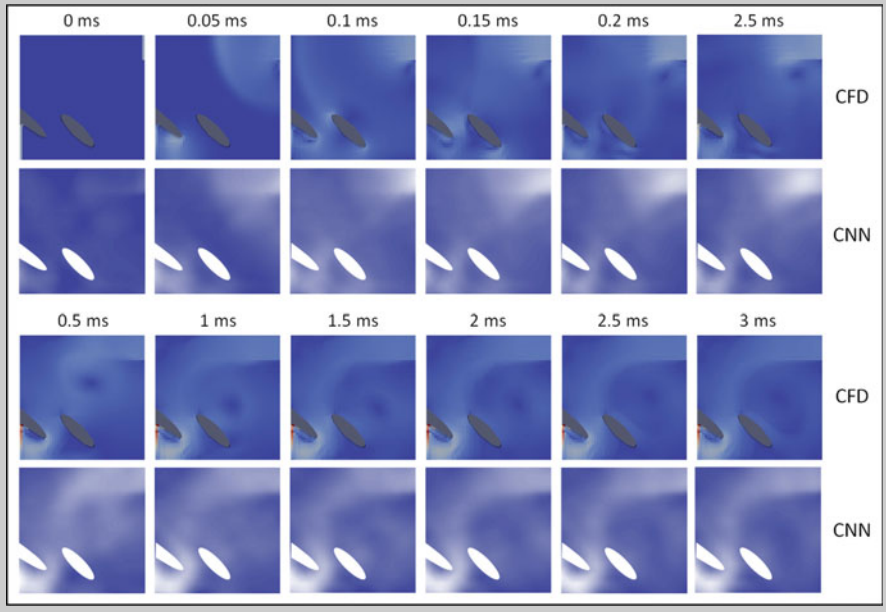

Fig. 5.71 Plate flow with asymmetrical incisions in comparison: CNN versus 3D-CFD

Sound Recognition

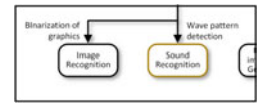

For over 120 million years, sound recognition has been one of the primitive survival instincts of all life forms. The sensitivity and performance of the sense of hearing can vary greatly. Speech and hearing together form the ability to communicate, and depending on lifestyle and living environment, the sense of hearing is evolutionarily adapted to enable the ability to communicate within individual species and to allow the auditory recognition of natural enemies.

The interaction of the ear and the brain as the central processing unit enables sound to be characterized for different features. The localization of sound combines the recognition of the **sound direction** and the **sound distance**. As an indication for the determination of the distance, the sound level or level differences of different sound sources relative to each other play an important role. The **frequency spectrum** of the sound provides the information about the sound source itself and can additionally be helpful for determining the distance to the source. As, for example, a distant sound is perceived as dull, a further characteristic is the **motion of a sound** that is perceived while one of the mentioned characteristics changes relative to the listener.

Sound recognition is a decade-old field of science that traditionally deals with pattern recognition theories. The underlying analysis methods use algorithms for data processing, feature extraction and classification of sound. More recently, the field has benefited enormously from the advances in artificial intelligence. Especially the data collection through the method of Big Data as a statistical analysis tool for real data has proven to be highly efficient. In combination with the deep learning network type (CNN), Sound Recognition is now evolving into a modern technology that aims to solve the processing of a sound according to human processing concepts. This is done by imitating neuronal and biochemical mechanisms underlying unconscious thinking. The power of modern computers helps to exceed the performance of a human brain by far.

Conventional method of sound recognition

Figure 5.72 shows a common sequence of different techniques for the sequential decoding and classification of sound features from the time domain [67].

Sound

A common sound recognition process starts with a sound being recorded, which is received by a microphone as a time signal. The higher the quality of the recording, the easier the recognition process can be designed. Background noises or room reverberation, for example, are

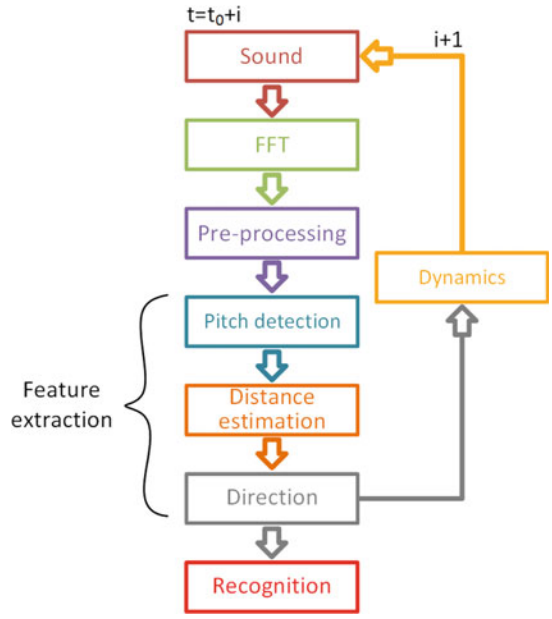

Fig. 5.72 Conventional Sound Recognition: Sequential extraction of individual sound features

unwanted effects that disturb the sound and make the later recognition process more difficult. The quality of the transduction unit in the microphone (conversion of a sound pressure into an electrical signal) can also have a great influence on the quality of the sound recording.

FFT

In a few cases, the information of a sound wave can be sufficient to extract features for sound recognition. However, the variability and the resulting complexity of sounds usually require the execution of a Fast Fourier Transformation (FFT) and the transformation of the wave signal into its spectral components. From this, all relevant frequency orders with the associated amplitudes and phase information are obtained, by which the characteristics of a sound signal are established; see retrospectively Sect. 3.5. The FFT is intended for periodic signals with a fixed periodic length. If a recorded sound is variable (dynamic), a fixed period length must be cut out of the sound signal.

Pre-processing

Pre-processing plays an important role in eliminating irrelevant sources on the recorded audio soundtrack, which later facilitates the accuracy of the recognition process. It includes the filtering of background noise, smoothing of dynamic noise, endpoint detection for periodic closure of a sound signal (for non-periodic signals), determination of a suitable window function and suppression of reverberation and echo.

Pitch Detection
Pitch detection is used to characterize dominant tones. This ensures that only frequencies with a high energy density compared to others in the overall spectrum are sorted out. The consideration of the cleaned spectrum can be important for the classification of a noise source.

Distance estimation
The distance between the microphone and the sound source, especially with moving sound sources, can be estimated by the sound pressure level. For this purpose, a relative calculation is made in relation to existing background noise.

Direction
If a sound source is moving, it may also be of interest to consider the direction of movement relative to the microphone. This can be realized if several microphones (at least 2) are mounted in opposite directions, so that the relative change of the different sound pressure levels can be taken as a reference.

Dynamics
In the process phase "FFT", the problem of the periodicity of a sound signal was mentioned as a prerequisite for a Fourier synthesis. If a sound is non-periodic, this problem can be solved in the last phase by stringing together many non-periodic signals of the FFT. The result is a quasi-continuous picture of a tone, which allows examining and evaluating even time-dependent signals.

Sound recognition with AI
Sound recognition based on neural networks corresponds in principle to a classification of the supervised learning method (see Sect. 5.4.1). While CNNs only allow images as inputs, sound recognition is performed using the same principles of image recognition. After an acoustic sound signal has been transformed into a spectrogram, i.e. into a graphical representation, using the FFT method, a CNN method can be applied. Fig. 5.73 shows exactly this process sequence [68].

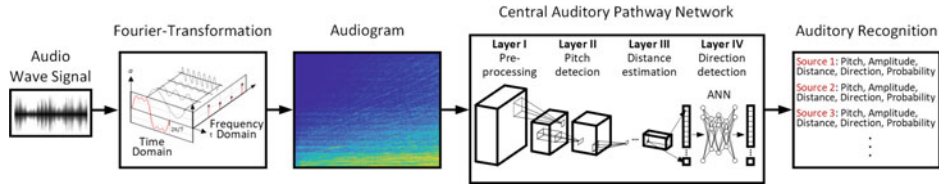

Fig. 5.73 Sound Recognition: Sequential extraction of individual sound features by CNN

Noise vibration and harshness (NVH), i.e. the acoustic data acquisition and analysis of structure-borne and airborne sound, is one of the major topics in the development of motor vehicles and offers far-reaching application potential for sound recognition. Some important applications are listed as follows:

- Body and chassis
  - NVH and structural dynamics for car body vibrations especially for lightweight components in the medium frequency range;
  - Eigenvalue analyses of brakes;
  - Rolling noise in the passenger compartment and for driving past depending on tire profile and wheel suspension;
  - Aeroacoustics: Audible vibrations in the vehicle interior due to external currents and sound pressure.
- Powertrain
  - Engine acoustics, torsional vibration dampers and injection systems;
  - Valve train;
  - Transmission and differential gear.
- Electric mobility and vehicle electronics
  - Electrical drive, battery and power electronics (PCU);
  - Electronic boards and control units (ECU) and GCU.

Voice Recognition has been used for many years in criminal investigations for the automated comparison of stored data. It is also used for identification monitoring, alarm systems and personal identification at banks. Acoustic oceanography and the science of animal noises and communication behavior have provided sound recognition with great insights over the last decade. More conventional in use are natural speech recognition systems like Siri and Alexa or music recognition applications like Shazam and Soundhound, which use the same techniques of artificial intelligence.

Example 14: Powertrain acoustics

Powertrain acoustics offers a wide range of applications for the sound recognition process. This is due to the fact that acoustic measurement data can be generated easily, but spectral analyses can only be differentiated at great expense. Depending on the measurement signal, the data can vary by different levels of uncertainty due to measurement noises. An acoustic engineer is therefore often faced with the task of breaking down measured sound signals, which are composed of a superposition of different noise sources, into their individual components. Along with extensive experience, components of special frequency spectrums can be assigned to a noise source—the task becomes more complex when destructive interference causes signal sources to be canceled out so that they cannot be recovered again.

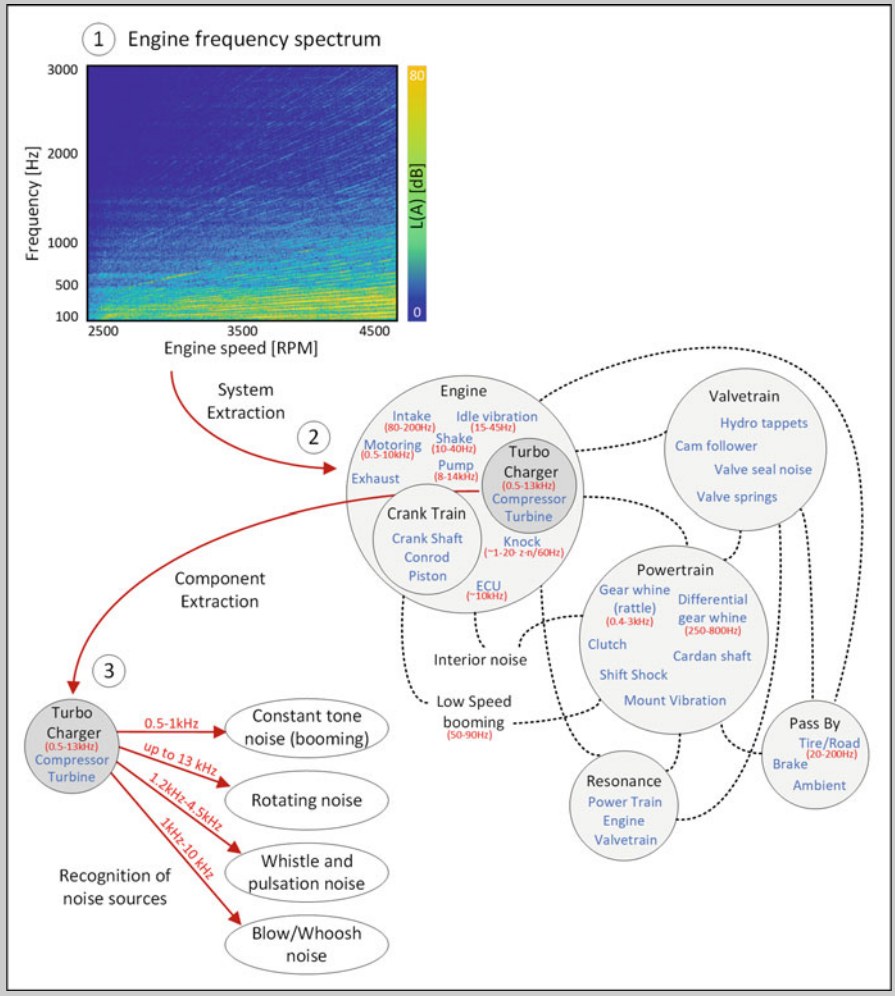

Fig. 5.74 Sound recognition applied to the frequency spectrum of an engine to recognize turbocharger specific noises

As can be seen in the next example, a CNN is fed by the frequency spectrum of a recorded sound that was measured on a motor. The model is able to separate all superimposed sounds from each other and assigns them to individual systems. Furthermore, it determines individual noise sources, as in the example of the turbocharger, and splits these into individual frequency ranges. The sound signal is then completely characterized, which enables the acoustic engineer to make a detailed pre-diagnosis of the existing system (Fig. 5.74).

5.6.2 Generative Adversarial Network (GAN)

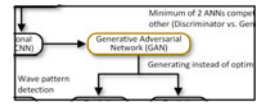

Generative Adversarial Networks (GAN) are part of a highly advanced group of algorithms developed in 2014 by a US computer scientist named Ian Goodfellow, which has established itself remarkably fast for artificial intelligence applications. The concept, which was originally based on the supervised learning method, has now also proven to be very powerful for unsupervised and reinforcement learning. The special feature of a GAN is that two neural networks are used simultaneously—a so-called generator and a discriminator. These networks compete with each other—while the generative network generates synthetic data, i.e. data that does not originate from reality, and real data is simultaneously fed into the system. The discriminator faces the challenge of evaluating the incoming data and checking it for authenticity. The interaction of these neural networks promises a highly efficient and autonomous training.

While the discriminator divides a given input into a cascade structure in order to perform a feature characterization on different levels, the way the generator works is contradictory. In each feature level, it is able to change properties by a reciprocal convolution. The following example shows the functioning of a generator and a discriminator by the example of microscopic fracture structures of a metal material (Fig. 5.75).

The GAN is interpreted as a competitive process because of the way it works. The training goal of the generative network is to increase the error rate of the discriminative network, i.e. to fool the discriminator by generating data that appear realistic so that the discriminator classifies them as non-synthesized.

If the discriminator is fed with a real and a synthetically generated image, it generates a function $D(x)$ as an output signal, which corresponds to a probability x that states whether the input corresponds to a real image or not. The goal is to maximize the function $D(x)$. To measure a representative result, the cross- entropy function is used.

$$\max_{D} V(D) = E_{x_{t+1} \sim p_{data}}(x_{t+1})[log\, D(x_{t+1})] + E_{z \sim p_{noise(z)}}[log(1 - D(G(z)))] \quad (5.19)$$

The generator on the other hand also tries to generate images at a maximum possible value for $D(x)$.

$$\min_{G} V(G) = E_{z \sim p_{noise(z)}}[\log(1 - D(G(z)))] \quad (5.20)$$

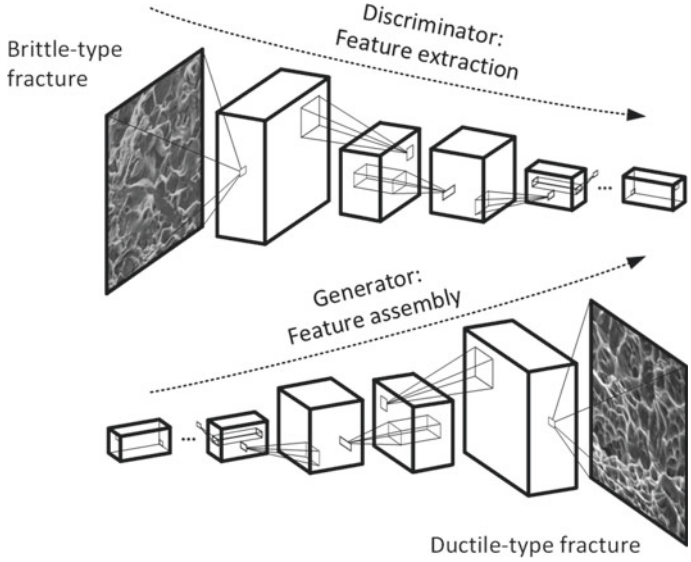

Fig. 5.75 Functioning of the discriminator (top) and the generator (bottom) at microscopic fracture structures of a metal material

In summary, a GAN is often interpreted as a MinMax game, where the generator G tries to minimize the function V and the discriminator D tries to maximize it (Fig. 5.76).

$$\min_G \max_D V(D, G) = E_{x_{t+1} \sim p_{data}}[\log D(x)] + E_{z \sim p_{noise(z)}}[\log(1 - D(G(z)))] \quad (5.21)$$

Monitoring and training are controlled by an agent. For a sample matrix (input matrix) $[x]$ with m dimensions $x_1, x_2, \ldots, x_m$ and a noise matrix $[z]$ with m dimensions $z_1, z_2, \ldots, z_m$, an agent transfers the following equation to the discriminator:

$$\nabla \Theta_D \frac{1}{m} \sum_{i=1}^{m} [log D(x^i) + log(1 - D(G(z^i)))] \quad (5.22)$$

The generator on the other hand is monitored with the following equation:

$$-\nabla \Theta_D \frac{1}{m} \sum_{i=1}^{m} [\log(1 - D(G(z^i)))] \quad (5.23)$$

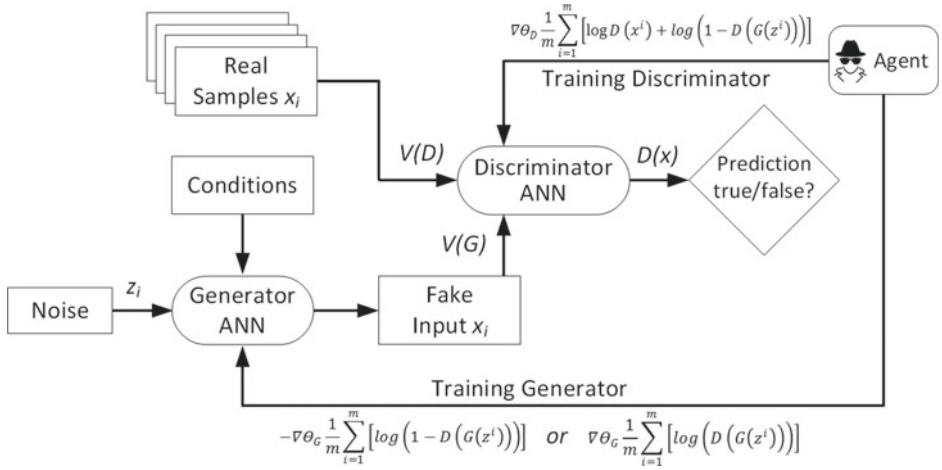

Fig. 5.76 Working process of a GAN

With the gradient descent method, one quickly encounters the problem that the discriminator defeats the generator early on due to its stronger function weighting, which means that in the early training stage non-real images can be quickly distinguished from real ones. To solve this problem, it is a good idea to program the GAN with an alternative function to retransmit the gradients [69]:

$$\nabla\Theta_D \frac{1}{m}\sum_{i=1}^{m}[\log(D(G(z^i)))] \tag{5.24}$$

GANs are currently still mainly used in the field of image processing and image generation. Among the best known applications are the realistic generation of photographs of human faces, manipulation of human poses, and "photo-aging" which is used by many cell phone applications. In the cartoon area, GANs are used to create new characters, and in the fashion design area to create suggestions for new patterns, designs and fresh inspirations. On the Internet, astonishing artworks are circulating that have been synthetically created with the help of existing works by famous artists and are amazingly similar to them. In the area of technical design, GANs are used in the modeling of 3D objects to generate new systems of objects and so to create fresh ideas, such as in the development of sports prostheses.

Example 15: Application of electronic control units

In the field of powertrain development, the basic idea of synthetic data generation can be transferred excellently to the base application of ECUs, the application of hybrid strategies or the power application of GCUs and PCUs. In principle, huge amounts of data are required to cover different stationary and transient operating ranges. For an internal combustion engine, a base application usually starts with the mapping of the air path for the steady state. For this purpose, the air mass flow is represented as a function of 1. intake valve timing, 2. exhaust valve timing, 3. boost pressure, 4. wastegate position, 5. throttle position and 6. engine speed. This is also done for different 7. ambient temperatures and 8. ambient pressures. The strategic procedure may differ depending on the manufacturer. Due to the 8D system shown here, a very rough subdivision of all parameters into 5 categories each already results in $5^8 = 390.625$ *combinations. Even modern space-filling methods (see retrospective Sect. 4.3) are easily overstrained by an enormous measuring and simulation effort when a thorough and error-free application is desired.*

These types of problems can be greatly tackled by the concept of GANs. It is able to provide enormous help in this respect by independently generating a massive amount of virtual data that imitate real data. This eliminates the need for test-based generation by test bench measurements or simulation-based data generation, which saves a lot of time. Fig. 5.77 illustrates a flowchart for this.

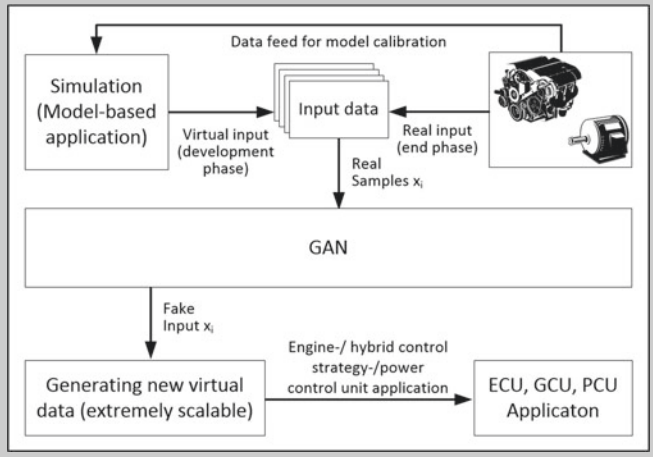

Fig. 5.77 GAN for an extremely scalable generation of data

5.7 Software

The science of data is a young and promising field that is developing rapidly, especially in the provision of data-based application software. This chapter intends to give an overview of ways for data handling and the underlying possibilities with regard to AI features, in the midst of numerous options. Which software and library package is the best one is left to the discretion of the respective application and may vary depending on it.

Many languages are now in use by data scientists and are very useful for individual applications. Among the most popular and widely used languages are Python, Scala and R, which have prevailed in the field of machine learning. Their now versatile and powerful libraries set them apart from individual solutions. Last but not the least, the constant development of additional package solutions provides the users a high degree of flexibility. Compared to commercially available simulation software tools for industrial applications, which were discussed in detail in Sect. 4, machine learning tools presented here are open-source solutions that can bring about significant cost savings in the value creation of industrial development processes.

For open-source software solutions, the source code is public and the copyright holder allows users to modify and adapt it for their own individual purposes. Because of the flexible applicability and the freedom that is offered, open-source solutions enjoy a very high acceptance.

Especially for students and other academic fields, open-source solutions offer free or low-cost access and a platform to an open community that is always in exchange to support each other. This accelerates the development process of the software automatically. Compared to commercial software, open-source solutions are considered safe to use. Possible errors in the code that were overlooked by the original developers of a program can be quickly detected and corrected under their own steam. By informing the community, an otherwise typical software update and, combined with a new release process is eliminated and hence, a substantial amount of time can be saved.

In terms of stability and long-term project planning, open-source software offer further significant advantages over proprietary software. As a rule, they are based on open standards to ensure flexible integration. Even after development projects have died, tools are available to users for an indefinite period of time.

In addition to the idea of a community, values and principles such as sustainability, efficiency and cost savings are increasingly becoming the focus of digital corporate structures. Combined with the idea of lean management and the associated low-process and transparent development structures, open-source solutions are a revolutionary era. Not only as individual solutions for academic institutions and small companies as before, but especially for medium-sized and large companies, they are becoming more popular than ever.

Python

Python is a language for very general applications with a large number of stored and elaborated libraries. It is suitable for computer scientists, mathematicians and especially for

engineers. It can be used for beginners and advanced machine learning applications as well as data analysis, operation and visualization.

Scala
Scala offers ideal solutions in dealing with Big Data. The combination of Scala and Spark allows the computing power of computers or graphic cards to be used optimally through cluster computing. This balances the high computing load especially with huge amounts of data, which is unique for Scala. The language has many powerful libraries for machine learning with close links to engineering. In the area of data analysis and visualization possibilities, Scala has a disadvantage compared to its competitors.

R
R was initially developed for statistical calculations and analyses and for historical reasons offers a range of high-quality packages for statistical data acquisition and visualization. Due to its strong interface and formatting capabilities to different syntax, R is especially well suited for research purposes due to this flexibility. Compared to its competitors, R is currently less suitable for applied purposes such as engineering.

Each of these languages is more or less suitable for certain types of tasks. The choice of a preferred programming language can be very subjective, so the developer should always choose the tool that is most convenient for him.

After the most suitable programming language has been selected, a further decision has to be made on the selection among available **Machine Learning** libraries. Depending on which AI application is preferred (Natural Language Processing, Search Tree, Supervised Learning, Unsupervised Learning, Reinforcement Learning, Deep Learning, etc. (see Fig. 5.5), a large number of different libraries are available. With the help of **visualization** packages, data operations can be post-processed and results visualized. Depending on the visualization option, this can lead to a better understanding and interpretation of the corresponding data. Libraries for **mathematics and engineering sciences** offer the possibility to make numerical data manageable and to perform complex mathematical operations and scientific calculations. These packages are also used to handle data that is difficult to interpret, such as text content. As the main component of data science, the field of **data operation and analysis** provides libraries that can be used to collect, clean and pre-processed data for subsequent analysis. Finally, packages for **research** support the idea of combining variable formats from different sources of syntax in order to provide the user the greatest possible freedom in handling (Table 5.3).

The following figure lists 20 popular libraries for each of the programming languages presented. This can help to give an overview in which category libraries can be assigned and which individual strengths and weaknesses have to be taken into account when searching for the best individual solution. The diagram shows only a brief outline among countless libraries that are available on the market and are being expanded with continuous growth [70].

Tab. 5.3 Open-source software and examples of some libraries for the application of AI

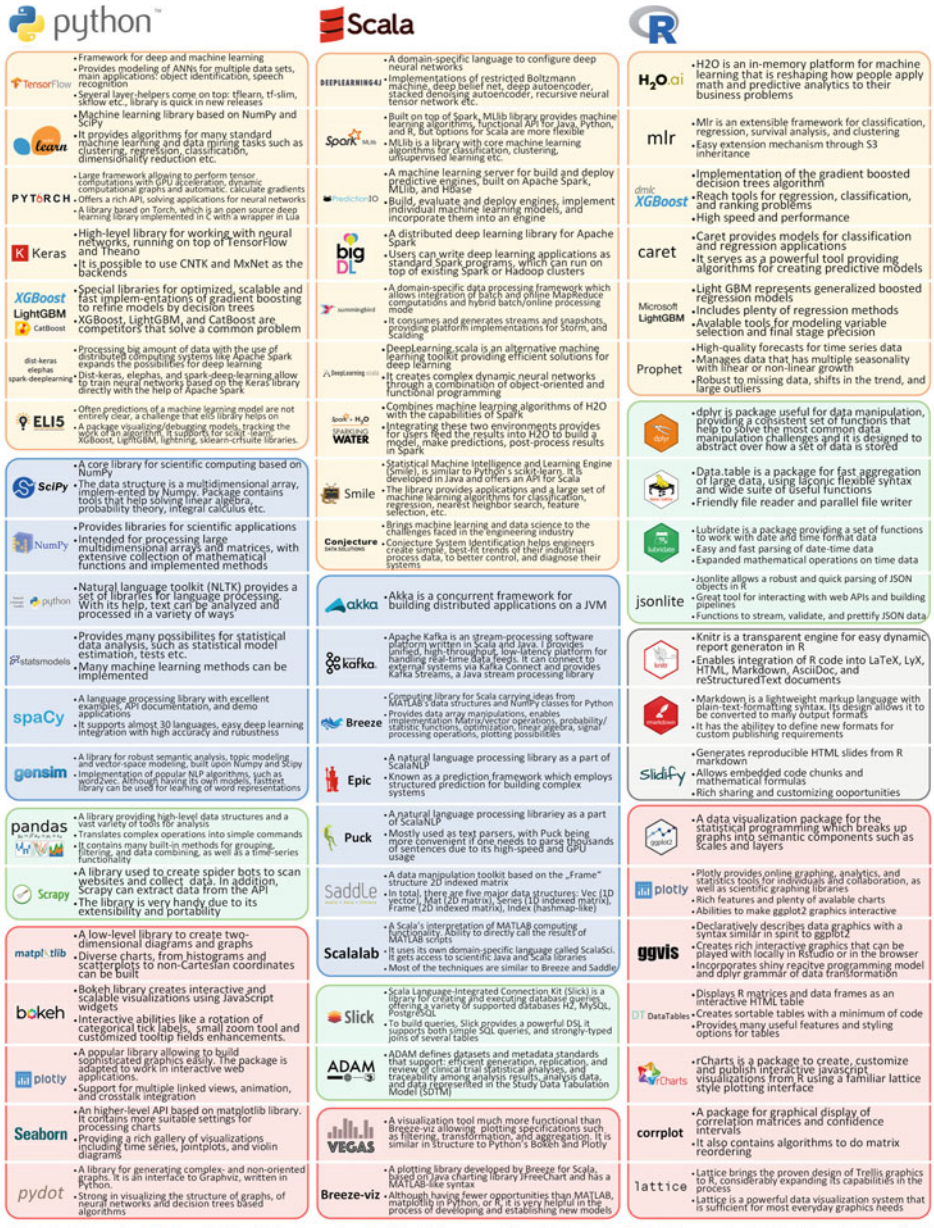

Correction to: Powertrain Development with Artificial Intelligence

Correction to:
Chapter 5 in: A. Mirfendreski, *Powertrain Development with Artificial Intelligence*, https://doi.org/10.1007/978-3-662-63863-7_5

Figures 5.28, 5.40 and 5.41 were replaced for legal reasons.

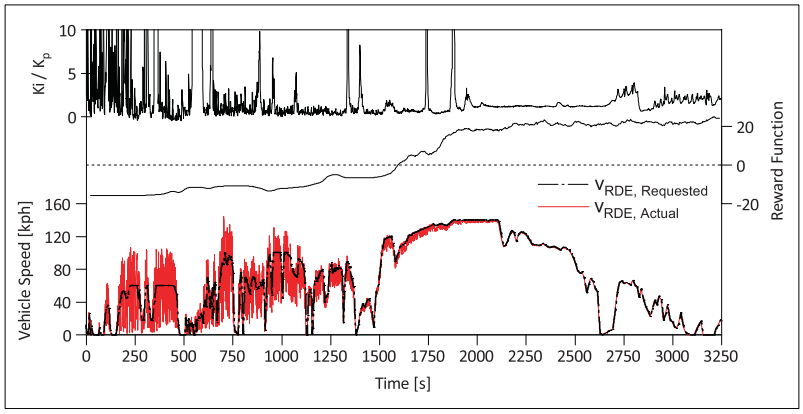

Fig. 5.28 Adaptive RDE speed control

The updated version of this chapter can be found at https://doi.org/10.1007/978-3-662-63863-7_5

A. Mirfendreski, *Powertrain Development with Artificial Intelligence*,
https://doi.org/10.1007/978-3-662-63863-7_6

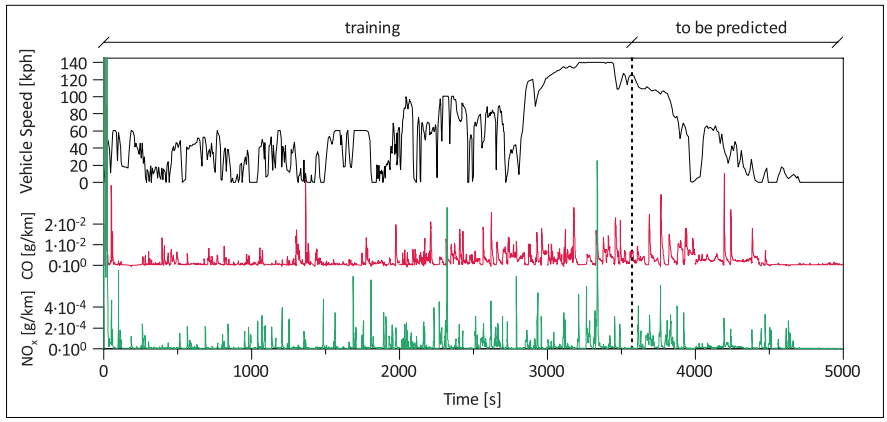

Fig. 5.40 Training and prediction of CO, NO_x emissions of the RDE test procedure

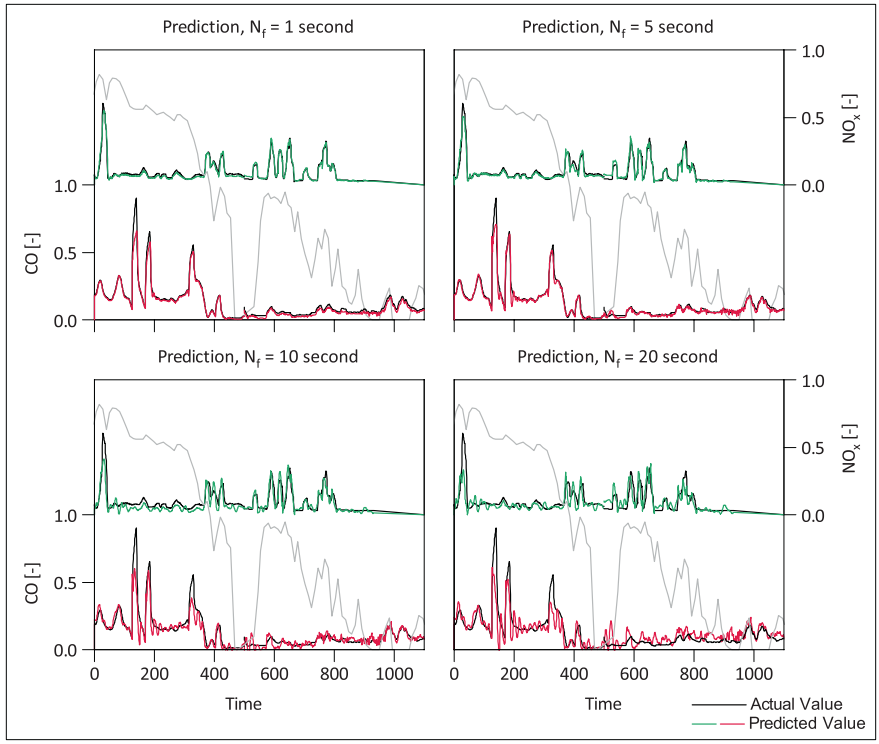

Fig. 5.41 Prediction of CO and NO_x in RDE for different future times steps N_f

Bibliography

1. R. Liedtke, *Die Industrielle Revolution* (UTB. Böhlau, Köln, Weimar, Wien, 2012). 978-3825233501
2. E.J.B.D.S. Montague, *Schöne Alte Automobile* (Gondrom, Bayreuth, 1978)
3. G. Goldbeck, *Gebändigte Kraft: Die Geschichte Der Erfindung Des Otto-Motors* (Moos, München, 1965)
4. J.H. Ferziger, M. Perić, *Numerische Strömungsmechanik* (Springer-Verlag, Berlin, Heidelberg, 2008). 978-3-540-68228-8
5. G.P. Merker, *Grundlagen Verbrennungsmotoren: Funktionsweise, Simulation*, 7th edn. (Messtechnik. Springer Vieweg, Wiesbaden, 2014). 978-3-658-03195-4
6. Gamma Technologies, editor. *GT Suite Flow Theory Manual Version 7.5*. Westmont, USA, 2015
7. L. Guzzella, C.H. Onder, *Introduction to Modeling and Control of Internal Combustion Engine Systems* (Springer-Verlag, Berlin, Heidelberg, 2010). 978-3-642-10775-7
8. M. J. W. Schouten, H. J. van Leeuwen. *Die Elastohydrodynamik: Geschichte und Neuentwicklungen*. volume 1207, Fulda, 1995. Eindhoven University of Technology, VDI Berichte
9. T. Mang, *Encyclopedia of Lubricants and Lubrication* (Springer-Verlag, Berlin, Heidelberg, 2014). 978-3-642-22647-2
10. C.H. Venner, A.A. Lubrecht, *Multi-Level Methods in Lubrication* (Tribology and Interface Engineering. Elsevier, Burlington, 2000). 9780080537092
11. E. Justi, *Spezifische Wärme Enthalpie* (Entropie und Dissoziation technischer Gase. Springer-Verlag, Berlin, Heidelberg, 1938). 978-3-642-99333-6
12. F. Zacharias. *Analytische Darstellung der thermodynamischen Eigenschaften von Verbrennungsgasen*. PhD thesis, Technische Universität Berlin, Berlin, 1966
13. T. Allison. *JANAF Thermochemical Tables, NIST Standard Reference Database 13*. National Institute of Standards and Technology. 10.18434/T42S31
14. G. Woschni, Die Berechnung der Wandverluste und der thermischen Belastung der Bauteile von Dieselmotoren. MTZ - Motortechnische Zeitschrift **31**, 491–499 (1970)
15. G. Hohenberg, *Experimentelle Erfassung Der Wandwärme in Kolbenmotoren* (Technische Universität, Graz, Habilitationsschrift, 1980)
16. K. Huber. *Der Wärmeübergang schnelllaufender, direkteinspritzender Dieselmotoren*. Dissertation, Technische Universität, München, 1990

A. Mirfendreski, *Powertrain Development with Artificial Intelligence*,
https://doi.org/10.1007/978-3-662-63863-7

17. M. Bargende. *Ein Gleichungsansatz zur Berechnung der instationären Wandwärmeverluste im Hochdruckteil von Ottomotoren*. Dissertation, Technische Hochschule, Darmstadt, 1991
18. H.G. Hahn, *Elastizitätstheorie: Grundlagen Der Linearen Theorie Und Anwendungen Auf Eindimensionale, Ebene Und Räumliche Probleme* (Vieweg + Teubner Verlag, Wiesbaden, 1985). 978-3-663-09894-2
19. F. Ziegler, *Technische Mechanik Der Festen Und Flüssigen Körper* (Springer-Verlag, Wien, 1998). 978-3-211-83193-9
20. G. Mueller, M. Möser, *Numerische Methoden Der Technischen Akustik* (Fachwissen Technische Akustik. Springer-Verlag, Berlin, Heidelberg, 2017). 978-3-662-55409-8
21. M. Bossert. *Einführung in die Nachrichtentechnik*. Technik 10-2012. Oldenbourg-Verlag, München, 2012. ISBN 9783486708806
22. J.W. Cooley, J. Tukey, *An Algorithm for the Machine Calculation of Complex Fourier Series*, Bell telephone system technical publications, vol. 4990. (Bell Telephone Laboratories, New York, 1965)
23. T. Butz. *Fouriertransformation für Fußgänger*. Springer-Verlag, Wiesbaden, 7. aktualisierte Aufl., 2011. ISBN 978-3-8348-8295-0
24. P. Jochem, *Alternative Antriebskonzepte Bei Sich Wandelnden Mobilitätsstilen* (KIT Scientific Publishing, Karlsruhe, 2012). 978-3-86644-944-2
25. International Council On Clean Transportation (ICCT). *CO_2 Emission Standards for Passenger Cars and Light-Commercial Vehicles in the European Union: Policy update*, 2019. URL www.theicct.org
26. J. Brokate, E. D. Özdemir, U. Kugler. *Der Pkw-Markt bis 2040: Was das Auto von morgen antreibt: Szenario-Analyse im Auftrag des Mineralölwirtschaftsverbandes*. Deutsches Zentrum für Luft- und Raumfahrt e.V., 2013
27. J. Adolf, C. Balzer, A. Joedicke, U. Schabla, K. Wilbrand, *Shell PKW-Szenarien Bis 2040: Fakten* (Trends und Perspektiven für Auto-Mobilität. Shell Deutschland Oil GmbH, Hamburg, 2014)
28. F. Bergk, K. Biemann, C. Heidt, W. Knörr, U. Lambrecht, T. Schmidt. *Klimaschutzbeitrag des Verkehrs bis 2050*. Umwelt Bundesamt, Heidelberg, edition 56, 2016
29. P. Hofmann, *Hybridfahrzeuge: Ein Alternatives Antriebskonzept Für Die Zukunft*, 2nd edn. (Springer-Verlag, Wien, 2014). 978-3-7091-1780-4
30. A. Ovens. *Bekanntmachungen zur Fahrzeugsystematik: Übersicht der Bekanntmachungen.* Kraftfahrt-Bundesamt, 2019. URL https://www.kba.de/DE/Statistik/Bekanntmachungen
31. *Infographics & Animations: Extracting business value from the 4 V's of big data*. IBM and Gartner, Stamford (Connecticut), USA, 2016. URL https://www.ibmbigdatahub.com/infographic
32. Q. Xiao. *Constructions and Applications of Space-Filling Designs*. PhD thesis, University of California, Los Angeles, 2017
33. S. D. Arnott, P. A. Lindsay. *Reducing Uncertainty in Systems Engineering through Defence Experimentation*. Researchgate GmbH, 2015
34. E. Aronson, T. Wilson, R. M. Akert. *Sozialpsychologie*. Psychologie. Pearson Studium, München, 6., aktualisierte Aufl., 2010. ISBN 3-8273-7084-1
35. A. Newell, J.C. Shaw, H.A. Simon, *Report On A General Problem-Solving Program* (Pittsburgh, Pennsylvania, USA, 1958)
36. F. Eisenführ, M. Weber, T. Langer. *Rationales Entscheiden*. Springer-Lehrbuch. Springer-Verlag, Berlin, Heidelberg, 5., überarb. und erw. Aufl., 2010. ISBN 978-3642028489
37. P. Kuhlmann, *Künstliche Intelligenz: Einführung in Machine Learning, Deep Learing, Neuronale Netze*, 1st edn. (Robotik und Co., Hannover, 2018). 9781983196065
38. V. Vowinkel. *Kommt die technologische Singularität?* HP Humanistischer Pressedienst, 2016. URL https://hpd.de/artikel/kommt-technologische-singularitaet-13480

39. R. Freshman. *Technological Singularity and A.I.: What is Technological Singularity?* Blog at WordPress.com, 2016. URL https://robertsfreshmanphysics.wordpress.com
40. I. Seifert, M. Bürger, L. Wangler, S. Christmann-Budian, M. Rohde, P. Gabriel, G. Zinke, *Potenziale Der Künstlichen Intelligenz Im Produzierenden Gewerbe in Deutschland: Studie Im Auftrag Des Bundesministeriums Für Wirtschaft Und Energie (BMWi) Im Rahmen Der Begleitforschung Zum Technologieprogramm* (Begleitforschung PAiCE, Berlin, 2018)
41. P. Hart, N. Nilsson, B. Raphael, A Formal Basis for the Heuristic Determination of Minimum Cost Paths. IEEE Transactions on Systems Science and Cybernetics **4** (2), 100–107 (1968). https://doi.org/10.1109/TSSC.1968.300136
42. H. Braun, *Neuronale Netze: Optimierung Durch Lernen Und Evolution* (Springer-Verlag, Berlin Heidelberg New York, 1997). 3-540-62614-X
43. R. van Loon. *Machine learning explained: Understanding supervised, unsupervised, and reinforcement learning*. 2018. URL https://bigdata-madesimple.com/machine-learning-explained-understanding-supervised-unsupervised-and-reinforcement-learning
44. A. Mirfendreski, *Entwicklung Eines Echtzeitfähigen Motorströmungs- Und Stickoxidmodells Zur Kopplung an Einen HiL-Simulator* (Springer Fachmedien, Wiesbaden, 2017). 978-3-658-19328-7
45. W. Kinnebrock. *Neuronale Netze: Grundlagen, Anwendungen, Beispiele*. Oldenburg-Verlag, München, Wien, 2., verbesserte Aufl., 2018. ISBN 3-486-22947-8
46. J. von Neumann, First draft of a report on the EDVAC. IEEE Annals of the History of Computing **15**(4), 27–75 (1993). https://doi.org/10.1109/85.238389
47. D. Kriesel. *A brief introduction to neural networks*, 2007. URL http://www.dkriesel.com/en/science/neural_networks
48. K. Debes, A. Koenig, H. M. Gross. *Transfer Functions in Artificial Neural Networks: A Simulation-Based Tutorial*. brains, minds, media, 2005. URL http://www.brains-minds-media.org
49. S. Hochreiter, Y. Bengio, P. Frasconi, J. Schmidhuber. *Gradient flow in recurrent nets: the difficulty of learning long-term dependencies*. In S. C. Kremer, J. F. Kolen, editors, *A Field Guide to Dynamical Recurrent Neural Networks*. IEEE Press, 2001
50. A. Géron, *Hands-on Machine Learning With Scikit-Learn, Keras, And Tensorflow: Concepts, Tools* (And Techniques. O'Reilly Media, Sebastopol, 2019). 1492032646
51. G. Xavier, Y. Bengio. *Understanding the difficulty of training deep feedforward neural networks*. In Yee Whye Teh, Mike Titterington, editors, *Proceedings of the Thirteenth International Conference on Artificial Intelligence and Statistics*, volume 9 of *Proceedings of Machine Learning Research*, p. 249–256, Chia Laguna Resort, Sardinia, Italy, 2010. JMLR Workshop and Conference Proceedings. URL http://proceedings.mlr.press/v9/glorot10a.html
52. K. He, X. Zhang, S. Ren, J. Sun. *Delving Deep into Rectifiers: Surpassing Human-Level Performance on ImageNet Classification*. In *2015 IEEE International Conference on Computer Vision (ICCV)*, p. 1026–1034. IEEE, 2015. ISBN 978-1-4673-8391-2
53. R. Tadeusiewicz, *Sieci Neuronowe* (Problemy Współczesnej Nauki i Techniki. Informatyka. Akademicka Oficyna Wydawnicza RM, Warszawa, 1993). 838576903X
54. J.A. Freeman, D.M. Skapura, *Neural Networks: Algorithms, Applications, and Programming Techniques* (Addison-Wesley, Reading, Massachusetts, 1992). 0-201-51376-5
55. G. Breard, L. Hamel, Evaluating Self-Organizing Map Quality Measures as Convergence Criteria, in *ICDATA' 18*. ed. by R. Stahlbock, G.M. Weiss, M. Abou-Nasr (CSREA Press, United States, 2018). 1-60132-481-2
56. T. Kohonen, T. S. Huang, M. R. Schroeder. *Self-Organizing Maps*, volume v.30 of *Springer Series in Information Sciences Ser*. Springer-Verlag, Berlin, Heidelberg, 3rd ed., 2000. ISBN 978-3-642-56927-2

57. R.S. Sutton, F. Bach, A.G. Barto, *Reinforcement Learning: An Introduction*, 2nd edn. (Adaptive Computation and Machine Learning series. MIT Press Ltd, Massachusetts, 2018). 9780262039246
58. A. Tang et al., Canadian association of radiologists white paper on artificial intelligence in radiology. Canadian Association of Radiologists journal **69** (2), 120–135 (2018). https://doi.org/10.1016/j.carj.2018.02.002
59. P. Radhakrishnan. *A Medium publication sharing concepts, ideas, and codes: What are Hyperparameters? And how to tune the Hyperparameters in a Deep Neural Network?* Medium, 2017. URL https://towardsdatascience.com
60. R. Fullér. Fuzzy logic and neural nets in intelligent systems. In C. Carlsson, editor, *Information systems day*, TUCS general publications, p. 74–94, Turku, Finnland, 1999. Turku Centre for Computer Science. ISBN 951-29-1604-5
61. K. Wolff, R. Kraaijeveld, J. Hoppermanns. Objektivierung der fahrbarkeit. In K. Becker, editor, *Subjektive Fahreindrücke sichtbar machen, IV*, Haus der Technik - Fachbuchreihe. Expert, 2009. ISBN 978-3-8169-2936-9
62. T. Epelbaum. *Deep learning: Technical introduction*. URL http://arxiv.org/pdf/1709.01412v2
63. W. Zhu, Y. Ma, Y. Zhou, M. Benton, J. Romagnoli. *Deep Learning Based Soft Sensor and its Application on a Pyrolysis Reactor for Compositions Predictions of Gas Phase Components*. In M. R. Eden, M. G. Ierapetritou, G. P. Towler, editors, *13th International Symposium on Process Systems Engineering : PSE 2018*, volume 44, p. 2245–2250. Elsevier, 2018. ISBN 978-0-444-64241-7
64. A. Dertat. *Applied Deep Learning - Part 4: Convolutional Neural Networks*. Medium, 2017. URL https://towardsdatascience.com
65. D. Forsyth, J. Ponce, *Computer Vision: A Modern Approach* (N.J. and London, Prentice Hall, Upper Saddle River, 2003). 978-0-13-085198-7
66. J. Hui. *GAN - Some cool applications of GAN*. 2018a. URL https://jonathan-hui.medium.com
67. B. C. Kamble. *Speech Recognition Using Artificial Neural Network – A Review*, volume 3. 2016. 10.15242/IJCCIE.U0116002
68. M. A. Escabi. *Biologically Inspired Speech and Sound Recognition*, 2020. URL https://escabilab.uconn.edu/biologically-inspired-speech-and-sound-recognition/
69. J. Hui. *GAN — What is Generative Adversarial Networks GAN?* 2018b. URL https://jonathan-hui.medium.com
70. ActiveWizards Group LLC. *Comparison of top data science libraries for Python, R and Scala*. New York, USA, 2010-2020. URL https://activewizards.com/blog/comparison-of-top-data-science-libraries-for-python-r-and-scala-infographic/